Revolutionizing T cell Therapy for Pancreatic Cancer: Harnessing the Power of T cell Receptor Exchange Mice

A DISSERTATION
SUBMITTED TO THE FACULTY OF THE
UNIVERSITY OF MINNESOTA
BY

Meagan Renae Rollins

IN PARTIAL FULFILLMENT OF THE REQUIREMENTS
FOR THE DEGREE OF
DOCTOR OF PHILOSOPHY

Advisor: Dr. Ingunn Stromnes

March 2023

Acknowledgements

There are many people that I must thank for helping me achieve this goal it's with their love, support, inspiration, and guidance that this work was possible.

To my mentor Ingunn Stromnes, I wanted to take a moment to express my gratitude for the opportunity to work with you. Your guidance and support have been invaluable to me, and I have learned a great deal from you. I appreciate your commitment to the team and the lab, and I am grateful for the work you do to help us succeed.

I want to thank my lab. When I started in the lab, we were a mere four people, since then it certainly has grown. Adam Burrack, Jonah Butler, Eddie Cruz, Alex Tsai, Zoe Schmiechen, Jackson Raynor, Antonio Rizzo, Cara-Lin Lonetree, Maren Pautsch, Iris Wang, Ellen Spartz, Anna Panek and Ebony Miller: It has been an honor working alongside all of you. You have all been friends, resources, incredibly hard workers, and great people to enjoy a beer or the occasional tequila shot with. I must also individually thank a few members of the lab whom without I wouldn't have gotten as much done or stayed sane without.

Adam, since the first day I rotated in the lab, I learned so much from you not only about biking, exercise, and raising three wild Burrack children but about experimental grit, maximizing data to be collected in a single experiment, and getting over the finish line. You have taught me a great deal about patience and the importance of laughter. Forever I will be thankful.

Ellen Spartz, my dear, you made lab an absolute joy, laughter was contagious, and your imaging skills were beyond. I thank you both for your important experimental contributions and assistance in data collection and analysis.

To Ebony Miller. Ebony joined the lab at a time when we were short staffed and drowning in work. She knew absolutely nothing about immunology and yet by the time summer hit she was arguably more knowledgeable than most first year graduate students. She was one of the brightest people I have ever known. Her daily encouragement, and light is missed dearly.

To my parents Ron and Diane Rollins. You both have always been there supporting me and my goals even when you didn't quite understand what I was doing.

Thank you always for the endless snacks and dinners you have sent to me throughout this journey and the endless number of lessons you have taught me in life that have allowed me to achieve this goal.

I want to thank my sisters Kate, Emily, and Grace, who always offered laughs, a dash of chaos, and always a little tomfoolery when we got together and were adequately caffeinated. To my brother Tony, you always taught me to be fearless, smart, to surround myself with trustworthy people. I miss you and having a beer with you after a hard day.

Thank you to my wonderful college friends who have always been there to support me with endless bottles of wine, celebrity gossip, delicious food and above all not talking about science. Katie, Emily, and Sarah, you all have made this journey with me, and I will always be thankful for bever meet up weekends at the winery, weddings, and getting to experience all the joys of life.

To the hype queen network, Emma, Lila, Paul, and Laura, I am beyond happy that our paths in life crossed. Forever will I be thankful for my experience at the Mayo Clinic because I couldn't have asked for better friends in life. You all have inspired me, allowed me to vent, and supported me through the tough ups and down with countless care packages, flowers, and gifts in the mail and of course not to mention the many drag brunches that we can't remember.

To my wonderful partner Michael, you have added a richness and joy in my life that is truly immeasurable. You added balance to my lab schedule, laughter when it all got hard, perspective when I got overwhelmed. I appreciate that you listen and try to understand what exactly it is that I do and work on, even when it all goes completely over your head. I am so happy for us to be able to be on the other side of this degree and be able to enjoy the best that life can provide for us. But most of all I can't wait to end at a round at even par for once and not overshoot my putts to the basket by 10 feet.

I need to thank my therapist, Erin. Mental health management isn't easy in grad school, but you have always challenged me when I needed it, listened, pushed me to put in the work and celebrated my success. You have taken me through a journey of grief, anxiety, ADHD, and helped me rediscover my own inner strength and overall helped me

become a more stable and confident human being. For this I will be forever thankful and grateful.

To my scientific inspiration, my mentor, and friend Rachel Gibbons Johnson, you have always been there supporting and encouraging me. When I lacked faith and belief in myself, you always knew I could do it and more importantly you told me this. You inspired my love of CD8+ T cells, Cancer Biology, Hamilton, and Trampled by Turtles. Your classes were and will always be my favorite classes I've ever taken in higher education. I fell in love with immunology and cancer immunotherapies in you research lab and you taught me how to be a good mentor and teacher through your patience and your endless willingness to just jump in whenever and wherever help is needed. Including the countless times, you have offered and taken time to read, edit, and give your thoughts on my writing. Without you, I wouldn't be where I am today and the impact you make on your students' lives should never be forgotten.

To my cohort. The gifs, memes, and endless number of games nights and text chains are what got me through grad school. Nothing I write here feels like enough so in twenty years let's all go hang out on my yacht. Thank you for to the good times and good vibes in the hardest times of my life.

A huge thank you to those who run the MICaB program: Ryan Thorsen, Megan Ruf, Ameeta Kelakar. Ryan and Megan, literally our work as graduate students wouldn't be possible without you thank you for constantly solving program issues so that we can focus on the research. Y'all are a blessing.

To the Center for Immunology, you all have created a wonderful and vibrant learning environment. Truly, I have been honored to be your colleague for the past five years.

Thank you to my thesis committee, Dr. Vaiva Vezys, Dr. Mike Farrar, Dr. Branden Moriarty, Dr. Kaylee Schwertfeger, and Dr. Steve Jameson. You have all been and immense resource and support. I have really enjoyed working with you, collaborating with you, absorbing your wisdom and knowledge. I am going to really enjoy sharing a St. Paddy's Day beer with you all next.

Abstract

Pancreatic ductal adenocarcinoma (PDA) is a lethal cancer characterized by a suppressive tumor microenvironment (TME) including elevated levels of TGFβ. The adoptive transfer of T cell receptor (TCR) engineered T cells specific to mesothelin (Msln) can effectively target PDA, but efficacy is limited by the suppressive TME that promotes engineered T cell dysfunction. T cell receptor (TCR) transgenic mice represent an invaluable tool to study antigen-specific immune responses. In the pre-existing models, a monoclonal TCR is driven by a non-physiologic promoter and randomly integrated into the genome. Here, we create a highly efficient methodology to develop T cell receptor exchange (TRex) mice, in which TCRs, specific to the self/tumor antigen mesothelin (*Msln*), are integrated into the *Trac* locus, with concomitant *Msln* disruption to circumvent T cell tolerance. We show that high affinity TRex thymocytes undergo all sequential stages of maturation, express the exogenous TCR at DN4, require MHC class I for positive selection and undergo negative selection only when both *Msln* alleles are present. By comparison of TCRs with the same specificity but varying affinity, we show that *Trac* targeting improves functional sensitivity of a lower affinity TCR and confers resistance to T cell functional loss. By generating P14 TRex mice with the same specificity as the widely used LCMV-P14 TCR transgenic mouse, we demonstrate increased avidity of *Trac*-targeted TCRs over transgenic TCRs, while preserving physiologic T cell development. To test the hypothesis that TGFβ is a major driver of engineered T cell dysfunction in PDA, we knocked out *Tgfbr2* using CRISPR/Cas9 in *in vitro* activated Msln-specific TRex cells. The loss of Tgfbr2 signaling in high affinity (1045) Msln-specific TRex T cells drive increases in markers of effector T cells such as Klrg1, Cxcr3, and CD44. When transferred into orthotopic PDA tumor bearing mice, both *Tgbr2*-WT and *Tgbr2*-/- engineered T cells traffic to tumors driven by increased frequency and number of cDC1 and cDC2 dendritic cells. With vaccination, the engineered T cells cause a 10-fold reduction in tumor weight at day 13 post tumor and are highly proliferative. Tumor infiltrating *Tgbr2*-/- cells upregulated IFNγ, TNFα, and Granzyme b and decreased markers of terminal exhaustion PD-1 and Lag3. Our studies suggest, interfering with TGFβ signaling can alter T cell fate prior to transfer and maintain effector differentiation within the TME promoting cytotoxic Klrg1+ T cells at the expense of PD-1+ exhausted T cells and leading to tumor control.

Table of Contents

List of Tables

List of Figures

Chapter 1: Introduction

1.1 The vertebrate immune system

The immune system is composed of a diverse network of a cells, soluble proteins, and factors that are vital to an organism's ability to clear pathogens such as viruses and bacteria, cancer, and to bring the overall system back to homeostasis. The process of recognition, response, and clearance is controlled by the two branches of the immune system, adaptive immune system, and the innate immune system. The innate immune system serves as the first line of defense against pathogens; composed of physical barriers such as skin and mucous membranes or major cellular components such as endocytic and phagocytic cells that drive inflammatory processes. Innate immune cells rapidly respond via pattern recognition receptors in a matter of minutes to hours and recruit other immune cells to sites of infections and inflammation in the body[1]. While these cells are fast, their recognition is non-specific meaning the innate immune response is not able to recall a specific pathogen or encounter. Edward Jenner, an 18th century scientist, and pioneer of immunology established the terminology of vaccines and vaccination in his paper "*Inquiry into the causes and effects of the variolae vaccinaie*". His findings showed that by giving a vaccination, an injection, of the weaker cow pox (vaccinia) virus, one could develop long lasting immunity to the much deadlier smallpox virus[2]. Since this initial observation, we have elucidated that this response is attributed to a memory response generated by the adaptive immune system.

The adaptive immune system is composed of two major cell types, T cells and B cells. Compared to the innate immune system, several key differences can be identified, indispensably every T cell and B cell will express a uniquely rearranged cell surface

receptor that recognizes a highly specific antigen, B cell receptor (BCR) and T cell receptor (TCR) respectively. Briefly, these clonally unique antigen receptors result from variations in the amino acid sequence at the antigen binding site. Both receptors contain two variable regions V_H and V_L in BCRs and Vα and Vβ (also possible V_γ V_δ) in the TCRs and are generated by a process of somatic DNA recombination (also known as VDJ recombination). This process involves recombination of gene segments (variable (V), diversity (D), and joining (J) segments), of which there are multiple copies of each of these gene segments that can be joined together to generate the unique antigen binding site. The repertoire of possible gene segment rearrangements is over 5 $x10^{13}$ possible BCRs, whereas TCR diversity for an α:β TCR pairing is greater than 10^{18} different TCRs[3]. This endless potential of TCRs and BCRs allows for recognition of an almost infinite number of pathogens and self-derived mutated proteins (neoantigens). Unfortunately, this diverse repertoire also opens immense opportunity for T cells and B cells to recognize of self-antigens propelling autoimmunity. To ensure distinguishing of self vs non-self T cells and B cells are subject to an 'education training program' at their site of development, where their antigen receptors will be tested by presentation of self-antigens to ensure self-reactive B cells and T cells are deleted from the repertoire.

T cells play a crucial role in the immune system as they are powerful and fantastic killers, meaning their activation and functions must be highly regulated to prevent self-recognition. One source of regulation is that T cells are only able to recognize antigens, small protein fragments, presented on Major Histocompatibility Complexes (MHC). T cells are divided into categories by their surface coreceptor (CD4+ or CD8) expression into CD4+ helper T cells or CD8+ cytotoxic T cells. CD4+ helper T cells recognize antigen

peptides 13-16 amino acids long (a.a.) in the context of MHC II, which is presented by special innate immune cells known as antigen presenting cells (APC)[3,4]. CD8+ cytotoxic T cells recognize antigen peptides 8-10 a.a. long presented by MHC I, which is presented on the surface of almost all nucleated cells. The adaptive immune response of CD8+ T cells in response to cancer will be the focus of this thesis work.

1.2 T cell Development

1.2.1 Overview

Immune cells originate in the bone marrow as pluripotent hemopoietic stem cell (HSC) and through specific signaling pathways will differentiate and give rise to lymphoid or myeloid lineages[3]. An HSC will give rise to an immature T cell by upregulating notch signaling, which in turn signals the immature T cell to leave the bone marrow and migrate to the thymus. There, it will undergo TCR rearrangement, thru the processes of positive and negative selection, before being released as a mature T cell into the peripheral circulation.

1.2.2 TCR rearrangement

Immature T cells enter the thymic medulla as double negative (DN) cells, which means they lack the expression of CD4+ and CD8+ coreceptors as well as lacking a rearranged T cell receptor (TCR). A TCR consists of an α chain and β chain or a γ:δ chain. This work will focus exclusively on α:β T cells going forward. Both the α and β chains are composed of a variable (V) and a constant (C) amino-terminal region. While the constant chain is as aptly named and constant in all TCRs, the variable chain is composed gene segments that undergo somatic DNA recombination to form a complete and unique

Vα and Vβ amino-terminal regions. The TCR β chain is comprised of three gene segments: V_β (variable segment), D_β (or diversity segment), and J_β (or joining segment), while the TCR α chain is composed of only two gene segments, V_α and J_α. To progress to a functional TCR, the T cell must successfully undergo the process of somatic DNA recombination, or better known as V(D)J recombination, to generate functional α and β chains.

Upon Notch1 stimulation with thymic stromal cells, immature DN thymocytes traffic further into the thymic cortex where they upregulate two critical transcription factors, TCF1 and GATA3. TCF1 and GATA3 initiate several T cell lineage specific genes, most critical being *Rag1* and *Rag2* [3–5]. RAG-1 and RAG-2 are recombinase proteins that facilitate V(D)J recombination in the TCR β chain, which undergoes recombination first. Once a successful rearrangement of all three TCR β gene segments occur, the new TCR β chain will pair with a pre-TCRα (pTα) and CD3 proteins and form a pre-TCR complex driving proliferation and allelic exclusion[6]. Once formed, the process of allelic exclusion inhibits rearrangement of any other TCR β chains by downregulating RAG1/2 and transitioning the immature thymocyte from a DN to an immature double positive (DP) thymocyte that expresses both the CD4+ and CD8+ co-receptors.

Immature DP thymocytes will begin to once again express RAG1/2 and initiate the TCRα gene segment rearrangements. The TCR α gene segments will continue to rearrange until there is a successful TCR α chain that pairs with the TCR β chain and undergoes positive selection[6–8].

1.2.3 Positive and negative selection

Positive selection is the process where the newly rearranged α:β TCR is tested on its ability to bind MHC presented on cortical thymic epithelial cells (cTEC)[9]. cTECs present self-antigen on MHC I and MHC II to DP thymocytes which can recognize and weakly bind self-MHC. These weak interactions subsequently induce positive survival signals that allow thymocytes continue down the development path to a mature single positive (SP) T cell[9]. DP thymocytes that positively select self-MHC I will downregulate the CD4 coreceptor and become an immature CD8+ SP thymocyte. Thymocytes that positively select self-MHC II will downregulate the CD8+ coreceptor and become an immature CD4+ SP thymocyte. Thymocytes that fail positive selection, do not recognize either self-MHC, have another chance to rearrange the TCR α chain again. TCRs that fail to productively rearrange their TCRα chain the second time will die by neglect and never make it out of the thymus. Once, positive selection has occurred, mature SP CD4+ and CD8+ thymocytes will migrate to the medulla region of the thymus where they will interact with medullary thymic epithelial cells (mTEC) and undergo negative selection.

As mentioned, T cells have immensely large number (10^{18}) of possible TCRs that can be generated due to the diversity that is generated in VDJ recombination. It is inevitable that self-reactive T cell clones will be generated through this process. Negative selection is the process of which the body eliminates self-reactive clones out of the T cell repertoire[10]. mTECs are the key regulators of negative selection due to their expression of the transcription factor gene autoimmune regulator (*AIRE*). AIREs primarily drives the transcription of genes encoding tissue-specific antigens, such as insulin, that would not normally be expressed in the thymus. Its multidomain structure allows it to also anchor

multimolecular complexes involved in initiation and gene transcription and can further drive mRNA diversity by favoring alternative splicing[11]. The expression of AIRE allows for mTECs to present a wide diversity of self-antigens on MHC in the thymus in various orientations that would normally never be expressed in that tissue[7,11]. Strong affinity binding of a SP thymocyte to self-peptides presented on MHC drives induction apoptotic pathways and cell death eliminating that cell from escaping into the periphery. When a SP thymocyte binds self-peptide:MHC complexes within a 'goldilocks' affinity, not too weak not too strong, it will undergo another round of rapid proliferation and traffic from the thymus into secondary lymphoid organs (SLO, i.e. spleen and lymph nodes) as a fully mature CD4+ or CD8+ T cells[12].

1.3 CD8+ T cells in adaptive immunity

1.3.1 Overview

CD8+ T cells are critical in monitoring all cells in the body and have a potent ability to kill host cells that present signs of malignant transformation or intracellular infection[4]. The immense number of infectable host cells that naïve CD8+ T cells would have to survey is not possible when compared the rare number of naïve CTL that can recognize any given epitope (~1 in 10^6-10^7)[13]. To increase the opportunity for antigen encounter and immune surveillance, CD8+ T cells perpetually circulate through and temporally reside in SLOs where dendritic cells (DC) present antigens on MHC I. The role of dendritic cells will be discussed later in this section.

1.3.2 Naïve Trafficking

Naïve CD8+ T cells express selectins that are vital in homing, a process of bringing leukocytes into tissues. L-selectin (CD62L) on naïve CD8+ T cells binds to vascular addressins CD34 and GlyCAM-1 on high endothelial venules (HEV), bringing them into the lymph node from the blood stream. Naïve CD8+ T cell also express LFA-1 which bind ICAM-1 on HEV, to enable adhesion and diapedesis through tight endothelial junctions. Once in the lymph node, naïve CD8+ T cells expressing CCR7 are driven by chemotactic gradients to the T cell zone, where dendritic cells are producing the ligands CCL21 and CCL19 in the T cell zone. In the T cell zone, T cells will scan activated DCs that have drained from sites of infection or have collected particulate antigen from surrounding lymph for their cognate pMHC[3]. A single antigen presenting DC within an SLO can be contacted by ~5,000 T cells/hour[14]. If the naïve T cell doesn't find its cognate pMHC, S1PR1, a G-protein coupled receptor, will draw the naïve T cell out into circulation through a high chemokine gradient of it ligand sphingosine 1-phosphate (S1P) and will leave the lymph node through the efferent lymphatic vessels[15–18]. Naïve CD8+ T cells repeat this process of continuous circulation until they are activated or die.

"With great power, comes great responsibility[19]", and with a strong killing response CD8+ T cell activation is tightly regulated to inhibit aberrant activation and killing of host cells. CD8+ T cell activation involves multiple signals and co-stimulatory molecules that are required to mount an effective immune response. Dendritic cells are a heterogenous innate immune cell population that in the absence of an ongoing inflammatory event continuously survey the blood, lymph, SLO, and other peripheral non-lymphoid tissues[13,14,20]. Often thought of as the bridge between the adaptive and innate immune

systems, DCs are critical in internalizing and presenting self and non-self-antigens by proteolytically cleaving peptides and loading them onto MHC I and MHC II molecules. Conventional DC (cDC) are particularly specialized APCs critical in priming and activating T cells. cDCs at steady state are considered immature and are highly inefficient and slow at generating and loading peptides on MHC[20]. However, after encountering a danger signal through pathogen recognition receptors (PRR), cytokines receptors, and/or toll-like receptors, cDCs undergo a maturation process driving transcriptional changes that streamline antigen uptake, degradation, and intracellular transport[14]. Additionally, mature activated cDCs upregulate and stabilize MHC molecules on the surface, increase levels of co-stimulatory molecules CD80 (B7-1) and CD86 (B7-2), and increase chemokines such as CCR7, that drive trafficking back to a lymph node to facilitate antigen presentation to T cells.

1.3.3 CD8+ T cell activation: Three-signals of activation

As mentioned above CD8+ T cells require an array of signaling events to become activated. Traditionally, we categorize three critical and required signals for T cell activation: TCR: peptide MHC (pMHC), co-stimulation, and cytokines. All three signaling events coinciding will drive rapid proliferation and differentiation of naïve CD8+ T cells into effector CD8+ T cells that will then migrate to inflamed tissue where they produce cytokines such as interferon-γ (IFNγ) and Tumor necrosis factor α (TNFα), and cytolytic granules such as Granzyme b. Without all three signals a CTL will undergo the process of peripheral tolerance, clonal deletion, or anergy[3,21].

The first signal required for activation comes from the T cell through the TCR recognizing it cognate peptide and MHC I. The TCR will interact and contact pMHC through the variable domains. The TCR:pMHC interaction is stabilized by the CD8+ co-receptor which acts as a non-antigen specific receptor for MHC and thus increases the duration for which the TCR:pMHC interact[4]. The interaction between TCR:pMHC drives initial signal transduction through co-receptor associated kinase LCK which phosphorylates immunoreceptor tyrosine-activation motif (ITAM) on the CD3 complexes and the ζ chains associated with the TCR[22–24]. TCR signaling induces confirmational changes on the T cell in LFA-1 (CD11a) that greatly increase its affinity for ICAM-1 and ICAM-2 that also stabilizes the interaction by creating the immunological synapse with the APC[25–27]. Downstream intracellular signaling from the engaged TCR leads to upregulation of transcription factors, namely, AP-1, NFAT, and NFκB for IL-2 cytokine production, cytoskeleton reorganization, adhesiveness, and metabolism[23,28,29,29–32].

Even if a T cell is engaged and the co-receptor is ligated it will not fully proliferate or differentiate into an effector T cell without engagement of co-stimulatory molecules such as CD28 on the naïve T cell. The second signal for activation comes from CD28 engaging with CD80 and CD86 on the same APC its engaging TCR signaling with[3,4,13,20,33]. At a high level, CD28 co-stimulatory signaling drives T cell proliferation, cytokine production, and cell survival by amplifying the downstream signaling responses to TCR engagement. Critically, CD28 signaling induces maximal activation of the signaling molecule PLCγ which is vital in production of IL-2[23,34]. The third signal for required for activation is IL-2 cytokine signaling. Cytokines are small soluble proteins secreted by cells that act as a communication channel between cells by altering the behavior or the properties

of a cell through autocrine (self) or paracrine (another cell) actions. Cytokine production isn't limited to immune cells and can be produced by many other cell types in the body. IL-2 is a fundamental cytokine in the immune system that works in autocrine and paracrine manners to promote T cell proliferation and survival[4,13,18]. The IL-2 α chain (CD25) is one of three chains, β and γ chains, that can compose the IL-2 receptor. CD25 expression is induced downstream of CD28 co-stimulation. This is necessary as CD25 has a higher affinity for IL-2 than that of the baseline expressed heterodimer β and γ chains alone[34,35]. When complexed into the trimeric IL-2 receptor, T cells are sensitive to very low concentrations of IL-2, allowing for little IL-2 in the environment to sustain T cell proliferation and survival[33–36]. Other co-stimulatory molecules such as ICOS, CD2, CD40, 4-1BB, and OX40 on T cells interact with ICOSL, CD70, CD40L, 4-1BBL and OX40L on APCs respectively to further facilitate T cell activation, differentiation, and effector functions. Mice deficient in these receptors show diminished and reduce T cell responses to infection, highlighting the importance of costimulatory signaling in activation[13,33–37]. Other cytokines such as IFNγ, IL-12, IL-4, TGFβ, IL-6, and IL-23 provide the differentiation cues necessary to induce effector functions, T cell subset fate (CD4+ T cells) and tissue homing receptors[28,38–43]. T cells that receive all three signals will undergo an immense proliferation dividing every 4-6 hours, 15-20 times, generating a massive clonal population of differentiated effector T cells that can then enter circulation and traffic to the site of infection or malignancy driven by chemokine and cytokine gradients[15,17,18,24,44–47]. T cells require all three signals for activation. Without them the T cell will be rendered dysfunctional, and as such they will downregulate cytotoxic molecules, upregulate

exhaustion markers such as PD-1, Tox and Lag3 and even enter the apoptosis pathway[4,21,37,48–52].

On top of receiving all three signals T cells also must overcome mechanism to inhibit T cell activation through inhibitory receptor signaling through engagement of Programmed Death 1 (PD-1), B and T lymphocyte attenuator (BTLA), and CTLA-4 (CD152) expressed on T cells. CTLA-4 has a higher affinity for CD80 and CD86 than that of CD28 and engages CD80/86 in a different orientation that allows it to bind multiple CD80/86 receptors at once driving immense competition for limited numbers of costimulatory molecules on APCs[33,53,54]. PD-1 and BTLA both contain immunoreceptor tyrosine-based inhibitory motifs (ITIM). Engagement of these receptors drive recruitment of phosphatases that inhibit will inhibit intracellular signaling of T cell activation and can also induce cellular apoptosis through release of Bim[55–58]. CTLA-4 and PD-1 have become of great interest in the treatment of cancer of which will be discussed later[54,59–62].

1.3.4 CD8+ T cell effector functions

After proliferation and differentiation effector CD8+ T cells (T_{eff}) in the SLO microenvironment can be divided into two different subsets, short lived effector cells (SLECs) and memory precursor effector cells (MPECs)[63–66]. The majority of the cells in the microenvironment at the start will be KLRG-^{high}, CD127^{low}, CD27^{low}, BCL-2^{low} SLECs that act to clear the ongoing infection or malignancy[66–68]. These are thought to be short lived at the expense of having highly increased effector functions. Whereas MPECs are KLRG-1^{low}, CD127^{high}, CD27^{high} and BCL-2 ^{high} and are thought to be longer lived at the expense of decreased effector functions in comparison to SLECs.

Once a T_{eff} has trafficked to and entered a site of infection or malignancy, it's time to do the job, destroy infected or malignant cells. T_{eff} can kill through direct or indirect mechanisms. Direct T_{eff} killing is started by CD2 and LFA-1 ligand interactions that allow the T cell to roll along the cells looking for cognate pMHC presentation on the target cell[29,69–71]. A target cell displaying cognate antigen will be tightly bound by the CD8+ T cell and an immunological synapse, where the TCR and co-receptors will cluster at the cell surface, will form. The immunological synapse creates a cytoskeletal "seal" between the target cell and the effector CD8+ T cell creating a focused area for the release of effector molecules by CD8+ T cells, thus protecting adjacent cells from off-target killing[25–27]. Cytotoxic effector molecules released by T_{eff} fall into two broad classes cytotoxins and cytokines. Cytotoxins are pre-stored cytotoxic granules that can be released by CD8+ T cells upon engagement of the TCR by a target cell. They can penetrate through any lipid bilayer and induce apoptosis within a matter of minutes in the effected cell thus their release must be tightly regulated[4,25,72]. Cytotoxic molecules produced by T_{eff} include perforin, granzymes (such as granzyme B), and granulysin. Perforin binds to the cell surface of the target cell and generates a pore while the granzymes and granulysin can enter the target cell to induce apoptosis through various pathways[73]. Effector CD8+ T cells also express FAS ligand (CD178) which when engaged with the target cell expressing FAS (CD95) will drive the intracellular apoptosis pathways[74,75].

Effector cytokines, unlike cytotoxins, are produced newly by T cells only after activation and released into the microenvironment. CD8+ T cells produce a variety of effector cytokines upon activation such as IFNγ, TNFα and LTα. Effector cytokines cellular actions are largely restricted to MHC II expressing cells or cells that express the

specific cytokine receptor but often act to mediate the effects of T cell killing[76,77]. One example of mediation of the effects is the cytokine IFNγ. IFNγ drives upregulation of MHC I expression on the surface of cells and increases intracellular MHC I machinery, such as β2m and Tap-1, expression[78]. This causes cells within the infection or tumor microenvironment to present more peptide on the surface and increase the chances of cytolytic killing by a CD8+ T cell[25,77–79].

After an infection or malignancy has been essentially cleared by the adaptive immune response 90-95% of the expanded CD8+ T cell population with die by apoptosis. This "clonal contraction" is driven by both intrinsic and extrinsic pathways of apoptosis through loss of pro-survival cytokines (IL-2), an upregulation BIM through loss of BCL-2 production, and induction of CD95 signaling[80,81]. It was originally proposed that the contraction phase was linked to antigen clearance, as timing of contraction coincides frequently, but studies at most show a casual link rather than causation[81–83]. The 5-10% of clonal cells left behind of will seed and become the long-lived memory pool[14,66] with many of these being generated from MPECs.

1.3.5 CD8+ T cell Memory

As discussed earlier the adaptive immune system differentiates itself from the innate immune system because it can form lifelong memory to specific pathogens. Memory T cells (T_{mem}) require lower threshold signals for activation than that of naïve T cells. Thus, T_{mem} can respond more rapidly and robustly to their cognate antigen with every subsequent to re-exposure[66,84–86]. It has also been shown that this re-activation of memory T cells can essentially go on forever, well past the life span of a research mouse[87]. Memory CD8+ T

cells differentiate from MPECs following the contraction phase into three different memory subsets, central memory (T_{CM}), resident memory (T_{RM}) and effector memory (T_{EM})[66]. T_{CM} and T_{EM} are circulating memory populations unlike that of the T_{RM} population which stays within the tissue and does not recirculate in blood or lymphatics. T_{CM} populations, marked by expression of $CD62L^{high}$, $CCR7^{high}$, and S1PR1, restrict themselves to recirculation of blood and lymph trafficking and surveying through SLO like that of naïve T cells. T_{EM} populations, marked by $CD44^{high}$, $CD11a^{high}$, generally lack $CD62L^{low}$ and $CCR7^{low}$, and recirculate through the blood and lymphatics. T_{EM} populations can survey the both the SLO and non-lymphoid tissues (NLT) for antigen re-encounter. The T_{RM} population is generally characterized by CD69 and CD103 expression and are retained in the NLT and do not recirculate. Markers for the T_{RM} population are heterogenous and seem to change dependent on the NLT of which they reside in[65,66,86]. Each of these populations play a distinct role in protecting humans from reinfection and from cancer reoccurrence.

1.4 Cancer Immunosurveillance

1.4.1 Historical Overview

In 1908, German scientist Paul Ehrlich won jointly a Nobel prize for his work in establishing the field of immunology. It was his work that first suggested that the immune system could be responsible for treating tumors[88]. Ehrlich is also responsible for the discovery of one of the first chemotherapeutic agents to treat cancer. This work laid dormant though until the mid-1950's before being recognized by Frank McFarlane Burnet and Lewis Thomas who formalized and further developed Ehrlich's theories in their

"immune surveillance" hypothesis, which states cells of the immune system will detect and destroy tumor cells[89]. The importance of this hypothesis was lost for almost forty years and it wasn't until 1990's that we would be able to confirm that Burnet and Thomas were right[90]. We now know that the immune surveillance hypothesis is true but more complicated than once thought by Burnet and Thomas. We have fully come to recognize that the immune system plays at least three distinct roles in preventing cancer: 1. protecting against viral infections including suppressing virally-instigated tumors, 2. preventing prolonged establishment of an inflammatory environment that facilitates tumorigenesis by driving prompt resolution of inflammation and contraction after pathogen clearance, and 3. eliminating malignant cells that co-express ligands for activating receptors on innate immune cells[90]. The immunosurveillance hypothesis languished to fully account for how cancer responds to and evolves through the immune response[91].

1.4.2 Elimination, Equilibrium, and Escape: the battle for survival

Cancer immunosurveillance is just one phase of cancer immunoediting that has now been established to occur into three phases, elimination phase, equilibrium phase, and the escape phase. Cancer immunoediting defines the concept that there is a dual role of the immune system in response to cancer, a host-protective and tumor–sculpting[90,92,93]. The first phase, elimination, is whereby the innate and adaptive immune systems work in an organized fashion to destroy the emerging tumor, leading to the destruction and elimination of the tumor from the body before it is clinically apparent. In IFNγ -/- mice there is an increased susceptibility to developing spontaneous and chemically induced tumors. This work established the central role that IFNγ plays in acting on the malignant cell itself and

IFNγ enhances recognition of these cells by the immune system[94]. Additionally, lymphocyte-deficient RAG-/- mice are highly susceptible to chemical carcinogen 3′-methylcholanthrene (MCA) induced tumors[95]. Tumors derived from RAG2-/- mice and implanted into immunocompetent WT hosts were rejected more frequently than tumors that were derived in immunocompetent mice and implanted into immunocompetent WT hosts[95]. These studies not only established the role that lymphocytes play in the elimination of cancer, but also revealed that in immunocompetent hosts tumors that develop are less immunogenic.

Tumor cell variants that survive the elimination phase by becoming less immunogenic will then enter the equilibrium phase. In equilibrium, CD8+ T cells prevent tumor outgrowth but also fail eliminate the tumor. This process is thought to be the longest phase and could possibly take place over years, extending throughout the lifetime of the host. These tumor cells can seed themselves into tissues and lay dormant showing up later in life[96]. Immunocompetent mice treated with low-dose MCA for an extended period of time failed to develop evident tumors[97]. When treated with monoclonal antibodies (mAbs) to deplete T cells and IFNγ, effectively ablating the adaptive immune response, tumors rapidly appeared at the original MCA injection site in half of the mice. Showing that the mice were harboring undetectable cancer cells[97]. It was further exposed in this study that it is the adaptive immune system, specifically IL-12, IFNγ, CD4+ T cells and CD8+ T cells, that is required to maintain equilibrium of the tumor cells.

Making it a distinct phase from elimination which requires synergizing of both the adaptive and innate immune response for clearance[97]. Further, these and other studies have highlighted the critical importance of CD8+ T cells for tumor cell recognition and killing.

CD8+ T cells require cross-presentation of antigens, tumor neoantigens or tumor associated antigens, within the draining lymph node to drive activation and trafficking into tissues. At this time it has been well established that cross-presenting XCR1+ conventional type I DC's (cDC1) are the critical APC that migrates into tumors driven chemotactic gradients such as CCL4/5 and its ligand CCR5 or XCR1/ XCL1, gets licensed by CD4+ T cells via CD40/CD40L interactions, and are a critical producer of IL-12 which drives anti-tumor CD8+ T cell differentiation.[44,98–102] . Subsequently, cDC1's produce CXCL9/10 which is the ligand for CXCR3 expressed on CD8+ T cells and has been shown to be a critical interaction for driving effector and stem-like memory cell fates that drive effective responses to PD-1 immune checkpoint blockade (ICB)[68,103–105]. It is possible that the selective pressure put on tumor cells during the equilibrium phase drives immunoevasive mutations, such as loss of MHC I, that reduces immunogenicity leading to escape[79].

The escape phase is defined by tumor cells that have acquired the ability to circumvent immune recognition, destruction, and/or drive immune dysfunction. Immune escape the phase at which tumor burden becomes so great can be clinically detected. Escape can occur due to a host of reasons including tumor cell population changes, the tumor microenvironment (TME) becomes overly suppressive towards immune cells, or immune system deterioration due to aging. Mechanisms of escape have been widely published including the loss of tumor antigen which can happen through 1. emergence and outgrowth of tumor cells that lack expression of immune targeted antigen 2. loss/downregulation of MHC I to present antigen 3. loss of antigen processing functions by tumor cell that is needed to process and load peptides onto MHC I[106]. This can be caused by selective

pressure by the immune system or by genomic instability which is central in malignant cancer cell formation and lifecycle[91,107,108].

Another mechanism of escape is driven by establishment of an immunosuppressive TME by the tumor cells producing immunosuppressive cytokines and recruiting immunosuppressive regulatory cells. Pancreatic ductal adenocarcinoma (PDA) is well known to established a highly immunosuppressive dense stromal fibroinflammatory TME that leads to immune cell exclusion[109–111]. Immunosuppressive cytokines such as vascular endothelial growth factor (VEGF), transforming growth factor-β (TGF-β), galectin, indoleamine 2,3-dioxygenase (IDO), IL-10, IL-6, IL-1β, CXCL12, produced by tumor cells are prevalent in PDA[109,112–114]. These cytokines lead to several mechanism of immune cell dysfunction including recruitment of other immunosuppressive immune cell recruitment such as regulatory CD4+ T cells (T_{reg}). T_{reg} cells in a normal pathogen immune response are important checkpoints to ensure CTLs do not end up activating and attacking self-causing autoimmunity[115–118]. CD4+ T_{reg} cells constitutively express the high affinity IL-2 receptor, CD25 allowing them to sequester IL-2 from the microenvironment to prevent CTL proliferation and survival[41,99,119]. Additionally, T_{regs} produce the inhibitory cytokines IL-10 and TGFβ, which work by downregulating CD80/CD86 and MHC II, and inhibit IL-2 and IFNγ production respectively[41,47,109]. This can lead to chronic TCR stimulation without costimulatory signals driving CD8+ T cell exhaustion[120–122]. T_{regs} can be recruited into the TME also by myeloid derived suppressor cells (MDSC). MDSCs are a heterogenous group of myeloid progenitor cells and immature myeloid cells that inhibit lymphocyte function. MDSCs are recruited into the TME by tumor cells secreting factors

such as prostaglandins, stem-cell factor (SCF), VEGF and IL-6[123]. MDSCs by producing and upregulating immunoinhibitory molecules, such as arginase 1 (Arg1), inducible nitric oxide synthase (iNOS), and reactive oxygen species (ROS), drive CD8+ T cell apoptosis[123]. Other cellular drivers of the immunosuppression in the PDA TME include tumor associated macrophages (TAM) and cancer associated fibroblasts (CAF), which can produce many of the same inhibitory factors talked about above such as TGFβ, IL-6, and IL-10[110,124,125].

While it may seem like a linear process there are no data that currently show that immunosurveillance and immunoediting happen in sequential and organized manner. It is entirely possible the immune response can out right eliminate malignant cells and never enter another stage, or equilibrium can occur first followed by escape of the malignancy, or worst of all the immune response fails to be mounted at all leading to immediate escape. External factors may influence the phase at which the flow directs, such as stress, age, diet, or medical interventions such as immunotherapies. Overall, the understanding of cancer immunosurveillance and immunoediting has driven the explosive discovery and use of cancer immunotherapies.

1.4.3 Cancer Immunotherapies

In 1891, William B. Coley injected a patient with inoperable Sarcoma, a type of bone cancer, with live streptococcal organisms to treat and shrink the cancer. His hypothesis was that the infection produced by the bacteria would have a side effect of shrinking the malignant tumor. He based this hypothesis from a patient record that had shown a patient with an inoperable neck tumor leave the hospital cancer free after developing erysipelas. Coley's hypothesis had worked and while the mechanism of "Coley's Toxin" at the time

was unknown it was used to treat more than a thousand patients. Despite the remarkable success seen, Coley's Toxin came under heavy criticism and skepticism from other doctors and scientists[126,127]. The cancer research field more willingly embraced the new radiation and chemotherapies and drove use of Coley's Toxin to fall out of use and by 1952 Coley's Toxin was no longer produced. Radiation, chemotherapy, and surgical resection became the standard therapy for treating cancer till the early 2000's when the foundational ideas from Ehrlich, Coley, Burnet, and Thomas resulted in the detailed enough fundamental and translational immunology research that led to the first clinical trials for cancer immunotherapies.

Cancer immunotherapies are defined as a therapy that uses the patient's own immune system therapeutically by boosting, stimulating, or altering immune components to all for the destruction of cancer. In the past decade, immune checkpoint blockades (ICB), which target negative regulators of T cell activation and their ligands via infusion of target specific antibodies (anti-PD-1, anti-PD-L1, anti-CTLA-4), have been shown to induce tumor regression in several types of advanced malignancies and have quickly become standard of care therapies[128–130] . ICB and other immunomodulatory therapies require, or at least appear to be most effective in patients, with pre-existing anti-tumor immunity and endogenous CD8+ T cell infiltration. Though sudden reactivation of these endogenous T cell responses can cause a wide spectrum of toxicities [131–133]. Toxicity in patients is likely associated with breaking immune tolerance to both the tumor but other tissues within the body as many of these same targeted checkpoints are critical in T cell tolerance and contraction of harmful immune responses[58,134]. ICB, while being one of the most hopeful and field-altering therapies to hit the clinic in decades is not universally effective for all

tumors. Many cancers, such as pancreatic ductal adenocarcinoma (PDA), are largely resistant to ICB therapies. Tumors with high mutational burden are thought to generate more neoantigens, generation from mutated proteins. Thus theses tumors produce more unique targets for endogenous T cell responses to target[132,135,136]. Even in the minor fraction of PDAs that have a high tumor mutational burden and thus probable numerous neoantigens, ICB is often insufficient for cure[104,129,137,138]. Thus, implementation of other immunotherapies, although maybe not as simple as or widely obtainable to treat all patients as an off the shelf therapy, must be considered.

Adoptive transfer of in vitro–expanded T cells that express a tumor-reactive TCR can eliminate solid tumors in advanced cancer patients[139–149]. Engineered TCR-based approaches have a significant advantage over chimeric antigen receptor (CAR) engineered approaches, as CAR T cell therapies cannot detect cross-presented antigen[45,90,94,150,151]. CARs are composed of an ectodomain variable region of an antibody, a transmembrane domain, and an intracellular CD3ζ^{+} co-stimulatory (CD28, 41BB) domain that leads to T cell activation and tumor cell killing in an HLA-independent manner. While CAR T cells are producing remarkable results in hematological malignancies[150–153], CAR T cell have not been effective thus far in solid tumors. In contrast to CARs, which contain CD3ζ and ITAM co-stimulatory signaling domains, engineered TCR therapies instead rely on host cell machinery for downstream signaling, allowing for more physiologic control of activation, contraction, and tolerance.

Clinical trials often transduce T cells with TCR-expressing γ-retroviral or lentiviral vectors because of their high transduction efficiency and stable integration into host DNA. However, the location of integration is unknown with this engineering strategy. In the

context of CAR-T cell therapy, unanticipated lentiviral vector integration in *TET2* and *CBL* caused enhanced clonal T cell expansion in two patients[154,155], proving the dangers of this non-specific approach. The lentiviral approach is highly efficient for screening and generating engineered TCR products, but as genome engineering strategies are advancing rapidly since the discovery of CRISPR, more targeted genomic approaches can be employed to reduce risk. Indubitably, targeting a CAR into the T cell receptor alpha constant (*TRAC)* locus by employing a recombinant adeno-associated virus to deliver the CAR construct in combination with by CRISPR/Cas9 *TRAC*-specific guide RNAs was shown to interfere with endogenous TCR chain expression and yield CAR T cells with enhanced functionality[156]. Until now, it remained to be determined whether a similar approach would be advantageous for engineered TCR T cells.

Significant technological advances in whole-genome sequencing have spurred the development of personalized neoantigen vaccines[147,148,157] and the transfer of personalized neoantigen-specific T cells. However, such a personalized approach is laborious and difficult to scale for numerous patients. Most TCR engineered T cell therapies in clinic are exploiting TCRs specific to commonly overexpressed self-/tumor epitopes such as Mesothelin, MART-1, WT-1. The hope that by picking these targets numerous patients could be treated with the same immunotherapy product but these are still limited because of TCR restriction to specific HLA molecules, a single cloned TCR is only fitting for only patients with the correct haplotype. There are also inherent risks when infusing large numbers of tumor-reactive T cells into patients. As tumor cells often have low antigen presentation, or can alter antigen presentation due to immunoediting, much focus has been

placed on obtaining high-affinity tumor-reactive TCRs[149] which come with a greater risk of off tumor toxicities and autoimmunity.

While the inherent risks exist for immunotherapies, such as TCR engineer cell therapies, these risks for those who are diagnosed with cancers without therapy options or genuinely poor outcomes seem worth it. The approval and integration of ICB, CAR T cell therapies, TCR T cell, cancer vaccine immunotherapies into the standard of care of patients has truly innovated not only the field of cancer biology but also that of immunology. Greater than that, cancer immunotherapies have changed hope and outcomes for millions of people who have or will be diagnosed with cancer and treated with these therapies. The focus of this dissertation is to better understand and innovate a promising Mesothelin-specific TCR T cell therapy in the context of pancreatic cancer.

1.5 Publications:
Chapter modified with permission from the following published article:

Rollins, M. R., Spartz, E. J., & Stromnes, I. M. (2020). T cell receptor engineered lymphocytes for cancer therapy. Current Protocols in Immunology, 129, e97. doi: 10.1002/cpim.97.

Chapter 2: Germline T cell receptor exchange results in physiological T cell development and function

2.1 Introduction

The understanding of antigen-specific T cell responses at steady state and in disease have benefited from the use of T cell receptor (TCR) transgenic mice. TCR transgenic mice have a monoclonal TCR randomly integrated into the mouse genome and TCR expression is driven by heterologous promoter fragments including MHC class I[158], CD2[159,160], or endogenous promoter and regulatory flanking regions[161,162]. Such models require substantial time to generate, have random TCR genomic integration, and the use of non-physiologic promoters may alter T cell functionality and hinder direct TCR comparisons.

Mesothelin (Msln) is a self-antigen overexpressed in many malignancies[163–169] and a promising target for cancer therapy[170]. Human MSLN-specific T cells are induced following vaccination demonstrating its immunogenicity[171]. Engineered T cells targeting MSLN are undergoing testing for the treatment of advanced malignancies[172–174]. Msln is also lowly expressed in the pleura, peritoneum and pericardium in mice and humans yet *Msln*$^{-/-}$ mice lack a discernible phenotype[175]. We previously characterized a panel of T cell receptors (TCRs) specific to Msln for pursuing a TCR engineered T cell therapy for cancer patient treatment[176]. We selected murine TCRs specific to Msln$_{406\text{-}414}$:H-2D^{b} because T cells reactive to this epitope were obtainable from both wild type (WT) and *Msln*$^{-/-}$ mice, thereby modeling TCR affinity enhancement[177]. The adoptive transfer of P14 TCR transgenic T cells[178] retrovirally transduced to express a high affinity murine Msln-specific TCR (clone 1045) accumulated in malignant sites, elicited objective responses and prolonged survival in an autochthonous pancreatic ductal adenocarcinoma (PDA) mouse

model[176]. The identical approach prolonged survival in the ID8 ovarian cancer model[179]. Finally, human CD8+ T cells transduced to express MSLN-specific TCRs kill pancreatic[176] and ovarian[179] cell lines *in vitro* supporting the translation of this approach (NCT04809766). However, using the above approach, TCR engineered T cells were ultimately rendered dysfunctional in the highly suppressive tumor microenvironment (TME)[176]. Concomitant blockade of multiple immune checkpoints[180] or macrophage depletion[181] failed to rescue intratumoral engineered T cell dysfunction. Thus, additional strategies are necessary to enhance TCR engineered T cell therapy of carcinomas.

Prior studies support that targeting chimeric antigen receptors (CAR)[182] or TCRs[183] into the physiological *TRAC* locus in primary human T cells confers potent antigen-specific T cell function. Previously, a CRISPR ribonucleoprotein (RNP) electroporation and adeno-associated viral (AAV) donor infection (CRISPR-READI) zygote engineering approach was shown to be a robust method for targeted gene engineering[184]. Thus, we sought to combine the above approaches to generate physiologically regulated and naïve tumor-reactive T cells as a robust tool to elucidate how to enhance T cell antitumor function.

Here, we identify a robust and efficient methodology for direct orthotopic TCR exchange into the endogenous *Trac* locus in murine zygotes, referred to as T cell receptor exchange (TRex). First, we target a high or low affinity Msln-specific TCR to the *Trac* locus while simultaneously disrupting the cognate self-antigen Msln and assess T cell development and function. Next, we rapidly generate P14 TRex mice and compare T cell development and function to historical P14 TCR transgenic mice. In sum, we identify a robust and highly efficient method to generate mice with more physiological expression of a desired antigen-specific TCR, allowing for a standardized source of antigen-specific T

cells. Further, our characterization of TRex mice reveals novel insights into T cell development and functionality.

2.2 Results

2.2.1 Targeting Msln-specific TCRs to Trac in primary murine T cells.

We previously cloned and validated two murine $Msln_{406-414}$:H-$2D^b$-specific TCRs[176]. The 1045 TCR was the highest affinity obtained from *Msln*$^{-/-}$ mice and the 7431 TCR was the highest affinity TCR obtained from wild type mice[176]. Both TCRs utilized Vα4 and Vβ9 and differed only in CDR3[176], which largely contributes to TCR specificity[185]. To develop an approach to target these TCRs to *Trac*, we first screened rAAV-GFP serotypes and identified rAAV6 to be superior at infecting activated primary mouse T cells without impacting viability (**Supplementary Fig. 2.1a-b**), similar to human T cells[186]. We cloned 1045 or 7431 TCRβ variable (V), TCRβ constant (C) and TCRα V, linked by a self-cleaving P2A element[187] and flanked by homology arms (HA) encoding endogenous *Trac* genomic sequences into rAAV6 (**Fig. 2.1a**). Two single guide RNAs (sgRNAs) specific to the beginning of *Trac* exon 1 complexed to Cas9 ribonucleoprotein (RNP) were tested independently in activated polyclonal T cells (**Fig. 2.1b)**, using a prior CRISPR protocol[188]. Both *Trac* sgRNAs caused TCR and CD3 loss in > 90% of T cells (**Fig. 2.1c**). While both sgRNAs reduced endogenous Vβ9, 1045 or 7431 TCR integrated only following *Trac* sgRNA 2 but not *Trac* 1 sgRNA (**Fig. 2.1d-e**). This is likely due to sgRNA 1 cutting within *Trac* exon 1 (**Supplementary Fig. 2.1c-d**). To assess TCR functionality, we restimulated the T cells with peptide-pulsed irradiated syngeneic splenocytes and quantified the frequency of Vβ9+ T cells 5 days later. Vβ9+ T cell

frequency ranged from 5-10% prior to restimulation (**Fig. 2.1g**) and increased to 38-70% following cognate antigen stimulation (**Fig. 2.1f**), corresponding to a 5-fold increase in T cell number. Thus, the targeted approach resulted in functional exogenous TCRs in primary T cells.

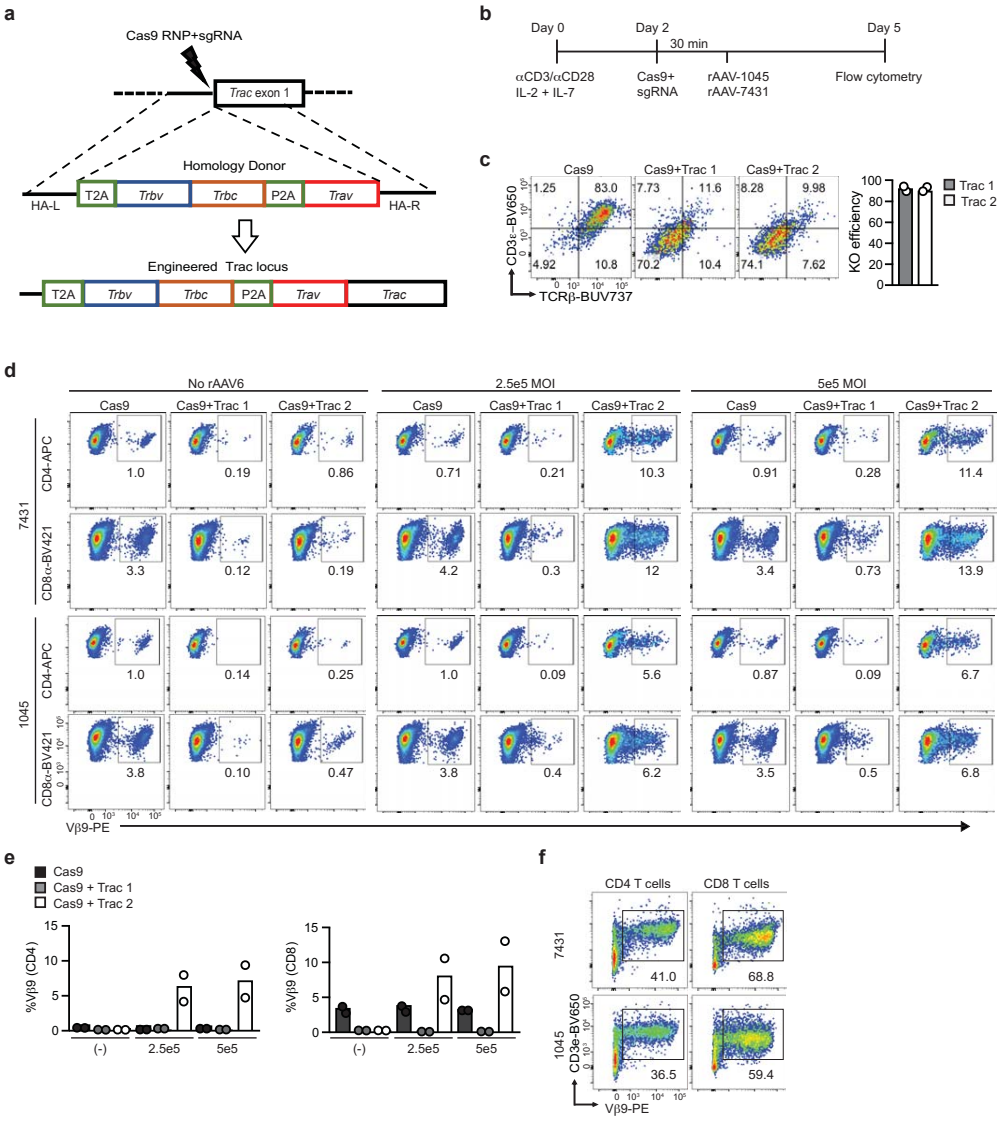

Fig. 2.1 Targeting Msln-specific TCRs to Trac in primary murine T cells.
a Schematic of TCR targeting to murine Trac. sgRNAs targeting the region upstream of *Trac* exon 1 were designed. Codon optimized 1045 or 7431 TCRβ variable (V), TCRβ Constant (C) and TCRα V, linked by a self-cleaving P2A is flanked by a left and right homology arm (HA-L, HA-R) and encoded by recombinant adeno-associated virus (rAAV) serotype 6. **b** Protocol for testing TCR targeting using CRISPR/Cas9 and rAAV. Polyclonal B6 splenocytes were activated with anti-CD3+anti-CD28, IL-2 and IL-7. Two days after T cell activation, splenocytes were electroporated with Cas9 RNP complexed to *Trac*-specific gRNAs, followed by addition of rAAV encoding TCRs. **c**. Knockout efficiency (KO) of *Trac* sgRNA 1 or 2 was measured by loss of TCRβ and CD3ε by flow cytometry on day 5 post activation. n=2 biologically independent experiments. **d** Representative flow cytometry plots of 1045 or 7431 TCR expression in murine T cells was determined by Vβ9 staining on day 5 after varying the multiplicity of infection (MOI). **e** Proportion of CD4+ or CD8+ T cells that express Vβ9 at the indicated MOIs on day 5. Data are mean ± S.E.M. and pooled from 3 independent experiments. **f** Frequency of donor TCR+ *Trac*-edited T cells 5 days post the second *in vitro* stimulation with $Msln_{406-414}$-pulsed irradiated splenocytes, IL-2 and IL-7.

2.2.2 Targeting TCRs into Trac sustains engineered T cell function and obviates Treg expansion.

We next compared the efficiency of retroviral transduction (RV) of P14 T cells (**Fig. 2.2a**) using our prior protocol[176] to CRISPR/Cas9 + rAAV-mediated TCR *Trac* knock-in (KI) of polyclonal T cells (**Fig. 2.2b**) using the gating strategy in **Supplementary Fig. 2.2a**. Vβ9+ CD4+ T cell frequency was comparable among RV and KI strategies whereas RV increased Vβ9+ CD8+ T cell frequency (**Fig. 2.2c-e**). While proliferation was similar among the two approaches (**Fig. 2.2f**), RV increased Vβ9+CD4+Foxp3+ Treg frequency (**Fig. 2.2g-h**). Foxp3 was not detected in CD8+ T cells as expected (**Fig. 2.2g, 2.2i**). We next measured cytokine production by RV and KI T cells following repetitive antigen stimulations. We found that Vβ9+ CD4+ T cells rarely produced cytokines (**Fig. 2.2j**). In contrast, a higher frequency of RV Vβ9+ CD8+ T cells produced cytokines following the 2nd *in vitro* stimulation compared to KI Vβ9+ CD8+ T cells (**Fig. 2.2k**). By the 3rd stimulation, a greater frequency of KI Vβ9+ CD8+ T cells produced cytokines compared to RV Vβ9+ CD8+ T cells (**Fig. 2.2k**). Despite distinct cytokine production profiles, Vβ9 mean fluorescence intensity (MFI) was similar in KI vs. RV T cells (**Supplementary Fig. 2.2b**). Thus, the KI approach permitted TCR engineering of polyclonal T cells, obviated Treg expansion, and maintained cytokine production after recurrent antigenic exposure. Both approaches appeared to require the *in vitro* expansion of effector T cells for TCR integration thereby prohibiting studies of naïve Msln-specific T cells and a limitation of the KI approach was the low KI efficiency.

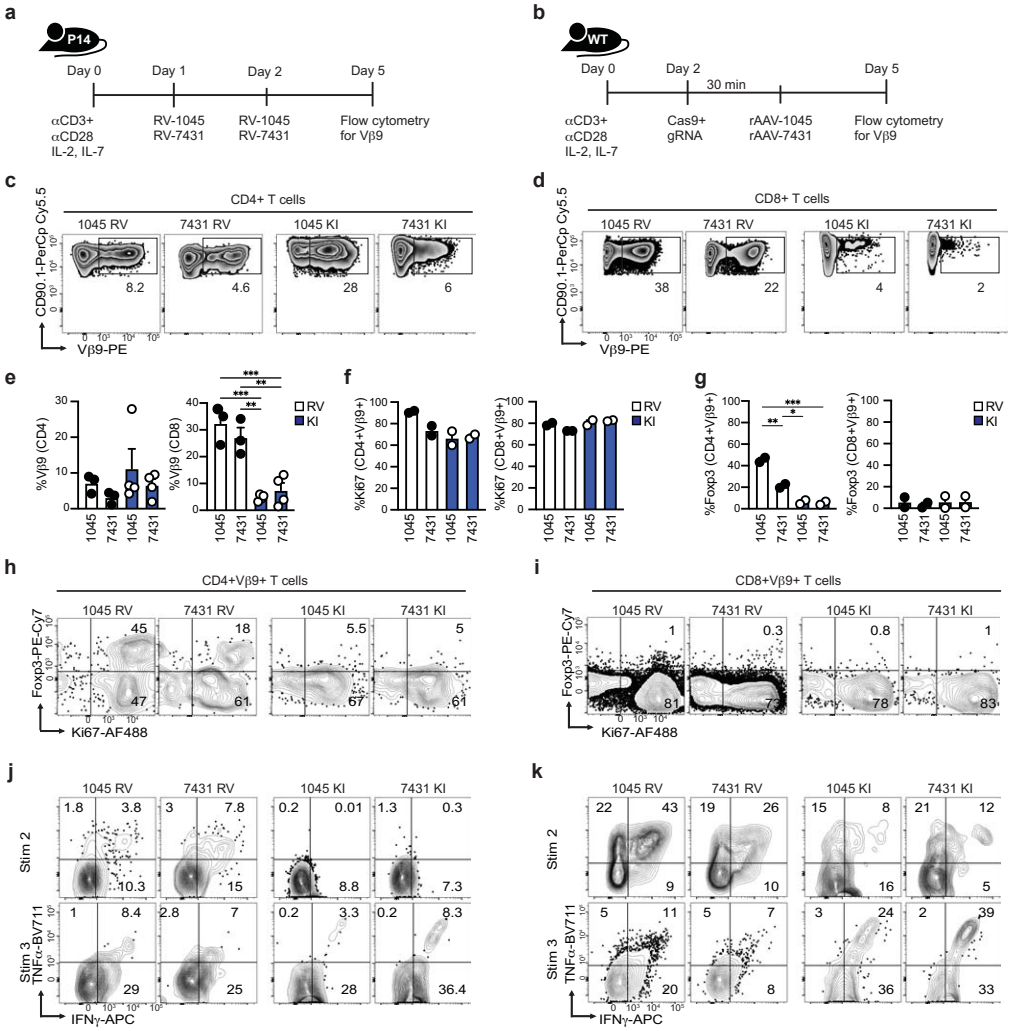

Fig. 2.2 Targeting TCRs to *Trac* sustains engineered T cell function and obviates Treg expansion.
a Schematic of retroviral transduction (RV) of P14 T cells with Msln-specific TCRs. **b** Schematic of CRISPR/Cas9 + rAAV TCR knock-in (KI) of polyclonal T cells with Msln-specific TCRs. **c** Donor TCR expression by CD4+ T cells 5 days post activation. **d** Donor TCR expression by CD8+ T cells 5 days post activation. **e** Quantification of **c** and **d**. n=2 biologically independent experiments. **f** Frequency of Ki67+Vβ9+ CD4+ or CD8+ T cells 5 days post activation. n=2 biologically independent experiments. **g** Frequency of Foxp3+Vβ9+ CD4+ or CD8+ T cells 5 days post activation. n=2 biologically independent experiments. **h** Representative plots gated on live CD4+Vβ9+ T cells. **i** Representative plots gated on live CD8+ Vβ9+ T cells. **j** Representative plots gated on CD4+Vβ9+ T cells. Intracellular cytokine staining was assessed after the second (Stim 2) or third (Stim 3) restimulation *in vitro* with Msln peptide-pulsed irradiated syngeneic splenocytes and IL-2 + IL-7. **k** Representative plots gated on CD8+ Vβ9+ T cells. Intracellular cytokine staining was assessed as in **j**. Data are mean ± S.E.M in e-g. n=3-6 mice per group. *p<0.05, **p<0.005, and ***p<0.0005. One-way ANOVA with a Tukey's posttest.

2.2.3 Rapid generation of Msln-specific TRex mice that lack Msln.

To create a standardized and reproducible source of naïve murine Msln-specific T cells, we sought to create Msln-specific TRex mice. To circumvent potential T cell tolerance to Msln, we tested 2 *Msln* exon 4-specific sgRNAs to concurrently knockout Msln. Both sgRNAs efficiently induced insertion-deletion mutations (indels) in 3T3 fibroblasts (**Supplementary Fig. 2.3a-e**). Both TCRs integrated in 40% of EL4 cells regardless of simultaneous *Msln* targeting (**Fig. 2.3a-b**). Thus, we next adapted the CRISPR-READI approach[184] to integrate the 1045 or 7431 TCRs (**Supplementary Fig. 2.3f-g**) in-frame with *Trac* while simultaneously disrupting *Msln* in murine zygotes (**Fig. 2.3c**). Using a junction PCR to detect exogenous TCR integration in one or both *Trac* alleles (**Fig. 2.3d**), 5/15 (33%) pups born were 1045 TCR heterozygous ($1045^{+/-}$, **Fig. 2.3e**). $1045^{+/-}$ pups exhibited increased CD8+ and decreased CD4+ circulating T cells compared to wild type (WT) mice (**Fig. 2.3f-g**, **Supplementary Fig. 2.3h**), consistent with forced expression of an MHC I-restricted TCR. In $1045^{+/-}$ pups, most CD8+ T cells expressed Vβ9 and Vβ9 was also enriched in CD4+ T cells (**Fig**. **2.3f-g** and **Table 2.1**). Indels in *Msln* were detected in 9/15 animals, including all $1045^{+/-}$ pups (**Table 2.1**).

We repeated this process with the lower affinity Msln-specific 7431 TCR and found 12/13 (92%) of the pups were 7431^{+} with 6/13 (46%) homozygous and 6/13 (46%) heterozygous for 7431 (**Fig. 2.3h**). Circulating T cells were significantly biased toward CD8+ T cells at the expense of CD4+ T cells in 7431^{+} pups (**Fig. 2.3i-j**, **Supplementary Fig**. **2.3h**). In $7431^{+/-}$ mouse #9, circulating T cells were markedly reduced, lacked Vβ9 (**Fig**. **2.3i**), and contained an additional PCR band (**Fig. 2.3h, Supplementary Fig. 2.3i**) suggesting *Trac* was cut yet the TCR failed to integrate correctly. In the remaining 7431^{+}

pups, most T cells co-expressed CD3 and Vβ9 (**Fig. 2.3i-j, Table 2.2**) and exhibited *Msln* indels rates consistent with bi-allelic disruption (**Table 2.2**). Representative *Msln* sequence analysis is shown in **Supplementary Fig. 2.3j-k**. We detected Msln in WT lung but not in lungs from 7431 or 1045 TRex mice homozygous for *Msln* indels (*e.g.*, *Msln*$^{-/-}$, **Fig. 2.3k**). Thus, we established an efficient method to target an exogenous TCR to *Trac* while disrupting a self/tumor-antigen in parallel.

#	ID	Sex	1045[&]	%CD8[Φ]	%Vβ9 (CD8)	%CD4	%Vβ9 (CD4)	%*Msln* KO[#Φ]	*Msln* In/Dels
1	3290	M	+/-	13	73.3	10.7	6.22	84%	+1/-7
2	3291	M	-/-	n.d.	n.d.	n.d.	n.d.	50%	-3/-8
3	3292	M	-/-	n.d.	n.d.	n.d.	n.d.	0%	none
4	3293	M	-/-	n.d.	n.d.	n.d.	n.d.	11%	+1
5	3294	M	+/-	13.7	52.4	6.09	4.19	93%	+4/+1/-1/-7
6	3295	M	+/-	11.3	26.7	5.23	2.75	10-50%	n.r.
7	3296	F	-/-	n.d.	n.d.	n.d.	n.d.	0%	none
8	3297	F	-/-	n.d.	n.d.	n.d.	n.d.	90%	+13/+1
9	3298	F	-/-	n.d.	n.d.	n.d.	n.d.	0%	none
10	3299	F	-/-	n.d.	n.d.	n.d.	n.d.	0%	none
11	3300	F	+/-	15.5	20.5	9.04	4.29	93%	-23
12	3301	M	+/-	8.91	42.3	6.29	2.39	40-50%	+1/-1/-2
13	3302	M	-/-	n.d.	n.d.	n.d.	n.d.	n.r.	n.r.
14	3303	M	-/-	n.d.	n.d.	n.d.	n.d.	45%	-1/-2
15	3304	M	-/-	n.d.	n.d.	n.d.	n.d.	47%	+1

Table 2.1. Analysis of T cells and Msln locus from 1045 TRex pups
[&]1045 knock-in was determined by junction PCR of tail DNA.
[Φ]n.d., not determined; n.r., no results indicating sequence analysis was attempted but data were inconclusive.
[#]Msln knockout was determined PCR amplification of *Msln* exon 1 followed by Sanger sequencing and Inference of Crispr Edits (ICE) analysis software (https://www.synthego.com/products/bioinformatics/crispr-analysis).

#	ID	Sex	7431[&]	%CD8[Φ]	%Vβ9 (CD8)	%CD4	%Vβ9 (CD4)	%Msln *Indel*[#Φ]	*Msln* Indel
1	3291	F	+/-	27.7	92.3	0.87	55.3	86*	-2, +4, -19
2	3292	F	-/-	9.98	2.31	12.5	1.24	0	none
3	3293	F	+/+	26.1	94.9	1.11	70.1	97*	-7
4	3294	F	+/-	31.3	92.6	1.0	59.8	97*	-4
5	3295	F	+/-	23.9	91.7	1.4	67	84*	-8
6	3296	M	+/+	25.7	74.4	1.1	95.5	91*	-5, +1
7	3297	M	+/-	27.9	91.6	1.9	57.9	95 (KO 47)	-7, -9
8	3298	M	+/+	24.1	91	1.0	64.2	95*	-1, -8
9	3300	M	+/-[Ψ]	5.25	0.98	3.67	0.68	86*	+1, -8
10	3301	M	+/+	25.4	93.7	0.97	69	97*	-8
11	3302	M	+/+	25.7	96.2	1.0	73	92 (KO 45)	-1, -6
12	3303	M	+/+	22.0	92.8	0.96	73.5	96*	+1
13	3304	M	+/-	26.4	88.8	0.89	50	97*	-4

Table 2.2. Analysis of T cells and Msln locus from 7431 TRex pups

[&]7431 knock-in was determined by junction PCR of tail DNA from pups

[Φ]n.d., not determined; n.r., no results indicating sequence analysis was attempted but data were inconclusive.

[#]Msln knockout was determined PCR amplification of *Msln* exon 1 followed by Sanger sequencing and Inference of Crispr Edits (ICE) analysis software (https://www.synthego.com/products/bioinformatics/crispr-analysis).

*Knockout score was identical to %Indel [Ψ]An additional band was detected between the WT and KI

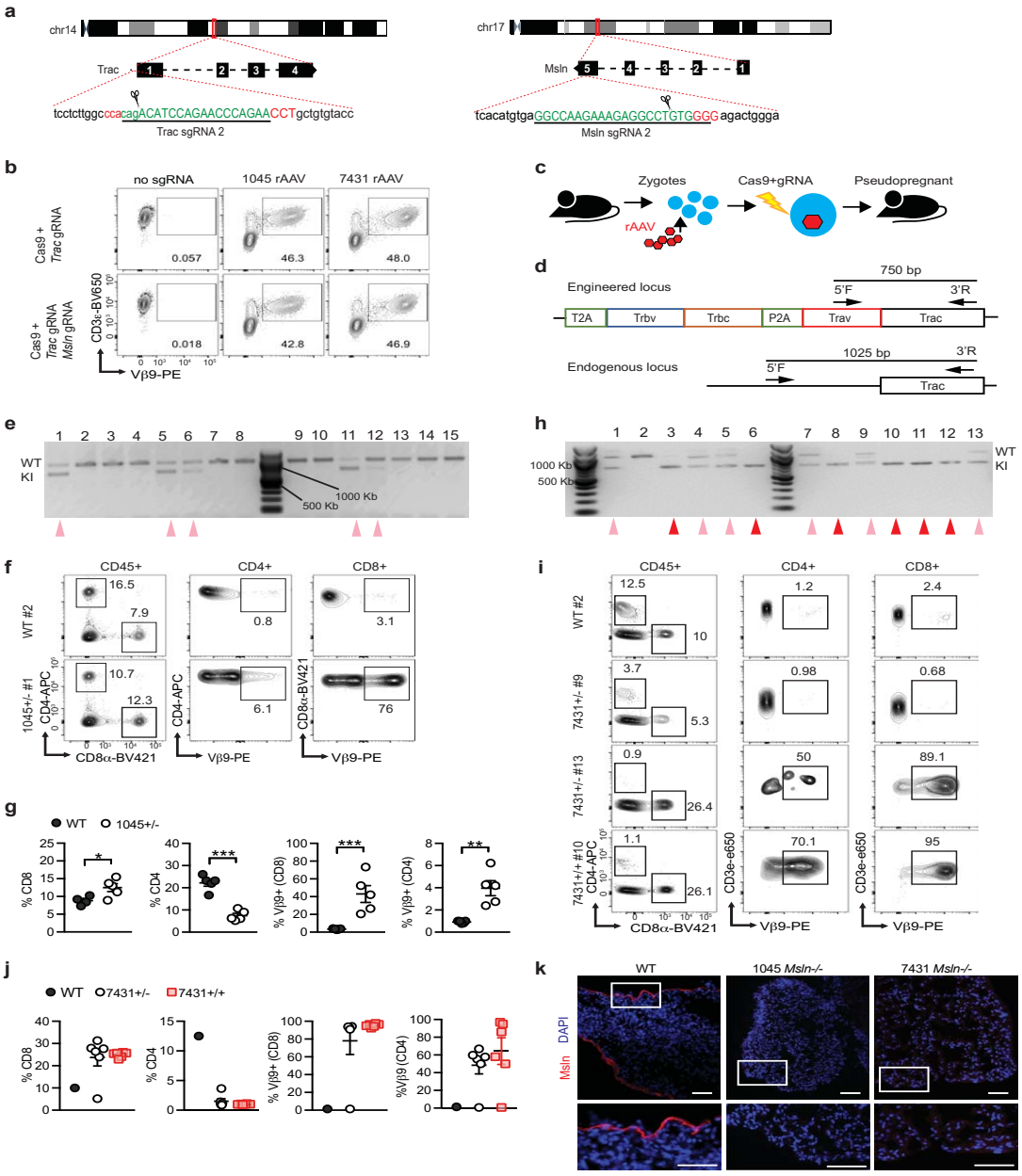

Fig. 2.3 Rapid generation of Msln-specific TRex mice that lack Msln.
a Sequence and target sites of sgRNAs targeting *Trac* exon 1 or *Msln* exon 4. **b** CD3+ EL4 cells were electroporated with *Trac* sgRNA or *Trac* and Msln sgRNAs complexed with Cas9 RNP, followed by rAAV-1045 or rAAV-7431. Msln TCR expression was determined by Vβ9. **c** Schematic for murine zygote engineering. **d** Junction PCR design to detect TCR integration. 5' Forward primers are located within the engineered locus to detect the exogenous TCR and in an intron region upstream of the endogenous *Trac* locus to detect the WT allele. A 3'Reverse primer was located in *Trac*. **e** PCR gel of junction PCR performed with DNA collected from the 15 pups born from 1045 engineered pseudo pregnant B6 females. 100 Kb ladder is located in the middle lane and 500 and 1000 Kb demarcated. Wild type (WT) indicates amplification of the endogenous locus while knock-in (KI) indicates amplification of the exogenous TCR upstream of the *Trac*. Pink arrows, $1045^{+/-}$ heterozygous pups. n=1 experiment. **f** T cell frequency in circulation (left, gated on live CD45+ cells) and frequency of Vβ9+ CD4+ (middle) or CD8+ (right) T cells in representative pups from e.

g Quantification of f. Each dot is an independent mouse. n=5 mice per group. Data are mean ± S.E.M. **h** Junction PCR from DNA isolated from the 13 pups born from the 7431-zygote engineered mice. 100 Kb ladder is located on left and middle lanes with 500 and 1000 Kb demarcated. Pink arrows indicate $7431^{+/-}$ pups and red arrows indicate $7431^{+/+}$ pups. n=1 experiment. **i** T cell frequency in circulation (left, gated on live CD45+ cells) and frequency of CD4+ (middle) and CD8+ (right) T cells expressing Vβ9 in representative pups from h. **j** Quantification of i. Each dot is an independent mouse and include n=13 animals from h. Data are mean ± S.E.M. **k** Representative immunofluorescent (IF) tissue staining of Msln (red) and DAPI (blue) in lungs from WT, 1045 *Msln* $^{-/-}$, and 7431 *Msln* $^{-/-}$ mice. Scale bar, 25 μM. Representative of 6 biologically independent animals.

2.2.4 High affinity Msln-specific T cells undergo central tolerance in a Msln dose dependent manner.

To investigate T cell development in TRex mice, we backcrossed 1045 TRex #11 (**Fig. 2.3e**) onto *Msln*$^{WT/WT}$, *Msln* $^{WT/-23}$ and *Msln*$^{-23/-23}$ background (referred to as *Msln*$^{+/+}$, *Msln*$^{+/-}$, and *Msln*$^{-/-}$, respectively, **Table 2.1**) and analyzed thymocytes in $1045^{+/+}$ offspring. Thymus weight (**Fig. 2.4a**) and CD45+ cell number (**Supplementary Fig. 2.4a**) were similar regardless of *Msln* status. Thymocyte maturation occurs through sequential differentiation program that is distinguished by CD4+ and/or CD8+ coreceptor expression[189]. The earliest thymocyte progenitors lack CD4+ and CD8+ (double negative, DN) and differentiate into CD4+CD8+ double positive (DP) followed by maturation into CD4+ or CD8+ single positive (SP) cells. The frequency and number of DNs and DPs were similar among the strains (**Fig. 2.4b-d**). In $1045^{+/+}$ *Msln*$^{+/-}$ and *Msln*$^{-/-}$ TRex mice, thymocytes were biased toward CD8+ SP (**Fig. 2.4b-d**). In contrast, CD8+ SP frequency and number were significantly reduced in *Msln*$^{+/+}$ as compared to *Msln*$^{+/-}$ and *Msln*$^{-/-}$ 1045 TRex mice (**Fig. 2.4c-d**, **Supplementary Fig. 2.4b**). These data suggest negative selection to *Msln* is gene dose dependent. Vβ9 was increased in most thymocyte stages in TRex vs. WT mice as expected (**Fig. 2.4e-f**) and Vβ9+ thymocytes downregulated CD24, consistent with maturation (**Fig. 2.4e**). Vβ9+ DP and Vβ9+ CD8+ SP numbers trended to be reduced

in *Msln*$^{+/+}$ as compared to *Msln*$^{+/-}$ and *Msln*$^{-/-}$ 1045$^{+/+}$ TRex mice (**Fig. 2.4g**), further supporting a gene dosage dependent induction of central tolerance.

The DN stage is further subdivided into DN1- DN4 based on CD25 and CD44 (**Supplementary Fig. 2.4c**)[190]. TCRβ is rearranged first at DN3[189]. Rapid cell proliferation and TCRα upregulation occurs in the transition from DN4 to DP stage and selection ensues for functional αβ TCR heterodimers on DP cells[191]. Since the 1045 TCR is integrated in *Trac*, it is expected that the donor TCR would be detectable at the DN4 stage. As such, Vβ9 was first detected at the DN4 stage cells in 1045 TRex mice (**Fig. 2.4h**), supporting more physiological TCR regulation and thymocyte maturation in TRex mice.

To assess if MHC I is required for T cell development, we backcrossed 1045$^{+/+}$ TRex mice to the *B2m*$^{-/-}$ mice, which lack functional MHC I[192]. Thymus weight trended to be smaller in 1045$^{+/+}$ *B2m*$^{-/-}$ vs. *B2m*$^{+/+}$ mice (**Fig. 2.4i**). CD8+ SP frequency was dramatically reduced in 1045$^{+/+}$ *B2m*$^{-/-}$ vs. *B2m*$^{+/+}$ TRex mice and a compensatory increase in DP frequency in 1045$^{+/+}$ *B2m*$^{-/-}$ mice was detected (**Fig. 2.4j-k**). CD8+ Vβ9+ and CD4+Vβ9+ T cell frequencies were reduced in 1045$^{+/+}$ *B2m*$^{-/-}$ TRex mice (**Fig. 2.4l**). Thus, MHC I is required for positive selection of TRex T cells.

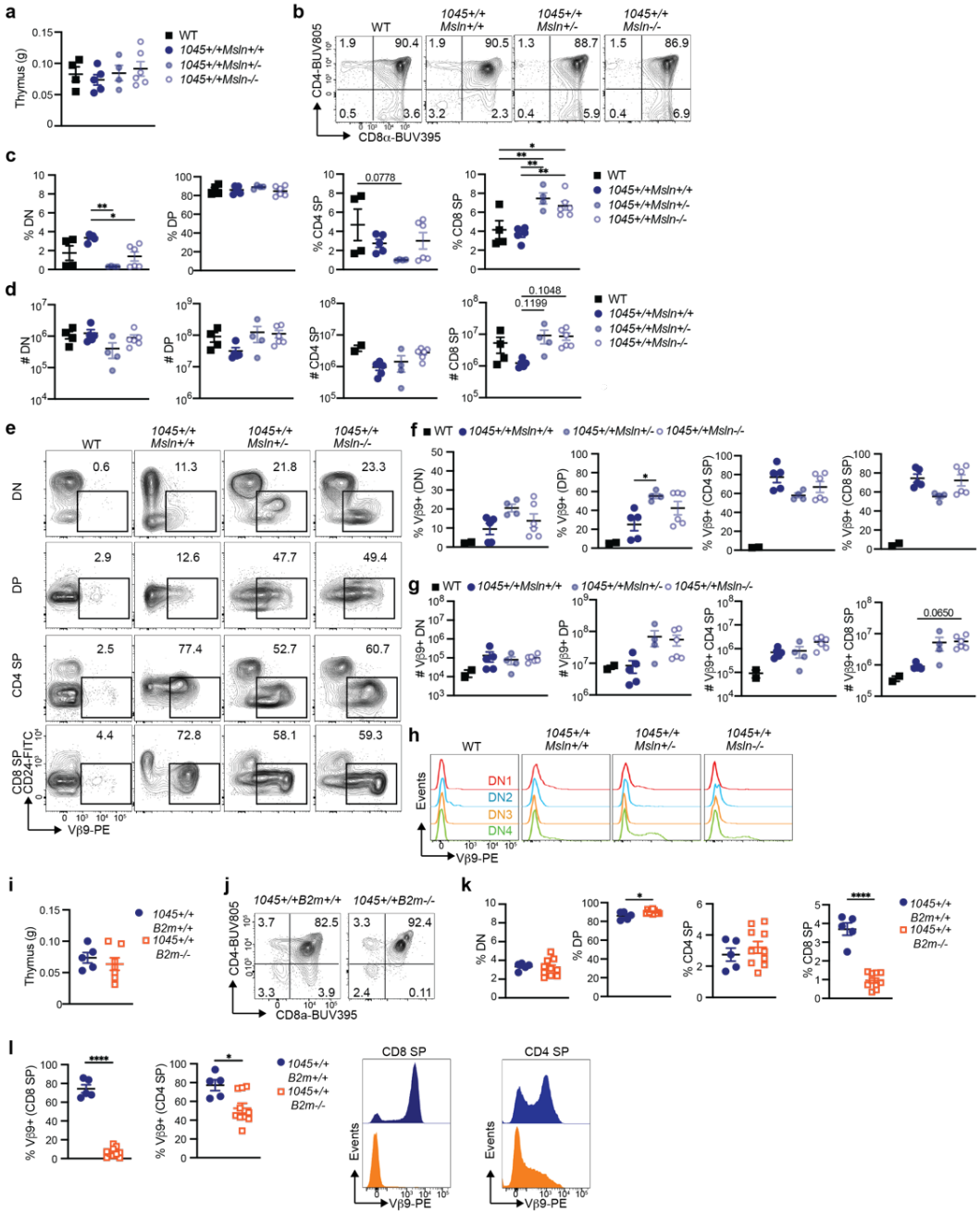

Fig. 2.4 High affinity Msln-specific T cells undergo central tolerance in a Msln dose dependent manner.

a Thymus weight in grams (g). n=4-6 biologically independent animals. Data are mean ± S.E.M. **b** Representative plots gated on live CD45+B220- thymocytes. **c** Frequency double negative (DN), double positive (DP), CD4+ single positive (CD4+ SP) and CD8+ single positive (CD8+ SP) among CD45+B220- thymocytes. n=4-6 biologically independent animals. Data are mean ± S.E.M. *p<0.05, **p<0.005. One-way ANOVA with a Tukey's posttest. **d** Mononuclear CD45+ cell number per thymus. Each dot is an independent mouse. Data are mean ± S.E.M. n=4-6 mice per group. *p<0.05, **p<0.005. Anova with a Tukey's posttest. **e** Representative plots of Vβ9 and CD24 of thymocytes in the indicated development stage. Numbers in plots indicate the frequency of Vβ9+ cells. **f** Vβ9+ cell frequency in each thymocyte developmental stage. n=4-6 biologically independent animals in 1045 cohorts and n=2 biologically independent animals in the WT group.

Data are mean ± S.E.M. *p<0.05, **p<0.005, ***p<0.0005, ****p<0.0001. One-way ANOVA with a Tukey's posttest. **g** Number of Vβ9+ cells each developmental stage per thymus. Each dot is an independent mouse. n=4-6 biologically independent animals in 1045 groups and n=2 biologically independent animals in the WT group. Data are mean ± S.E.M. *p<0.05. One-way ANOVA with a Tukey's posttest. **h** Representative Vβ9 staining of thymocytes in DN1-DN4. **i** Thymus weight. Data are mean ± S.E.M. n=5-10 biologically independent animals. **j** Representative plots gated on live CD45+B220- thymocytes. **k** Frequency of cells in each thymocyte stage. Data are mean ± S.E.M. n=5-10 biologically independent animals. *p<0.05, ****p<0.0001. Two-tailed unpaired Student's T test. **l** Vβ9 frequency among CD8+ SP and CD4+ SP thymocytes (Left) and representative histograms (right). Quantified data are mean ± S.E.M. n=5-10 biologically independent animals. *p<0.05, ****p <0.0001. Two-tailed unpaired Student's T test.

2.2.5 Peripheral 1045 T cells from Msln-/- or Msln+/- mice respond to specific antigen.

We next tested the functionality of peripheral T cells isolated from 1045 *Msln*$^{+/-}$ and *Msln*$^{-/-}$ mice. Most splenic T cells expressed Vβ9 in 1045$^{+/-}$ or 1045$^{+/+}$ mice (**Fig. 2.5a-d**). A higher frequency of CD8+ (**Fig. 2.5c**) and CD4+ (**Fig. 2.5d**) T cells expressed Vβ9 in 1045$^{+/+}$ vs. 1045$^{+/-}$ mice. Most splenic CD8+ Vβ9+ T cells exhibited a CD44^{low}CD62L^{+} naïve phenotype in *Msln*$^{-/-}$ and *Msln*$^{+/-}$ 1045 TRex mice (**Fig. 2.5c**) consistent with lack of self-antigen recognition when one *Msln* allele is absent. In contrast, a higher frequency of CD4+Vβ9+ T cells upregulated CD44 and downregulated CD62L in 1045$^{+/+}$ vs.1045$^{+/-}$ *Msln*$^{-/-}$ mice (**Fig. 2.5d**), a phenotype that was independent of self-antigen recognition.

To determine if 1045 T cells responded to specific antigen, we labeled splenocytes with a proliferation dye, incubated with Msln$_{406-414}$ and quantified T cell proliferation and activation after 3 days. We found that splenic CD8+ Vβ9+ T cells proliferated and upregulated CD25, CD69 and CD44 in response to Msln$_{406-414}$-pulsed APCs (**Fig. 2.5e-f**). In contrast, rare CD8+ Vβ9- T cells from the same TRex mice failed to respond to antigen (**Fig. 2.5e**). Presence of a single Msln allele did not impact 1045 T cell functionality *in vitro* (**Fig. 2.5e-f**). CD4+Vβ9+ T cells from 1045 TRex mice upregulated CD69 and CD25

following antigen recognition, yet proliferation was modest and CD44 was not further increased consistent with suboptimal CD4+ T cell activation (**Fig. 2.5g-h**).

As Tregs accumulated following P14 transgenic (Tg) T cell *in vitro* expansion (**Fig. 2.2g-h**), we compared Tregs from P14 Tg mice to 1045 and 7431 *Msln*$^{-/-}$ TRex strains. Tregs were disproportionately enriched among CD4+ T cells from P14 Tg compared to WT or TRex mice (**Supplementary Fig. 2.5a-b**). Tregs were biased toward a CD25-Foxp3+ subset in P14 mice (**Supplementary Fig. 2.5a-b**), potentially precursors to CD25+Foxp3+ Treg[118,193], and were more proliferative (**Supplementary Fig. 2.5c-d**). In contrast to T cells from WT mice, T cells from P14 transgenic mice activated with αCD3+αCD28 and IL-2 exhibited increased frequency of Foxp3+CD25+ Tregs (**Supplementary Fig. 2.5e-f**), and many did not express Vα2, the P14 TCRα chain (**Supplementary Fig. 2.5g**). Thus, endogenous TCR expression may be a prerequisite, but not the only factor contributing to disproportionate Treg expansion in P14 transgenic mice. Additionally, a higher proportion of CD4+ T cells were Treg in OT1 TCR transgenic[194] compared to WT mice (**Supplementary Fig. 2.5h**). Thus, the TRex approach may overcome Treg abnormalities in traditional TCR transgenics.

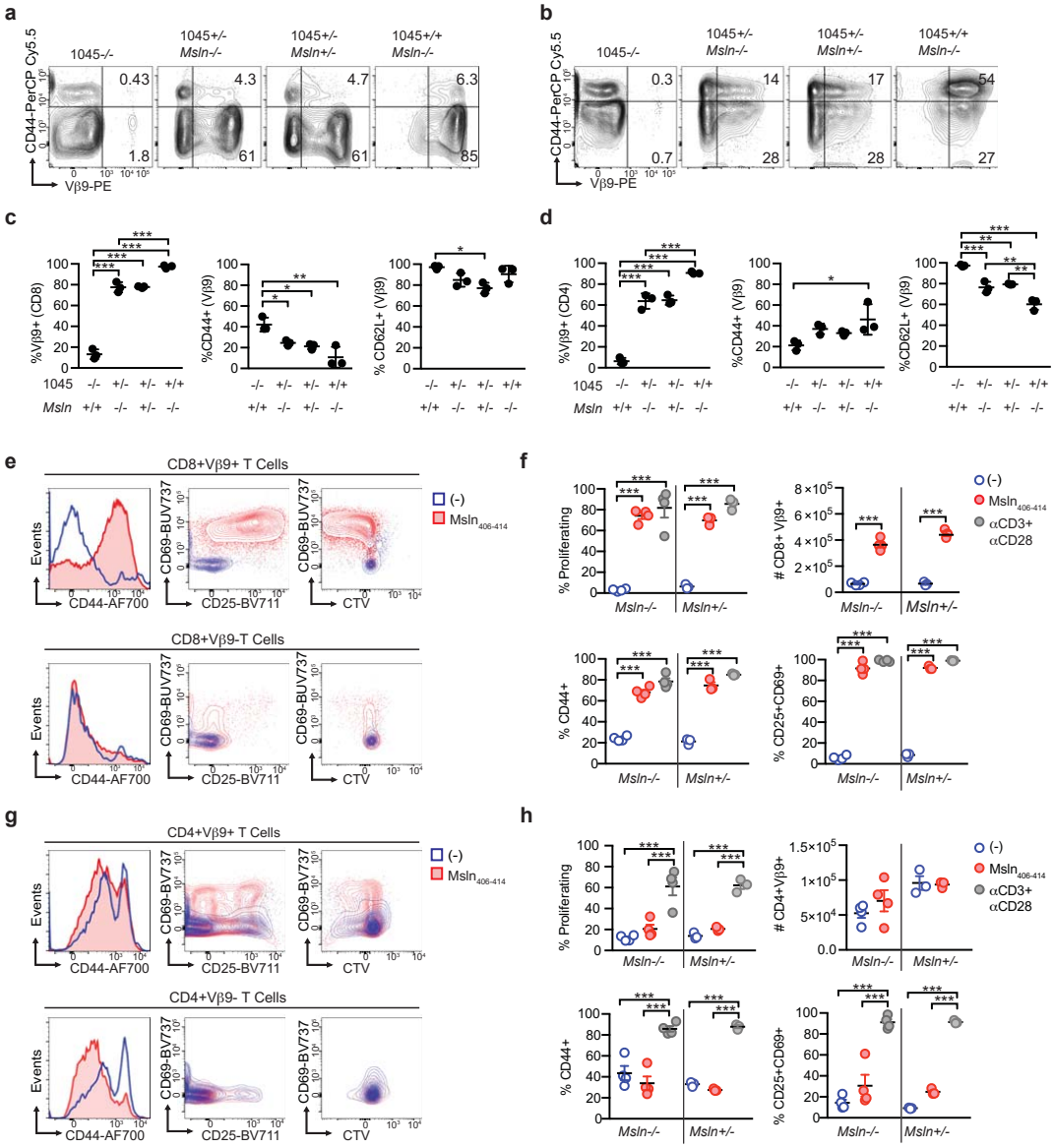

Fig. 2.5 Peripheral 1045 T cells from *Msln*$^{-/-}$ or *Msln*$^{+/-}$ mice respond to specific antigen.
a Representative plots gated on splenic CD8+ T cells. **b** Representative plots gated on splenic CD4+ T cells isolated from the indicated mouse strains. **c** Frequency of splenic CD8+ T cells that express Vβ9 (left) and frequency of CD8+ Vβ9+ T cells that express CD44 (middle) or CD62L (right). Data are mean ± S.E.M. n=3 biologically independent animals. *p<0.05, **p<0.005, ***p<0.0005. One-way ANOVA with a Tukey's posttest. **d** Frequency of splenic CD4+ T cells that express Vβ9 (left) and frequency of CD4+Vβ9+ T cells that express CD44 (middle) or CD62L (right). Data are mean ± S.E.M. n=3 biologically independent animals. ***p<0.0005. One-way ANOVA with a Tukey's posttest. **e** Representative plots gated on CD8+ Vβ9+ (top row) or CD8+ Vβ9- (bottom row) T cells on day 3 post ± Msln$_{406-414}$ peptide. **f** Quantification of e and results post αCD3+αCD28 on day 3. Data are mean ± S.E.M. Each dot is an independent mouse. *p<0.05, **p<0.005, ***p<0.0005. One-way ANOVA with a Tukey's posttest. **g** Representative plots of CD4+Vβ9+ (top row) or CD4+Vβ9- T cells (bottom row) on day 3 post ± Msln$_{406-414}$ peptide. n=4 biologically independent experiments. **h** Quantification of g and results from post αCD3+αCD28 on day 3. Data are mean ± S.E.M. n=4 biologically independent experiments. ***p<0.0005. One-way ANOVA with a Tukey's posttest.

2.2.6 TCR Trac targeting improves the functional avidity of a low affinity TCR.

We next compared the functionality of $7431^{+/+}$ and $1045^{+/+}$ T cells from *Msln*$^{-/-}$ TRex animals. Spleen weight (**Supplementary Fig. 2.6a**), CD45+ cell number (**Supplementary Fig. 2.6b**), and a bias toward the CD8+ lineage (**Fig. 2.6a**) were similar among the two strains. While splenic CD8+ T cell number was similar among the two TRex strains (**Supplementary Fig. 2.6c**), $1045^{+/+}$ *Msln*$^{-/-}$ mice exhibited increased splenic CD4+ T cell frequency (**Fig. 2.6a**) and number (**Supplementary Fig. 2.6d**). Over 95% of splenic CD8+ T cells expressed Vβ9 (**Fig. 2.6b**) and were naive (CD44-CD62L+) (**Fig. 2.6c**) in both TRex strains. ViSNE analysis[195], which reduces high-parameter data into 2 dimensions for visualization, confirmed a resting (CD25-Ki67-) T cell phenotype (**Supplementary Fig. 2.6e**).

Peptide:MHC tetramers can be a proxy for TCR affinity and functional avidity[176,196–198]. While naïve 7431 and 1045 CD8+ T cells stained similarly for Vβ9, 1045 CD8+ T cells stained brighter for $Msln_{406\text{-}414}$:H-$2D^b$ tetramer (**Fig. 2.6d**), supporting that the 1045 TCR is higher affinity and consistent with prior analysis[176]. Following *in vitro* activation with antigen and IL-2, TRex T cells upregulated CD44, yet maintained CD62L indicative of antigen experience and maintenance of memory potential (**Supplementary Fig. 2.6f**). Activated 1045 T cells stained brighter for tetramer (**Fig. 2.6d-e**) and T cells with the highest tetramer staining were also brightest for CD25 and CD69 (**Fig. 2.6e**). Thus, the TRex methodology still translates into differences in tetramer staining.

T-cells with high functional avidity respond to lower antigen concentrations which often correlate with effector T cell capacity[199]. Therefore, we compared 1045 and 7431 effector T cell cytokine production in response to titrating concentrations of antigen.

Unexpectedly, the functional avidity between 1045 and 7431 TRex effector T cells was similar (**Fig. 2.6f**). These results contrast with our prior analysis of 1045 and 7431 RV T cells in which 1045 RV T cells produce IFNγ with a log-fold greater sensitivity as compared to 7431 RV T cells[176]. While 1045 effector T cells produced more IFNγ and TNFα on a per cell basis in response to high antigen concentrations, both TCRs elicited similar cytokine amounts in response to low antigen concentrations (**Fig. 2.6g**). Thus, despite decreased tetramer staining consistent with a lower affinity TCR, 7431 TRex effector T cells exhibit a functional avidity comparable to 1045 TRex effector T cells suggesting *Trac* genomic location may enhance antigen sensitivity.

TCR downregulation after antigen recognition may be a protective mechanism to prevent pathology by autoreactive CD8+ T cells[200,201]. Directing a CAR to the *TRAC* locus in human T cells promotes CAR internalization and re-expression which delays effector T cell differentiation and acquisition of an exhausted phenotype[182]. Targeting TCRs to *TRAC* also conferred productive antitumor human T cells[202]. As such, we next compared TCR downregulation in TRex effector T cells 5 hours following a second antigenic stimulation. 1045 effector T cells downregulated Vβ9 to a greater extent than 7431 effector T cells (**Fig. 2.6h, Supplementary Fig. 2.6g**) whereas CD8α was similarly downregulated (**Fig. 2.6i, Supplementary Fig. 2.6g**). Additionally, TCR downregulation was more pronounced in 1045 vs. 7431 T cells at multiple timepoints (**Fig. 2.6j-k**). 1045 TRex T cells exhibited higher and prolonged CD25 and PD1 as compared to 7431 TRex T cells consistent with stronger TCR signaling (**Fig. 2.6j-k**).

It has been demonstrated that high affinity MHC I-restricted TCRs can engage CD4+ T cells due to peptide:MHC binding independent of CD8[203]. Strikingly, we found that over 90% of CD4+ T cells were Vβ9+ in 1045 and 7431 TRex mice (**Supplementary Fig. 2.6h**). CD4+ T cells stained brighter for tetramer in 1045 vs. 7431 TRex mice, despite comparable Vβ9 (**Fig. 2.6l**). A higher frequency of effector CD4+ T cells produced cytokines in response to Msln peptide in 1045 vs. 7431 TRex mice (**Fig. 2.6m**). IFNγ produced per cell was elevated in 1045 vs. 7431 CD4+ T cells (**Fig. 2.6n**). Thus, the MHC I-restricted high affinity 1045 TCR can elicit some function in CD4+ T cells.

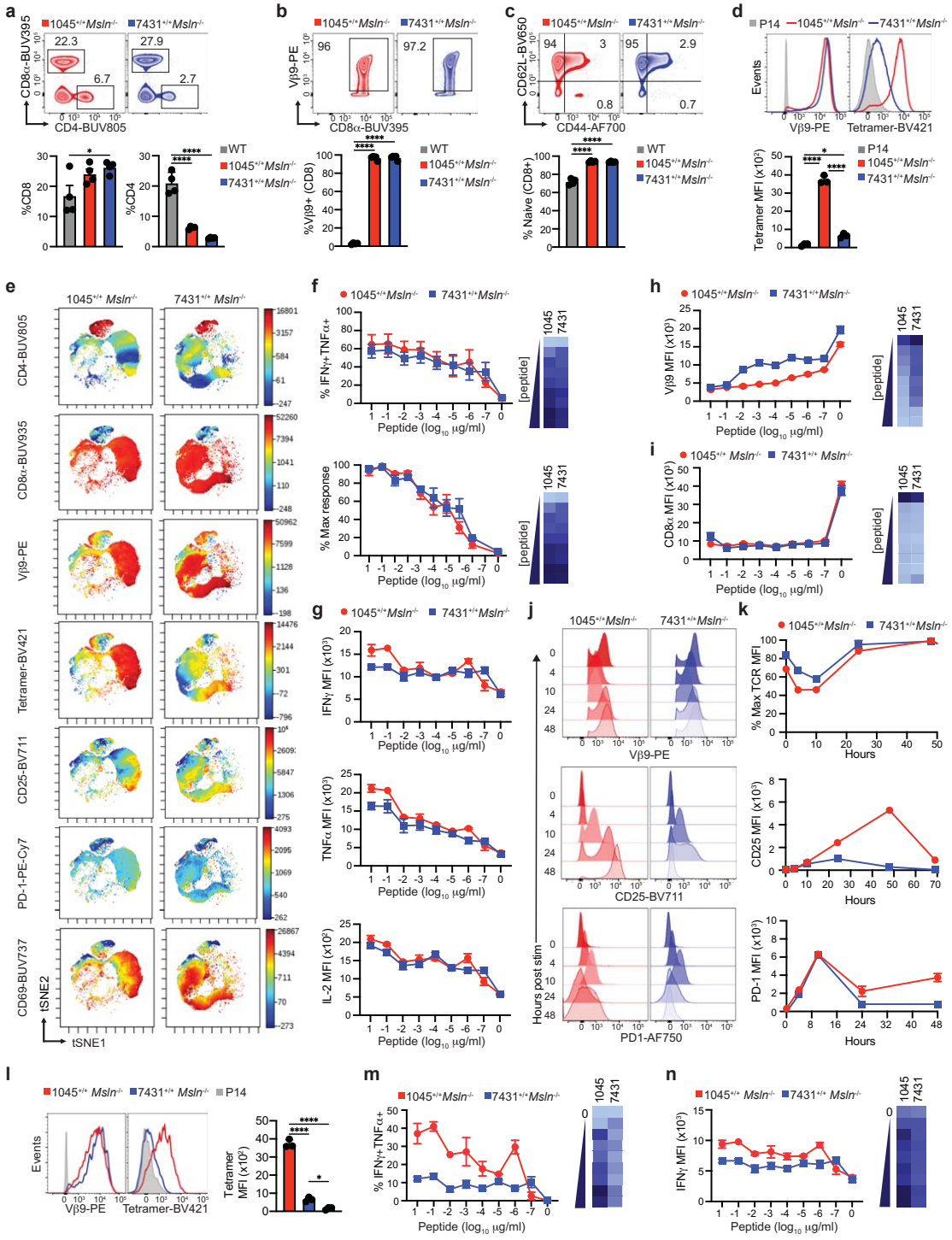

Fig. 2.6 TCR *Trac* targeting improves the functional avidity of a low affinity TCR.
a Frequency of splenic T cells. Plots (top) and mean ± S.E.M (bottom). n=4 biologically independent animals. **b** Frequency of splenic Vβ9+ CD8+ T cells. Plots (top) and mean ± S.E.M (bottom). n=4 biologically independent animals. **c** Proportion of splenic Vβ9+ CD8+ T cells that express CD44 and/or CD62L. Plots (top) and mean ± S.E.M (bottom). n=4 biologically independent animals. **d** Vβ9 and Msln$_{406-414}$:H-2D^{b} tetramer staining gated on CD8+ T cells and tetramer MFI. Data are mean ± S.E.M. n=4 biologically

independent animals. **e** ViSNE analysis of T cells day 6 post activation. **f** Frequency of effector CD8+ Vβ9+ T cells co-producing IFNγ and TNFα after antigen restimulation. Normalized maximum (below) and heat map of mean (right). Data are mean ± S.E.M. n=5 biologically independent animals. **g** Cytokine MFI gated on effector CD8+ T cells 5 h post APCs pulsed with titrating $Msln_{406-414}$. Data are mean ± S.E.M. n=5 biologically independent animals. Vβ9 (**h**) and CD8+ (**i**) downregulation 5 h post antigen. Data are mean ± S.E.M. n=2-3 independent biological replicates. Heat maps of mean (right). **j** Representative histograms of Vβ9, CD25, and PD-1 at the indicated timepoints post incubation with syngeneic splenocytes pulsed with 2 μg/ml of $Msln_{406-414}$. **k** Quantified data from j. n=3 biologically independent animals. Data are mean ± S.E.M. **l** Representative Vβ9 and $Msln_{406-414}$:H-$2D^b$ tetramer staining gated on splenic CD4+ T cells (left). Tetramer MFI is graphed as mean ± S.E.M. n=3 biologically independent animals. **m** Frequency of effector CD4+ T cells co-producing IFNγ and TNFα 5 h post incubation with splenocytes pulsed with titrating $Msln_{406-414}$. Heat map of mean (right). Data are mean ± S.E.M. n=2-3 biologically independent replicates. **n** IFNγ MFI by CD4+ T cells following a 5 h incubation with syngeneic splenocytes pulsed with titrating $Msln_{406-414}$ and heat map (right). Data are mean ± S.E.M. n=2-3 independent biological replicates. For all panels, *p<0.05, **p<0.005, *** p<0.0005, ****p<0.0001. One-way ANOVA with a Tukey's posttest.

2.2.7 Characterization of T cell development in P14 TRex mice.

To identify differences between the TRex approach and historical TCR transgenics, we generated P14 TRex mice. We first validated this approach by targeting the P14 TCR to *Trac* in EL4 cells (**Fig. 2.7a-b**). We next repeated the protocol established in 1045 and 7431 TRex mice for the P14 TCR in murine zygotes and confirmed P14 TCR integration at the *Trac* locus in pups by junction PCR (**Fig. 2.7b**). 19/52 pups (37%) showed P14 TCR integration in at least one *Trac* allele (**Fig. 2.7b-c, Table S2.3**), a frequency within the range of 1045 and 7431 TRex pups (**Fig. 2.7c**). Circulating T cell proportions were biased toward the CD8+ lineage and co-expressed Vα2 and Vβ8 in both $P14^{+/-}$ and $P14^{+/+}$ pups (**Fig. 2.7d**, **Table S2.3**). Thymus weight and immune cell number were similar among the strains (**Fig. 2.7e**). DN thymocyte frequency was increased in P14 Tg and was similarly low in P14 TRex and WT mice (**Fig. 2.7f-h**). DP and CD4+ SP frequency was decreased and CD8+ SP frequency was increased in both P14 Tg and TRex mice compared to WT mice (**Fig. 2.7f-h**). CD4+ SP number was decreased in P14 Tg compared to WT whereas CD8+ SP number was similarly increased in both P14 strains (**Fig. 2.7g**). P14 Tg thymus contained increased DN4 and decreased DN1-DN3 frequency as compared to P14 TRex

and WT thymus (**Fig. 2.7i-j**). While DN P14 Tg T cells were enriched for Vα2+Vβ8+ cells, TRex T cells became enriched for Vα2+Vβ8+ at later thymocyte development stages (**Fig. 2.7k-l**). Vβ8 was first detected at DN1 in P14 Tg thymocytes but at the DN4 stage in P14 TRex thymocytes (**Fig. 2.7m, Supplementary Fig. 2.7a**), the latter consistent with the known timing of TCRα expression in WT thymocytes. Only 20% of CD4+ SP co-expressed Vα2 and Vβ8 in P14 Tg whereas over 90% of CD4+ SP expressed the P14 TCR in TRex mice (**Fig. 2.7k**). Most CD8+ SP in TRex mice were CD3+Vα2+Vβ8+ (**Fig. 2.7k-l**, **Supplementary Fig. 2.7b-c**). CD3ε intensity was lower in CD4+ SP than CD8+ SP in P14 TRex mice and higher in CD8+ SP in TRex than Tg and WT mice (**Supplementary Fig. 2.7d**).

To assess endogenous Vβ in TRex mice, we stained thymocytes with a pool of FITC-conjugated antibodies specific to multiple murine Vβ alleles while excluding Vβ8, which was detected using a different fluorochrome using the gating strategy in **Supplementary Fig. 2.7e**. The Vβ panel detected 40-60% of endogenous Vβs in WT CD3+ thymocytes (**Fig. 2.7n**), an expected range since there are approximately 21 functional Vβ genes in mice[204]. A fraction of CD3+ thymocytes co-expressed low levels of an endogenous Vβ with Vβ8 in TRex mice (**Fig. 2.7n-p**). Endogenous Vβ was significantly decreased in in TRex CD8+ SP as compared to WT CD8+ SP (**Supplementary Fig. 2.7f**). P14 Tg and TRex DN4 thymocytes exhibited slightly increased dual Vβ frequencies compared to WT mice (**Supplementary Fig. 2.7g**). To investigate the frequency of dual Vβ T cells in circulation, we performed a similar analysis of T cells in the peripheral blood. Approximately, 20% of peripheral CD8+, CD4+

conventional (Tcon) and CD4+Foxp3+ cells (only 20% of the total CD4 population in TRex) co-expressed an endogenous and exogenous Vβ in P14 TRex mice (**Fig. 2.7p**, **Supplementary Fig. 2.7g-i**). In $1045^{+/+}$ $Msln^{-/-}$ TRex mice, 30-40% of peripheral CD8, CD4+ Tcon and Treg were dual Vβ+ (**Supplementary Fig. 2.7j**) revealing some interstrain variability in endogenous Vβ. To further investigate if thymocyte maturation is physiological in P14 TRex mice, we evaluated CD69 as it is downregulated in mature SP. CD69- CD8+ SP also expressed CD62L (**Supplementary Fig. 2.7k**), consistent with mature SP thymocytes. CD69- (mature) CD3+CD8+ SP thymocyte frequency was decreased in TRex mice as compared to P14 Tg and WT mice (**Fig. 2.7q, Supplementary Fig. 2.7l**). However, P14 Tg and TRex mice exhibited a 3-fold increase in mature CD3+CD8+ SP number as compared to WT mice (**Fig. 2.7r**), indicating CD8+ SP maturation is intact in TRex mice.

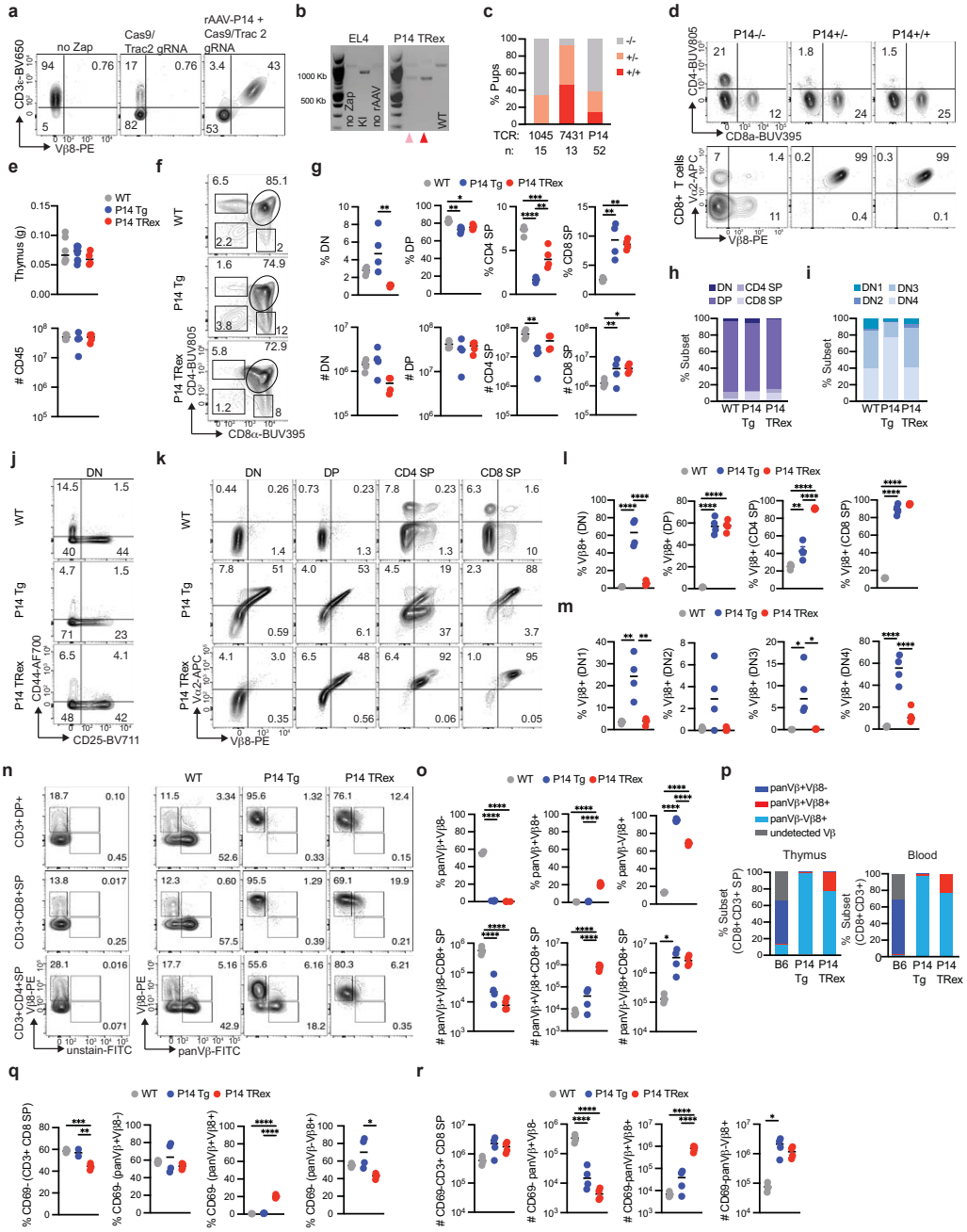

Fig. 2.7 Characterization of T cell development in P14 TRex mice.

a Frequency of EL4 cells that express Vβ8 and CD3ε on day 3 post electroporation with *Trac* gRNA 2 + Cas9 RNP ± rAAV-P14. No zap, negative control. **b** Donor P14 TCR integration was determined by a junction PCR of EL4 DNA (left image) or representative P14 TRex pups (right image). KI, knock-in. Pink arrow, $P14^{+/-}$ TRex pups; red arrow, $P14^{+/+}$ TRex pups. WT, wild type band. **c** Frequency of TRex pups with the indicated genotype. **d** Frequency of circulating CD4+ and CD8+ T cells (top, gated on live CD45+ cells) and frequency of Vα2+Vβ8+ among CD8+ T cells from P14 TRex pups. **e** Thymus weight in grams (g) and CD45 cell number per thymus from WT, P14 transgenic (Tg) or $P14^{+/+}$ TRex mice. **f** Plots are gated of CD45+B220- thymocytes. **g** Frequency (top) and number (bottom, per thymus) of double negative (DN), double positive (DP), CD4+ single positive (CD4+ SP) and CD8+ single positive (CD8+ SP) thymocytes. **h** Mean frequency of each subset among total CD45+B220-. **i** Mean frequency of DN1-DN4 subsets among

total DN. **j** DN1-DN4 plots are gated on CD4-CD8- DN thymocytes. CD44+CD25-(DN1), CD44+CD25+ (DN2), CD44-CD25+ (DN3), and CD44-CD25- (DN4). **k** Representative plots of Vβ8+Vα2+ staining gated on the indicated thymocyte subset. **l** Proportion of the indicated subsets that express Vβ8. **m** Proportion of DN subsets that are Vβ8+. **n** Plots of the indicated thymocyte subsets that express exogenous (Vβ8+) and/or endogenous (panVβ+) Vβ. **o** Frequency (top row) and number (bottom row, per thymus) of CD3+ CD8+ SP that express exogenous (Vβ8+) and/or endogenous (panVβ+) TCRβ. **p** Mean proportion of CD3+ CD8+ SP that express exogenous (Vβ8+) and/or endogenous (panVβ+) TCRβ in thymus or blood. **q** Frequency of mature CD69-CD8+ SP thymocytes among total CD3+ CD8+ SP and single or dual TCRβ+CD3+ CD8+ SP. **r** Number of CD69-CD3+ CD8+ SP per thymus (left) and number of single or dual TCRβ+CD69-CD3+ CD8+ SP thymocytes. For all quantified panels, data are mean ± S.E.M. n=4 mice per group. *p<0.05, **p<0.005, ***p<0.0005, ****p<0.0001. One-way ANOVA with a Tukey's posttest.

2.2.8 Targeting a TCR to Trac enhances exogenous TCR expression and antigen sensitivity.

We next compared peripheral T cell responses between P14 TRex and P14 Tg mice to fix the TCR specificity and precisely uncover the role of the genomic location. Spleen weights were similar among the strains (**Supplementary Fig. 2.8a**). CD8+ T cell frequency and number were increased in both P14 strains as compared to WT mice (**Fig. 2.8a, Supplementary Fig. 2.8b**). CD8+ T cells equally co-expressed Vα2 and Vβ8 among the two P14 strains (**Fig. 2.8b**), whereas more CD4+ T cells were Vα2+Vβ8+ in TRex vs. Tg mice (**Fig. 2.8b-c**). Most CD8+ T cells exhibited a naïve phenotype whereas most CD4+ T cells expressed CD44 in both strains (**Supplementary Fig. 2.8c**). TRex T cells expressed more CD3ε, Vα2 and Vβ8 ex vivo (day 0) and following activation (day 6) than analogous P14 Tg T cells (**Fig. 2.8d, Supplementary Fig. 2.8d**). CD8+ MFI was comparable ex vivo and modestly higher after activation in TRex T cells (**Supplementary Fig. 2.8d**). CD25 was also higher in CD8+ P14 TRex than Tg effector T cells (**Fig. 2.8d**). After primary activation, the kinetics of TCR internalization and re-expression were similar in TRex and Tg T cells (**Fig. 2.8e**), however, which suggests that factors other than the genomic location impact TCR downregulation. We next compared proliferation by incubating CTV-labeled

splenocytes with titrating concentrations of antigen and IL-2. At low antigen concentrations, TRex T cells were slightly more proliferative (**Fig. 2.8f**) and maintained higher TCR levels than Tg T cells (**Fig. 2.8f**). Providing exogenous IL-2 may compensate for differences in TCR signaling and proliferation, therefore we repeated the proliferation assay without IL-2. A greater frequency of TRex T cells were proliferating at low antigen concentration (**Fig. 2.8g**) corresponding to CD69 upregulation (**Fig. 2.8g**) and CD44, whereas PD-1 was not affected (**Supplementary Fig 2.8e**). Further, more TRex T cells had undergone ≥ 3 cell divisions (**Fig. 2.8h**) and trended to produce more IFNγ than analogous Tg T cells, particularly noticeable at lower antigen concentrations (**Fig. 2.8i**). CD69 MFI and frequency of cells expressing CD25 were also greater in TRex vs. Tg effector T cells (**Fig. 2.8i**). Thus, the data suggest that targeting a TCR to *Trac* may improve T cell responsiveness to antigen.

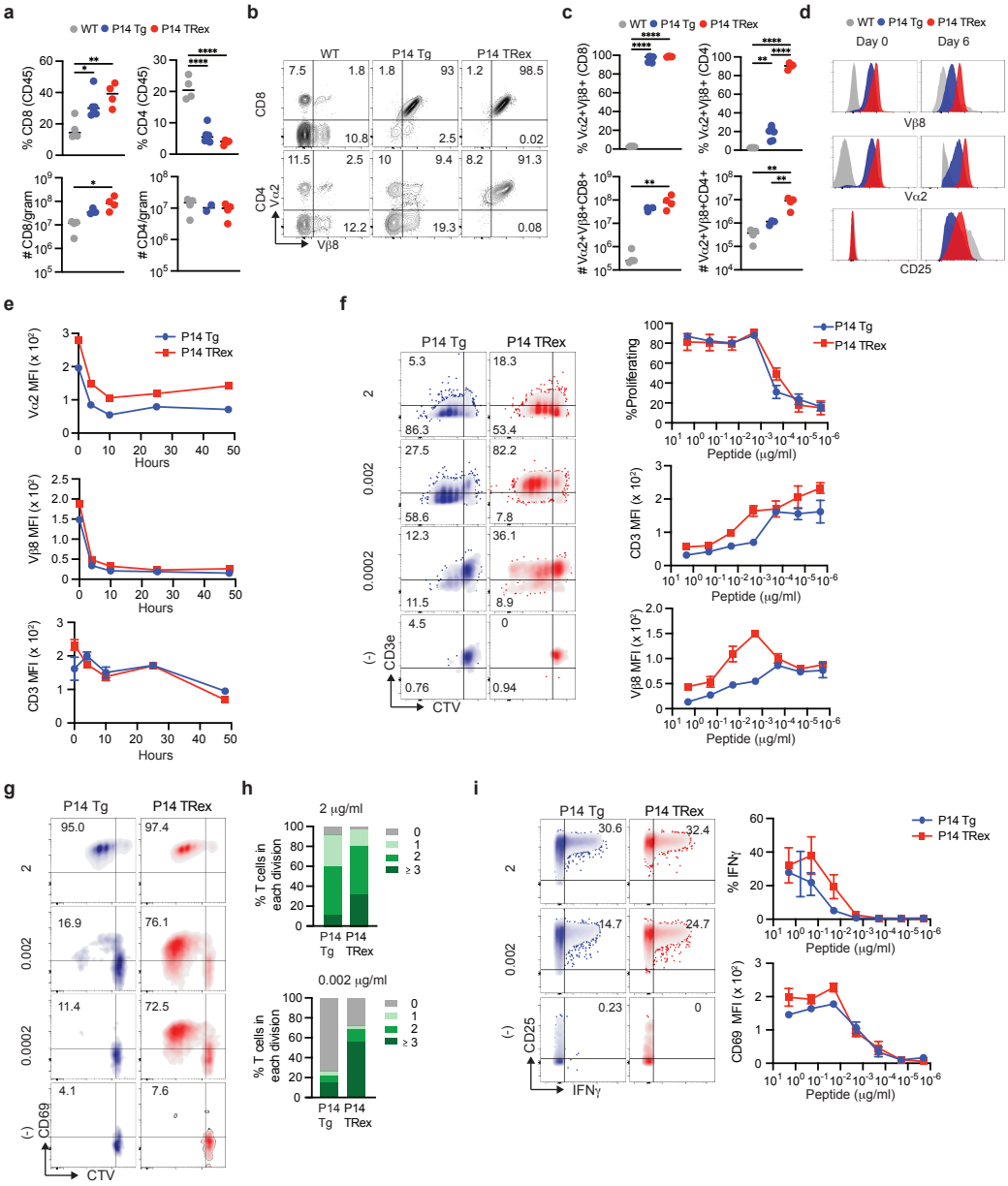

Fig 2.8. Targeting a TCR to Trac enhances exogenous TCR expression and antigen sensitivity.
a Frequency (top row) and number (bottom row) of splenic CD4+ and CD8+ T cells. Each dot is an independent mouse. Data are mean ± S.E.M. n=4 mice per group. *p<0.05, **p<0.005, ***p<0.0005, ****p<0.0001. One-way ANOVA with a Tukey's posttest. **b** Representative plots gated on splenic CD8+ (top row) or CD4+ (bottom row) T cells. **c** Frequency (top row) or number (bottom row) of Vα2+Vβ8+ splenic T cells. Each dot is an independent mouse. Data are mean ± S.E.M. n=4 mice per group. **p<0.005, ***p<0.0005, ****p<0.0001. One-way ANOVA with a Tukey's posttest. **d** Histograms of the indicated markers ex vivo (day 0) and on day 6 post *in vitro* activation with gp33 peptide and IL-2. Representative of n=3-4 mice per group. **e** Quantification of TCR chains and CD3 at the indicated hours post activation with 2 μg/ml of gp33 peptide. Data are mean ± S.E.M. n=4 mice per group. Significance was determined by unpaired two-tailed T-tests with Welch correction a False discovery rate (FDR) of 1% and a Two-stage step-up[205]. **p<0.005. ***p<0.0005, ****p<0.0001. **f** Proliferation gated on CD8+ T cells on day 3 post activation with

titrating doses of gp33 peptide (y-axis) and rhIL-2 (10 ng/μl). Significance was determined by unpaired two-tailed T-tests with Welch correction with an FDR of 1% and a two-stage step-up[205]. **p<0.005, ***p<0.0005, ****p<0.0001. **g** Proliferation gated on CD8+ T cells on day 3 post activation with titrating doses of gp33 peptide (y-axis) without exogenous IL-2. **h** Proportion of CD8+ Vβ8 + T cells among each division cycle on day 3 post activation. Data are mean. n=4 mice per group. **i** Proportion CD8+ T cells producing IFNγ and expressing CD25 (plots) or CD69 (graphed data on right) on day post activation. Data are mean ± S.E.M. n=4 mice per group. Significance was determined by unpaired two-tailed T-test with Welch correction with an FDR of 1% and a two-stage step-up[205]. *p<0.05.

2.3 Discussion

We develop a methodology to integrate a desired exogenous TCR into the physiological endogenous *Trac* locus in murine T cells and zygotes. We adapted the micro-injection free CRISPR-READI approach[184] by combining AAV-mediated donor TCR delivery with Cas9/sgRNA RNP electroporation to induce site-specific modifications in *Trac* and integrate the exogenous TCR. Contemporaneously, we induced *Msln* null mutations to circumvent T cell tolerance. We independently generate multiple TRex strains supporting high efficiency and reproducibility of this method. As Msln is overexpressed by many solid tumors[163–167,176], the 1045 and 7431 TRex mice will provide a standardized source of naïve T cells with physiological expression of TCRs specific to a native and clinically relevant tumor antigen to identify how to sustain T cell function in solid tumors.

TCR transgenic mice have improved our understanding of T cell development and differentiation. Considerations of this approach include multiple and random TCR integration into the genome resulting in non-physiologic TCR regulation[159–162,178] and premature TCRα and TCRβ expression at the DN1 stage impacting thymocyte development[206]. TCR rearrangement is a highly ordered and sequential process where TCRβ is rearranged in DN3 preceding TCRα rearrangement that can be initiated at DN4 transitioning to the DP stage. A productive TCRβ rearrangement prevents further Vα-to-

DJβ rearrangements at the DP stage, a process called allelic exclusion[204]. As a dsDNA break is directly upstream of *Trac* resulting in endogenous TCRα loss in TRex mice, we show exogenous TCR integration is critical for T cell development. We also demonstrate exogenous TCRα and TCRβ are initially expressed at DN4 and thymocytes undergo all the sequential stages of maturation in TRex mice. Indeed, MHC I is required for TRex T cell positive selection and negative selection of TRex T cells can occur when the target native antigen is sufficiently expressed. One consideration of the TRex approach is a fraction of TRex T cells express endogenous TCRβ in addition to the exogenous TCRβ. This is expected as the endogenous *Tcrb* locus remains intact in TRex mice. However, we identified that fewer TRex T cells express endogenous TCRβ than WT T cells and endogenous TCRβ cell surface expression is much lower in TRex T cells vs. WT T cells. Thus, post-transcriptional mechanisms for silencing endogenous TCRβ[207,208] may be playing a role. In the future, endogenous TCRβ could be deleted using CRISPR/Cas9 but this is complicated by the fact that exogenous TCRβ must remain intact. Alternatively, the TRex strategy could be applied directly in a TCRβ-deficient genetic background. An outstanding question, however, is the extent TRex T cells require expression of an endogenous TCRβ for development.

T cells that express high affinity self-reactive TCRs are susceptible to thymic negative selection, an essential central tolerance mechanism that safeguards against autoimmunity. Here, we identify that both copies of *Msln* are necessary for negative selection of high affinity Msln-specific T cells supporting a gene dosage dependent mechanism of central tolerance. Loss of a one *Msln* allele may reduce protein expression

on a per cell basis. Alternatively, as *Msln* expression has been reported in medullary thymic epithelial cells (mTECs)[209] and Aire-dependent genes can be stochastically monoallelically expressed in mTECs[210], *Msln* allele loss may reduce the number of Msln+ thymic APCs capable of mediating negative selection. Fezf2 elicits self-antigen expression in mTECs in an Aire-independent manner[211] and also represses some mTEC genes including *Msln*[212] suggesting *Msln* regulation by Fezf2 may necessitate that both alleles are intact for negative selection. MSLN is detected in Hassall's corpuscles, which are inflammatory, cornifying, terminally differentiated mTECs[213] in the normal human thymus[165] and single cell sequencing has identified *MSLN* in human thymic mesothelial cells and epithelial cells[214]. *MSLN* is also overexpressed in thymic carcinomas[215]. Thus, further investigation into the thymic cell type(s) that induce negative selection as well as the extent that a TCR affinity threshold exists for central tolerance are warranted.

Prior methods for engineering T cells to express an antigen receptor have primarily focused on the lentiviral transduction approach. In clinical trials, lentiviral-mediated CAR integration into *TET2* or *CBLB* caused infused CAR T cell clonal expansion in cancer patients[154,216]. Additionally, gene silencing and variable non-uniform receptor expression can occur following retroviral transduction of T cells[182,217,218]. We previously employed γ-retroviral vectors to transduce murine P14 Tg T cells with Msln-specific TCRs[176,219], an approach that necessitated 2 weeks of T cell expansion to obtain sufficient effector T cell numbers for preclinical adoptive T cell therapy studies[176,219]. In contrast to human T cells that can be sustained *in vitro* over multiple stimulations[143], maintaining murine T cell viability during repetitive *in vitro* stimulations is a challenge. Further, γ-retroviral vectors can only transduce proliferating cells, precluding the analysis of naïve Msln-specific T

cells that could model the activity of MSLN-based cancer vaccines[171,220]. Thus, the 1045 and 7431 *Msln*$^{-/-}$ TRex mice are a robust tool to track a native self/tumor-specific T cell response. During TCR transduction, exogenous TCRs must also outcompete endogenous TCR chains for CD3 complex and cell surface expression[221]. Exogenous TCR chains mispairing with endogenous TCR chains can result in unknown T cell antigen specificities thereby increasing the potential for toxicity during adoptive cell therapy[219] and may decrease exogenous TCR levels. Indeed, abrogating endogenous TCRβ improved antigen sensitivity in human TCR-transduced T cells[222]. Here, we demonstrate increased antigen sensitivity when the exogenous TCR is located within *Trac* even compared to TCR transgenic T cells with the identical antigen specificity. Many cancers are poorly immunogenic in part through defects in antigen processing and presentation. Thus, targeting an exogenous TCR to *Trac* may be beneficial in such settings. As engineered CD4+ T cells contribute to CAR T cell anti-tumor activity[223] our previous use of P14 TCR transgenic cells as a donor cell source for exogenous TCR transduction limited our assessment to CD8+ T cells. We show that the high affinity 1045 TCR has some functions in CD4+ T cells from TRex mice permitting future studies to potentiate the antitumor function of MHC I-restricted TCR engineered CD4+ T cells. Thus, Msln-specific TRex mice will permit efficient investigation into how to enhance antitumor T cells in cancer. Particularly, since all T cells express the Msln-specific TCR in TRex mice, experiments to further engineer the T cells to overcome the suppressive tumor microenvironment by expressing chimeric costimulatory proteins, cytokines or performing genetic screens are now feasible.

Our study supports that the genomic location of TCR can impact T cell functionality. Despite a lower affinity TCR, 7431 TRex effector T cells were as sensitive to low antigen as 1045 TRex effector T cells. While tetramer staining is not always a surrogate for T cell functionality[224,225], in the past, tetramer staining correlated with increased a higher functional avidity of 1045 RV T cells compared to 7431 RV T cells[176], supporting that TCR integration in *Trac* may improve antigen sensitivity of lower affinity TCRs. P14 TRex T cells were also more sensitive to antigen as compared to P14 transgenic T cells, which may be explained in part due to higher TCR expression in P14 TRex T cells. Since pups from multiple independent P14 TRex founders were analyzed, the heightened antigen sensitivity appears reproducible. Additionally, we identify that targeting a TCR to *Trac* sustained primary murine T cell function over multiple stimulations *in vitro* compared to transduced T cells. These data are consistent with a prior study of a CD19 CAR targeted to *TRAC*[182] and exogenous TCR replacement in in human T cells[183,202]. Thus, the TRex methodology is an exciting and robust technology to generate heritable alleles encoding a desired TCR and permit investigation into physiological TCR regulation on T cell behavior.

2.4 Methods

2.4.1 Animals

The University of Minnesota Institutional Animal Care and Use Committee approved all animal studies that conformed to ethical regulations for animal testing and research. Animals were co-housed in SPF vivarium which is maintained at a 14:10 hour light: dark cycle, at 68-70°F and 20-70% humidity range. Both female and male mice between the ages of 6-12 weeks old were used in this study. Mice for these studies were

euthanized according to IACUC approved methods of CO_2 or isoflurane overdose followed by cervical dislocation. C57BL/6J wild type (WT) mice were purchased from Jackson Labs (#000664). Pseudopregnant CD-1 female mice were purchased from Charles River Laboratory (#CD-1 022). Generation of TRex animals was performed in the Mouse Genetic Laboratory at the University of Minnesota. B6.129P2-B2mtm1Unc/DcrJ (*B2m*$^{-/-}$) mice backcrossed to C57Bl/6 strain for 11 generations were purchased from Jackson Labs (#002087) and backcrossed to 1045 TRex mice. P14 and OT1 TCR transgenic were kindly provided by Dr. David Masopust and Dr. Vaiva Vezys (University of Minnesota). P14 TRex and P14 Tg mice were on the *Rag*$^{+/+}$ background. P14 TRex mice were homozygous for the P14 TCR. Three independent P14 TRex founders were bred to generate homozygous F1 pups for the P14 TRex analysis.

2.4.2 rAAV serotype screening

Splenocytes from WT mice were activated *in vitro* with 1 μg/ml anti-CD3ε (145-2C11, BD Biosciences) and 1 μg/ml anti-CD28 (37.51, BD Biosciences) in the presence of 10 ng/μl recombinant human IL-2 (Peprotech) and 5 ng/μl recombinant murine IL-7 (R&D Systems) in T cell media (DMEM, 10% FBS, 2 μM L-glutamine, 100 U/ml penicillin/streptomycin, 25 μM 2-β-mercaptoethanol) at 37°C, 5% CO_2. After 2 days, activated T cells were centrifuged and incubated with rAAV serotypes (UPenn Vector Core) engineered to express GFP. After 3 days, GFP expression in live T cells was determined by flow cytometry.

2.4.3 Cell lines

EL4 cells are derived from a lymphoma induced in a C57BL/6N mouse by 9,10-dimethyl-1,2-benzanthracene and are commercially available (TIB-93, ATCC). NIH/3T3 fibroblast cell line isolated from a mouse NIH/Swiss embryo are commercially available (CRL-1658, ATCC). Both cell lines were cultured according to ATCC specifications and were negative for Mycoplasma.

2.4.4 TCR cloning into pAAV destination vector and virus production.

The *Trac* targeting TCR vectors were produced by first designing ~1 kb homology arms (HA) flanking the CRISPR sgRNA target site in exon 1 such that the high affinity (clone 1045[176]) or low affinity (clone 7431[176]) $Msln_{406-414}$:H-$2D^b$-specific or P14 TCR were inserted in-frame. A Furin (RRKR)-GSG-T2A element[226] was incorporated at the 5' end of the TCR insert site to facilitate co-translational separation from the residual peptide sequence of the endogenous Trac locus. The *Trac* HA-TCR-GSG-T2A sequence was synthesized as a gBlock Gene Fragments (IDT, Coralville, IA) with AttB sites and subcloned into pDONR221 using the Gateway BP Clonase II Enzyme Mix (ThermoFisher Scientific, Waltham, MA) to produce pENTR-mTRAC HA. TCR sequences were codon optimized and synthesized by Genscript and subsequently cloned into pENTR-mTRAC HA using Gibson Assembly[227]. Following sequence verification, the pENTR-mTrac HA-TCR was cloned into pAAV-Dest-pA using the Gateway LR Clonase II Enzyme Mix (ThermoFisher Scientific, Waltham, MA). pAAV constructs were sent to Vigene (1045 TCR) or SignaGen Laboratories (7431 and P14 TCR) for commercial AAV production. High titer virus ranged from 1.92 - 3 x 10^{13} gene copies (GC) per mL and was stored at -80°C.

2.4.5 Cas9 ribonucleoprotein and sgRNAs

Synthego sgRNAs were resuspended at 50 µM. 7 µl TrueCut Cas9 v2 (5µg/mL, ThermoFisher Scientific, A36498) was combined with 7 µl *Trac* sgRNA 2 or 7 µl *Msln* sgRNA 2 at a 1:1 molar ratio and mixed gently by pipetting similar to as described[188]. The *Msln* sgRNA was not used for generation of the P14 TRex mice. Two sgRNAs specific to murine *Trac* exon 1 were tested, including *Trac* sgRNA 1: UCUUUUAACUGGUACACAGC (-54220544) and *Trac* sgRNA 2: UUCUGGGUUCUGGAUGUCUG (-54220521). While both sgRNAs efficiently removed endogenous TCRs, only *Trac* sgRNA 2 resulted in exogenous TCR integration (**Fig. 1**) and was therefore used in all subsequent experiments. Two sgRNAs specific to murine *Msln* exon 4 were initially tested, *Msln* sgRNA 1: GGAGGUAUCUGACCUGAGCA (-25753010) and *Msln* sgRNA 2 GGCCAAGAAAGAGGCCUGUG (+25753054) and validated in murine B6 3T3 fibroblasts. *Msln* sgRNA 2 was selected for all subsequent experiments.

2.4.6 Primary murine T cell activation

Spleens were mechanically dissociated using a 40 µm filter. RBCs were lysed by resuspension in 1 ml ACK lysis buffer for 2 minutes. Lysis was quenched by addition of 10 mls of T cell media. T cells were centrifuged at 350 x g for 5 minutes at 4°C and resuspended in 10 ml of T cell media containing 10 ng/µl recombinant human IL-2 (rhIL-2, Peprotech), 5 ng/µl recombinant murine IL-7 (rmIL-7, R&D Systems), and 1 µg/ml anti-CD3ε (clone 145-2C11) and 1 µg/ml anti-CD28 (clone 37.51) (BD Biosciences). Alternatively, we used 10 ng/µl recombinant human IL-2 (rhIL-2, Peprotech) and 10 µg/ml

$Msln_{406-414}$ peptide (GQKMNAQAI, Genscript) or 10 µg/ml GP33 peptide (KAVYNFATM, Genscript) for studies evaluating antigen-specific T cell activation. Splenocytes were cultured in T25 flask for overnight at 37°C, 5% CO2. Cells were counted using a hemocytometer and Trypan blue exclusion. A total of 5 x 10^5 cells were transferred into a 12 well plates at and incubated at 37°C, 5% CO_2 for 24 h prior to editing, or for longer periods of time as indicated.

2.4.7 Superovulation and rAAV incubation

24-28-day old female C57BL/6J mice were purchased directly from Jackson Labs (000664) and were superovulated by i.p. injection of 5 IU/mouse of Pregnant Mare Serum Gonadotropin (PMSG, C1063, Sigma). After 47-48 hours, 5 IU/mouse of human Chorionic Gonadotropin (hCG, HOR-250, PROSPEC Protein Specialists) was injected i.p. in PMSG-treated females. Superovulating females were immediately crossed with C57BL/6J males at a 1:1 ratio to produce 1-cell zygotes. The next morning, zygotes were collected and washed using standard methods[228]. Briefly, cumulus-oocyte-complex were collected from the ampulla of the plugged females, treated in hyaluronidase (H4272, Sigma) in a 35 mm TC-treated dish (#353001, Falcon) containing 3.5 ml of modified Human Tubal Fluid (mHTF, http://card.medic.kumamoto-u.ac.jp/card/english/sigen/manual/medium/htf.html)[229] for 2 minutes to remove cumulus cells around the zygotes. The zygotes were then washed 2X in mHTF and then zona pellucida was thinned by briefly treating the zygotes in the Acidic Tyrode's solution (T1788, Sigma). Zygotes were subsequently washed 6X in M2 media (MR-051-F, Millipore), and incubated in 50 µl of mHTF containing rAAV (1.5 x 10^8 GC/µl) covered

by mineral oil (M8410, Sigma) in a 60 mm tissue culture dish (353004, Falcon) for 6 hours at a 37^{o} C, 5% CO_2.

2.4.8 Electroporation of zygotes with CRISPR Cas9 RNPs

TrueCut Cas9 (ThermoFisher Scientific, A36498) and sgRNAs were combined at a 1:1 molar ratio and incubated for 10 minutes at room temperature to generate ribonucleoprotein (RNP) complexes and stored on ice during transfer to the University of Minnesota Mouse Genetics Laboratory. Following 6-hour incubation with rAAV, zygotes were washed 1X in Reduced Serum Medium (OPTI-MEM, #31985-062, Gibco). Zygotes were transferred with a pipette and next mixed with 10 µl of OPTI-MEM, 2 µl of rAAV at 1.5 x 10^9 GC/µl (final concentration: 1.5 x 10^8 GC/µl), and 2 µl of 10X preformed RNP complex (Cas9+gRNAs to *Trac* and *Msln*). The electroporation was performed in a 1 mm gap electroporation cuvette (Cat# 5510, Molecular BioProducts) using the BioRad Gene Pulser Xcell according to the following parameters: square wave at 30V, 6 pulses with 3 ms duration and 100 ms interval. After the electroporation, zygotes were washed once in 1X OPTI-MEM and then transferred to the original mHTF drop for overnight culture. The next day, 2-cell embryos were transferred into pseudopregnant CD-1 females (Charles River Laboratory) and after 19 days, pups were born. Number of zygotes, embryos, CD-1 females, and pups born following zygote engineering using CRISPR/Cas9 and 1045, 7431 or P14 rAAV for generating TRex mice is in **Table S2.2**.

2.4.9 PCR Genotyping

DNA was isolated from ear snips using the REDExtract Kit (Sigma Aldrich). PCR was run using Q5 HiFi Master Mix (New England Biolabs) for *Trac* KO, *Msln* KO, and

Trac Junction PCR protocols using the following gene-specific PCR primers purchased from IDT: *Trac* KO forward, 5'-GCTAGATCCTAGGCTGTCATTTC-3', *Trac* KO reverse, 5'-CCAATGTCCTCTGTCATGTTCT-3', with an amplicon length of 579 bp; *Msln* KO forward, 5'- AGGTGGGTTCAGTACCTTTG-3', and *Msln* KO reverse, 5'-GATCAGCTCAGACTTGGGATAG-3', with an amplicon length of 698 bp. Amplification was run for 30 cycles at 95°C for 30 seconds, 55°C for 30 seconds, 74°C for 1 min. To assess exogenous TCR integration into the *Trac* locus, we created a *Trac* junction PCR using the following gene-specific PCR primers: Wild type (WT) Forward, 5'-CTCTGGTGTGAGTGCTATTC-3', 1045 and 7431 knock-in (KI) Forward, 5'-CCTGTTCTGGTACGTGAGATAC-3', P14 KI Forward, 5'-GTAGCTATGAGGATAGCACCTTT-3' and a junction universal reverse primer, 5'-CAAGAGAAGACAGGAAGGTGAG-3'. The WT amplicon length is 1025 bp, the1045/7431 KI amplicon length is 750 bp, and the P14 KI amplicon length is 742 bp. Amplification was run for 30 cycles of 95°C for 30 seconds, 60°C for 30 seconds, and 74°C for 1 minute. *Trac* and *Msln* KO PCR products were purified using a PCR Clean-Up Kit (Qiagen) and were subsequently submitted for Sanger sequencing through Eurofins genomics using both *Msln* and *Trac* forward and reverse primers described above. PCR was run on an Eppendorf Vapo Protect thermocycler. Sequence results were analyzed using Snapgene and Interference with Crispr Edits (ICE) software (https://ice.synthego.com). Mutant sequences were directly compared to WT control sequence. *Trac* junction PCR product was run on a 1.5% agarose gel and imaged in a UV transilluminator with ethidium bromide.

2.4.10 TCR targeting to Trac in primary murine T cells and EL4 cells.

EL4 lymphoma cells were sorted to >95% CD3+ purity. Primary T cells were activated with anti-CD3+anti-CD28 as described above and after 2 days, T cells were centrifuged for 10 minutes at 200 x g at 4°C. Primary T cells and EL4 cells were resuspended at 1 x 10^6-1 x 10^7 cells per ml in P4 solution with supplement (Lonza, V4XP-4024). Synthego sgRNAs were resuspended at 50 μM. 10X RNPs were generated by mixing Synthego sgRNAs and TrueCut Cas9 Protein v2 (ThermoFisher Scientific, A36498) at a 1:1 molar ratio and incubating at room temperature for 10 minutes. RNPs were diluted ten-fold in the cell suspension and cells were transferred to the nucleofection cuvette and incubated at room temperature for 2 minutes with the cover on. Using the Amaxa 4D Nucleofector, cells were pulsed with pulse code CM137 and allowed to rest 15 minutes in the cuvette. Cells were diluted 1:10 in prewarmed T cell recovery media (T cell media with no antibiotics) in the cuvette and allowed to recover at 37°C for 15 minutes. T cells were transferred to pre-warmed (37°C) T cell media containing rhIL-2 (10 ng/μl), rmIL-7 (5 ng/μl) and various virus concentrations of rAAV6 engineered to express the 1045 TCR (Vigene), 7431 TCR (Signagen), or P14 TCR (Signagen) homology donor DNA for a total of 30 minutes after nucleofection. T cells were returned to the incubator (37°C, 5% CO2) for an additional 3 days prior to flow cytometry and/or DNA sequencing analysis. Typically, EL4 and primary T cells were ~50% viable following this protocol.

2.4.11 Preparation of mononuclear cells from spleen and blood

Spleens were mechanically dissociated to single cells. RBCs were lysed by incubation in 1 mL of Tris-ammonium chloride (ACK) lysis buffer (GIBCO) for 1-

2 minutes at room temperature. 9 mL of T cell media was added to quench lysis. Cells were spun at 1400 rpm for 5 minutes at 4° C and resuspended in T cell media and stored on ice until further use. For PBMCs, 100-200 µl of blood was collected per animal in 20 mM EDTA in a 96-well round bottom plate. RBCs were lysed by resuspension in 150 µl ACK lysis buffer (GIBCO) for 10 minutes at room temperature. 1 mL of T cell media was added to quench cell lysis. Cells were spun at 350 x g for 5 minutes at 4°C, supernatant decanted. Cells were stored in T cell media on ice until further use.

2.4.12 Monoclonal antibody staining for flow cytometry.

Mononuclear cells were stained with various antibodies or $Msln_{406-414}$:H-$2D^b$-APC or -BV421 tetramer (1:100) in the presence of Fc block (αCD16/32) and a live/dead stain (Tonbo Ghost dye in BV510 or APC ef780). Antibodies were diluted 1:100 in FACs Buffer (2.5% FBS + PBS+ 1% NaN_3) unless otherwise indicated. All antibodies used for flow cytometry and T cell activation are described in **Table S2.3**. For intracellular Foxp3 and Ki67 staining, cells were fixed using Foxp3 transcription factor reagent (Tonbo) for 30 minutes at 4°C, washed and intracellular stained with diluted antibodies in permabealization buffer (Tonbo) and stained overnight. The next day, cells were washed 2X with perm/wash buffer and resuspended in FACs buffer. Cells not stained intracellularly were fixed in 0.4% PFA for 15 minutes at 4°C, washed 2X with FACS buffer and resuspended in FACs buffer. For dual TCRβ detection, thymocytes or PBMCs were stained with a panel of non-FITC antibodies including Vβ8 for 45 minutes at 4°C. Cells were washed 2X with FACS buffer and resuspended in a pool of anti-mouse TCR Vβ-

FITC antibodies (10 µl per reaction for each antibody, **Table S2.3**). Note that Vβ8.1/2 and Vβ8.3-FITC antibodies were excluded from the pooled TCR Vβ master mix. All samples were resuspended in FACs buffer and 100 µl of Countbright Absolute Counting Beads (Thermo Fisher). Cells were acquired with a Fortessa 1770 or Fortessa X-20 using Facs Diva software (BD Biosciences). Data were analyzed using FlowJo software (version 10).

2.4.13 Intracellular cytokine staining

Splenic mononuclear cells were activated *in vitro* with Msln or gp33 peptide (10 g/ml) or anti-CD3 + anti-CD28 as described above with rhIL-2 (10 ng/µl, Peprotech). On day 6 post activation, 1 x 10^5 effector T cells were centrifuged and resuspended with congenic (CD45.1+) pulsed with titrating concentrations of peptide-pulsed splenocytes at a 5:1 APC to T cell ratio. Cells were incubated in round-bottom 96-well plates in a total volume of 200 µl of T cell media + Golgiplug + Golgistop (BD Biosciences) for 5 hours at 37°C, 5% CO_2. Cells were centrifuged, and resuspended in cell surface antibodies including CD45.1 to exclude APCs and additional antibodies (**Table S2.2**) diluted in FACs buffer and incubated for 30 minutes in the dark at 4°C. Cells were washed 2X with FACs buffer, fixed and permeabilized (BD Biosciences Fixation Kit) and incubated with antibodies specific to IFNγ and TNFα diluted in permeabilization buffer overnight in the dark at 4°C. Cells were washed 2X and resuspended in FACs buffer and 100 µl of Countbright Absolute Counting Beads (Thermo Fisher). Acquisition was performed using a Fortessa 1770 or Fortessa X-20 using FACs Diva software (BD Biosciences). Data were analyzed using FlowJo software (version 10).

2.4.14 Cell Proliferation Assay

Live mononuclear splenocytes were counted using a hemocytometer and trypan blue exclusion. 2 x 10^6 splenocytes were incubated with 5 μM Cell Trace™ Violet (CTV) (Invitrogen) diluted in PBS and incubated for 20 minutes in the dark at 37°C, 5% CO_2. Cells were washed 4X with RPMI-10 to remove excess CTV and 7.5 x 10^5 CTV labeled splenocytes were plated in duplicate in 96-well round bottom plates in T cell media with 10-fold serial dilutions of gp33 or Msln peptide ± 10 ng/μl of rhIL-2. Cells were incubated in the dark for 3 days at 37°C, 5% CO2, stained for various cell surface markers and analyzed by flow cytometry. In Fig. 8i, duplicate plates were also set up in which Golgiplug + Golgistop (BD Biosciences) were added for 5 hours prior to cell surface staining, washing, fixing and intracellular staining for IFNγ as above. Data was acquired in the Center for Immunology on a Fortessa 1770 or Fortessa X-20 using FACs Diva software (BD Biosciences). Data were analyzed using FlowJo software (version 10).

2.4.15 ViSNE analysis

ViSNE analysis was performed by gating on total live T cells with default settings of 1000 iterations, 30 perplexity and theta of 0.5 using Cytobank software.

2.4.16 Msln406-414:H-2Db tetramer production

H-2D^b-restricted biotinylated monomer was produced by incubating Msln$_{406-414}$ peptide with purified H-2D^b and β2m followed by purification via Fast Protein Liquid Chromatography system (Aktaprime plus, GE health care) similar to as described[230]. Biotinylated monomer was conjugated to streptavidin R-APC or R-BV421 (Invitrogen) to produce fluorescent Msln$_{406-414}$/H-2D^b tetramer.

2.4.17 Cell numbers normalized to tissue gram.

The number of live CD45+ cells collected per tissue was determined by FlowJo analysis software and the equation: # CD45+ cells per tube (n) = (# Beads/# Cells) x (Concentration of beads x Volume of beads added). Total number of cells collected from the entire single cell suspension was determined by multiplying n by total number of stains. Cell numbers were normalized to tissue weight or organ as indicated.

2.4.18 Immunofluorescence

Tissues were embedded in OCT (Tissue-Tek) and stored at −80°C. 7 μm sections were cut using a Cryostat and fixed in acetone at −20°C for 10 min. Sections were rehydrated with PBS + 1% bovine serum albumin (BSA) and incubated for 1 hr with primary antibodies to rat anti-mouse Msln (MBL, B35, 1:100) diluted in PBS + 1% BSA at rt. Slides were washed 3X in PBS + 1% BSA and incubated with anti-rat AF546 (Invitrogen, 1:500) for 1 hr in the dark at room temperature. Stained slides were then washed 3X with PBS + 1% BSA, washed 3X with PBS, and mounted in DAPI Prolong Gold (Life Technologies). Images were acquired on a Leica DM6000 epifluorescent microscope at the University of Minnesota Center for Immunology using Imaris 9.1.0 (Bitplane).

2.4.19 Statistical Analysis

For power of 80%, the level of significance was set at 5%, 3-6 mice in each group were estimated and no data were excluded. Data are a minimum of 2 independent experiments.

Data were compiled using Microsoft Excel (v16.15.1) and all statistical analyses were conducted using Prism (version 9.0). Appropriate statistical methods were used to calculate significance as described in the figure legends. Unpaired, two-tailed student's T test was used to compare 2-group data unless otherwise indicated. One-way analysis of variance (ANOVA) and Tukey post-test were used for >2-group data. In Figure 8 panels e, f, and i, significance was determined by a unpaired T-test with Welch correction a false discovery rate (FDR) of 1% and a two-stage step-up[205]. Graphed data are presented as mean ± standard error of the mean (S.E.M.) unless otherwise indicated and $p<0.05$ was considered significant. *$p<0.05$, **$p<0.005$, ***$p<0.0005$, and ****$p<0.0001$.

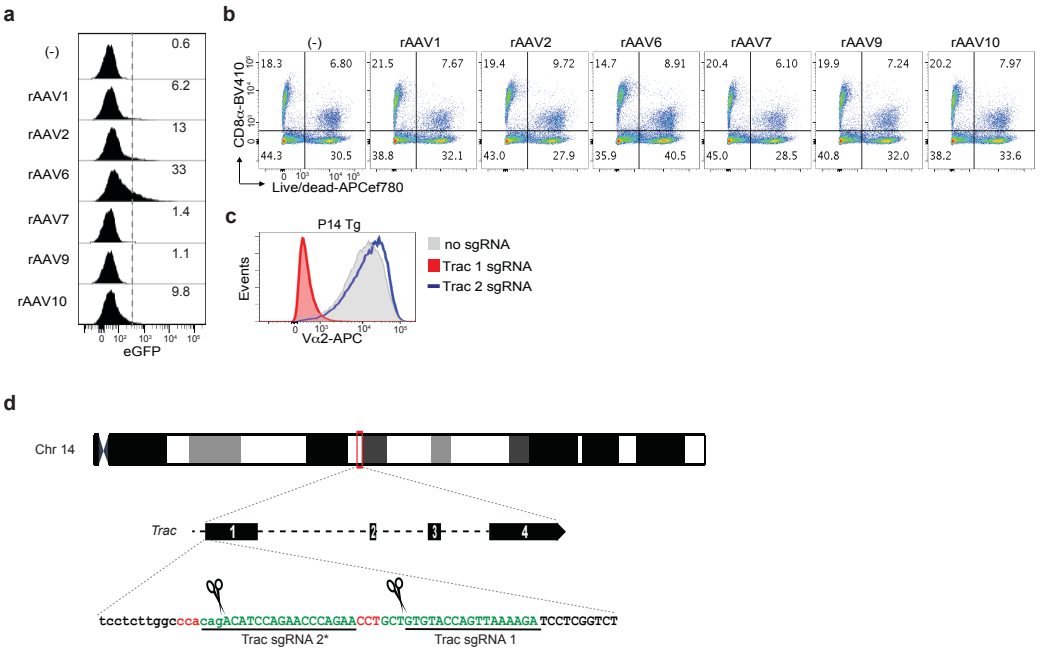

Fig S2.1. Characterization of rAAV serotype infection efficiency and *Trac* sgRNAs in primary activated murine T cells.

a rAAV-eGFP serotype infection efficiency in primary activated murine CD8+ T cells. Representative of 2 independent experiments. **b** Representative plots showing viability of rAAV-GFP infected T cells on day 3 post rAAV infection, which is day 5 post T cell activation. Representative of 2 independent experiments. **c** Vα2 expression in activated P14 T cells on day 3 post electroporation with *Trac*1 or *Trac*2 sgRNAs complexed to Cas9 RNP. *Trac* 2 sgRNA failed to interfere with transgenic TCR expression indicating it cuts outside of *Trac*. **d** Representation of *Trac1* and *Trac2* sgRNAs on murine chromosome 14.

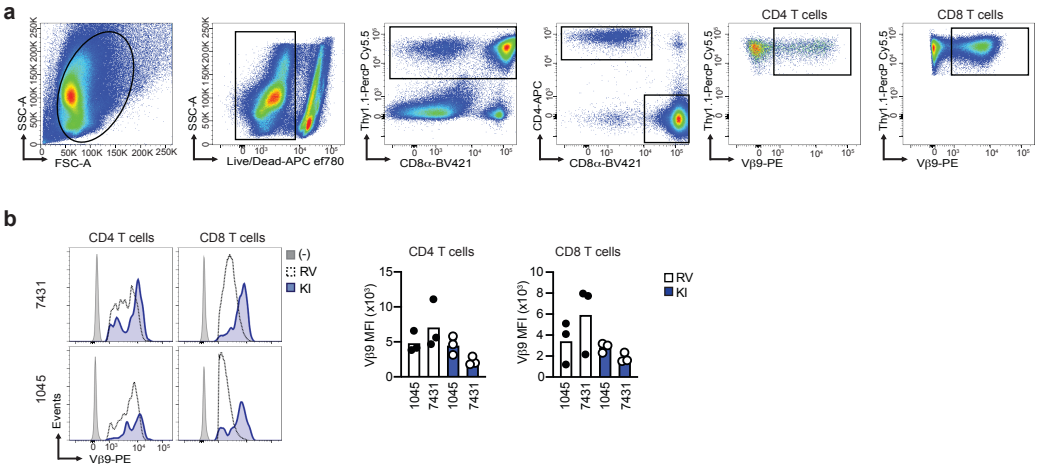

Fig S2.2. Comparison of retrovirally transduced T cells to CRISPR/Cas9 + rAAV6 *Trac*-targeted TCR knock-in T cells.

a Representative gating strategy for analysis TCR engineered T cells. **b** Representative histogram overlays (left) and mean fluorescence intensity (MFI, right graphs) following the retrovirally transduced (RV) or TCR knock-in (KI) approaches. **c** MFI is gated on CD4+Vb9+ or CD8+ Vb9+ T cells. Data are mean ± S.E.M. and are pooled from 2 independent experiments.

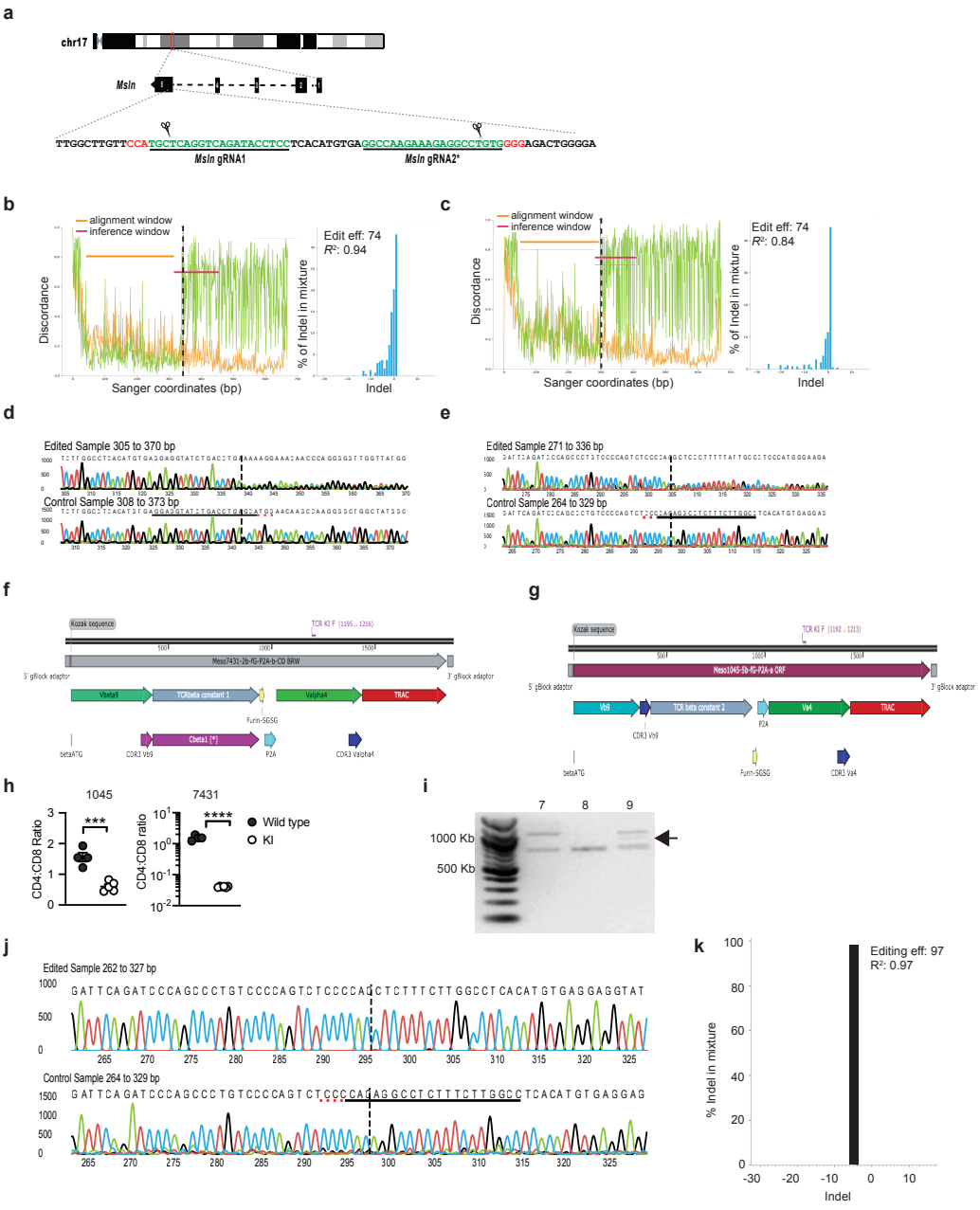

Fig S2.3. Generation of low and high affinity Msln-specific TRex mice that lack *Msln*.
a Simplified schematic of the 2 Msln-specific sgRNAs tested. Sanger sequencing and ICE analysis of 3T3 cells electroporated with *Msln* sgRNA #1 (**b**) or *Msln* sgRNA #2 (**c**) complexed with Cas9 RNP. Editing efficiency was determined by ICE analysis (https://ice.synthego.com/#/). Representative sequences of 3T3 cells that were nucleofected with Cas9 RNP complexed with Msln sgRNA #1 (**d**) or sgRNA #2 (**e**). Genetic maps of the 7431 TCR (**f**) and 1045 TCR (**g**). **h** CD4:CD8+ T cell ratio in the blood of 1045 and 7431 TRex F0 pups. n=4-6 biologically independent animals. **i** Magnified junction PCR results from 7431 TRex mice (#7-#9) showing an unexpected band in mouse #9 (see Fig. 3i). **j** Representative *Msln* exon 4 sequence from a 7431$^{+/+}$*Msln*$^{-/-}$ TRex mouse. **k** Percent indels in *Msln* exon 4 from j.

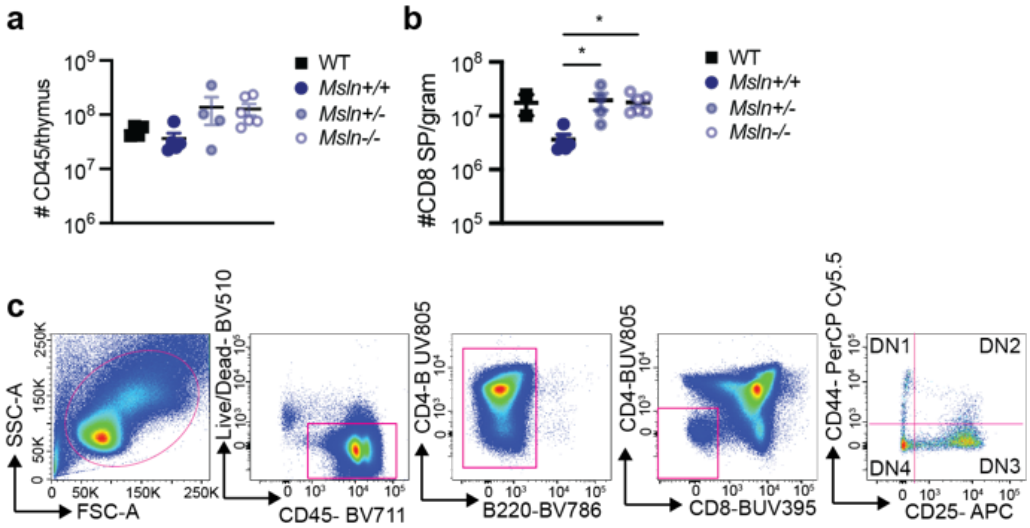

Fig S2.4. Thymocyte development in 1045 TRex mice with decreasing *Msln*.
a Number of CD45+ cells per thymus. Data are mean ± S.E.M. n=4-6 biologically independent animals. **b** Number of CD8+ SPs per thymus gram. Data are mean ± S.E.M. *p<0.05. One-way ANOVA with a Tukey's posttest was performed among the three 1045 cohorts which included n=4-6 biologically independent animals. WT, n=2 biologically independent animals. **c** Representative gating strategy for DN stage analysis. Note that the doublet exclusion gate is not shown.

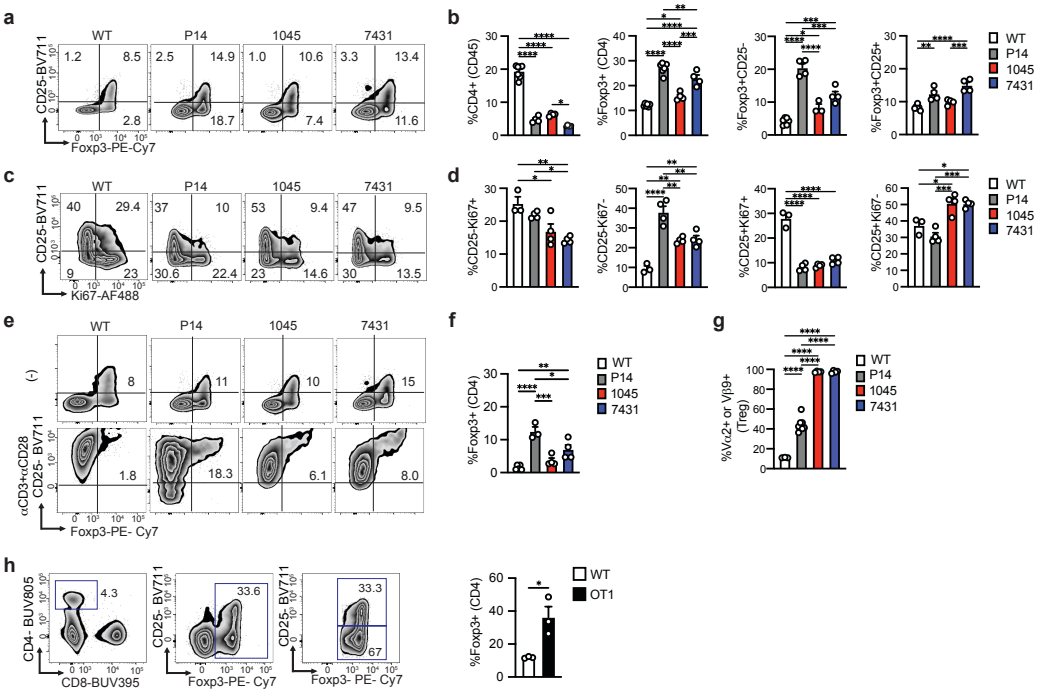

Fig S2.5. Bias toward Tregs in historical MHC class I TCR transgenic mice is obviated in TRex mice. 1045 and 7431 TRex mice are *Msln-/-* in all panels. **a** Representative plots gated on live CD4+CD3+ T cells. **b** Quantified data from a. Data are mean ± S.E.M. n=4-7 biologically independent animals per group. **p*<0.05, ***p*<0.005, ****p*<0.0005, and *****p*<0.0001. One-way ANOVA with a Tukey's posttest. **c** Representative Ki67 and CD25 plots are gated on live CD4+Foxp3+ splenic T cells. **d** Quantified data from c, gated on Foxp3+ Treg. Data are mean ± S.E.M. n=3-4 biologically independent animals per group. **p*<0.05, ***p*<0.005,****p*<0.0005, and *****p*<0.0001. One-way ANOVA with a Tukey's posttest**.** **e** Representative flow plots gated on CD4+ T cells on day 6 ± *in vitro* activation. **f** Quantification of e. Data are mean ± S.E.M. n=3-5 biologically independent animals per group. **p*<0.05, ***p*<0.005, and ****p*<0.0005. One-way ANOVA with a Tukey's posttest. **g** Proportion of CD4+Foxp3+ T cells that express Vα2 (binds P14 TCR) or Vβ9 (binds 1045 and 7431 TCR) on day 6 post activation. n=3-7 biologically independent animals. One-way ANOVA with a Tukey's posttest**.** *****p*<0.0001. **h** Gating strategy and frequency of Foxp3+ Tregs from representative OT1 TCR transgenic spleen and quantified data (right). Data are mean ± S.E.M. n=3 biologically independent animals per group. **p*<0.05. Unpaired two-tailed Student's t test.

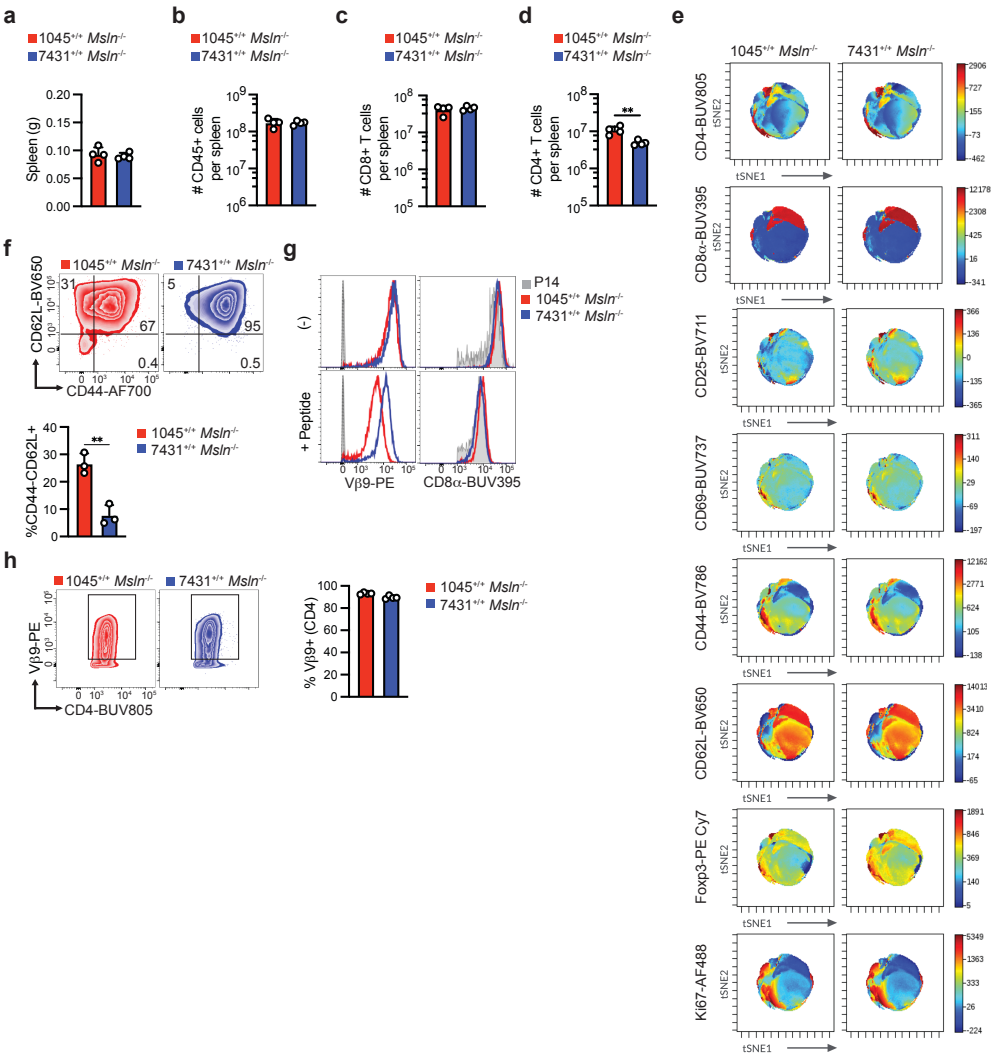

Fig S2.6. Comparison of low and high affinity T cells from TRex Msln-/- mice.
a Spleen weight in grams (g). Data are mean ± S.E.M. n=4 biologically independent animals per group. **b** Number of CD45+ immune cells per spleen. Data are mean ± S.E.M. n=4 biologically independent animals. **c** Number of CD8+ T cells per spleen. Data are mean ± S.E.M. n=4 biologically independent animals. **d** Number of CD4+ T cells per spleen. Data are mean ± S.E.M. n=4 biologically independent animals. $^{**}p<0.005$. Unpaired two-tailed Student's t test. **e** ViSNE analysis of total CD45+ splenocytes was generated using Cytobank. **f** Representative CD44 and CD62L staining on day 6 post *in vitro* activation with Msln406-414 peptide and recombinant IL-2. Data are quantified below as mean ± S.E.M. n=3 biologically independent animals. $^{**}p<0.005$. Unpaired two-tailed Student's t test. **g** Representative Vβ9 and CD8α staining gated on *in vitro* expanded effector T cells. P14 Tg T cells were treated identically to TRex T cells and used as a negative control for Vβ9 staining. **h** Representative plots gated on CD4+ T cells (left) and proportion of CD4+ T cells that express Vβ9. Data are mean ± S.E.M. n=4 biologically independent animals.

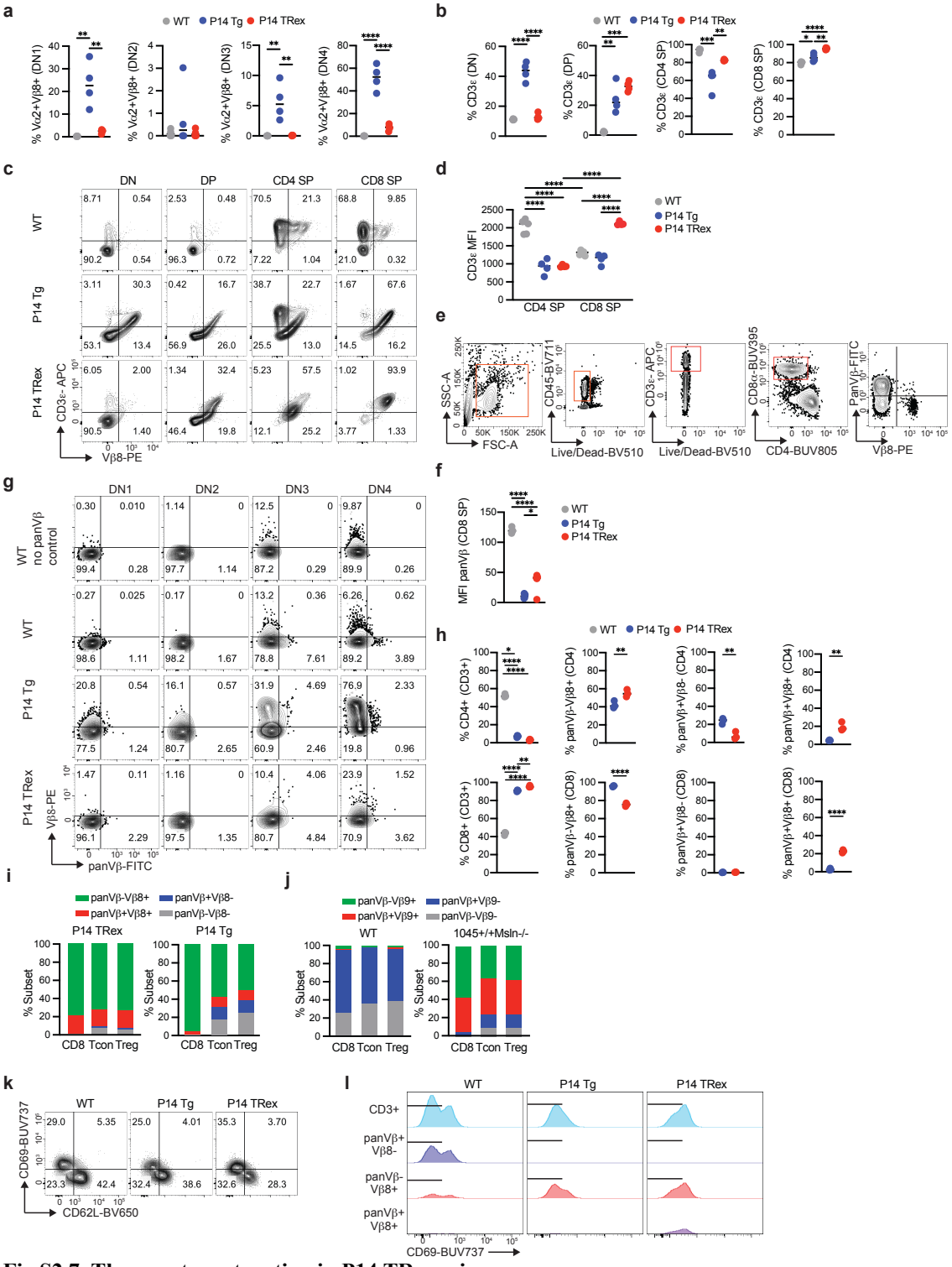

Fig S2.7. Thymocyte maturation in P14 TRex mice.

a Frequency of thymocytes in DN1, DN2, DN3 or DN4 that express Vα2 and Vβ8. n=4 biologically independent animals. **p<0.005, and ****p<0.0001. One-way ANOVA with a Tukey's posttest**. b** Frequency of DN1, DN2, DN3 or DN4 thymocytes that express CD3ε. n=4 biologically independent animals. *p<0.05, **p<0.005, ***p<0.0005, and ****p<0.0001. One-way ANOVA with a Tukey's posttest. **c**

Representative CD3ε and Vβ8 staining among the indicated thymocyte developmental stage. **d** CD3ε mean fluorescence intensity (MFI) of CD4+ or CD8+ SP thymocytes. n=4-5 biologically independent animals. ****p<0.0001. One-way ANOVA with a Tukey's posttest**. e** Simplified gating strategy for detecting dual TCR Vβ expressing cells. Note that an additional gate for excluding doubles is not shown. **f** PanVβ MFI of CD8+ SP thymocytes. n=4 biologically independent animals. *p<0.05 and ****p<0.0001. One-way ANOVA with a Tukey's posttest**. g** Representative Vβ8 and panVβ staining gated on thymocyte DN1-DN4 stages. **h** Frequency of CD4+ (top row) or CD8+ (bottom row) T cells in peripheral blood that express the exogenous (Vβ8) and/or endogenous Vβ. n=3 biologically independent animals. *p<0.05, **p<0.005, and ****p<0.0001. One-way ANOVA with a Tukey's posttest**. i** Mean proportion of circulating CD8+ T cells, CD4+ Foxp3- conventional T cells (Tcon) or CD4+Foxp3+ Treg that express a single or multiple Vβ from P14 TRex or P14 transgenic (Tg) mice. Data are mean of n=3 biologically independent animals per group. **j** Mean proportion of circulating CD8+ T cells, CD4+Foxp3- conventional T cells (Tcon) or CD4+Foxp3+ Treg that express a single or multiple Vβ from wild type (WT) or $1045^{+/+}$*Msln*$^{-/-}$ TRex mice. n=3 mice per group. **k** Representative CD69 and CD62L staining among CD3+CD8+ SP thymocytes. **l** Representative CD69 staining gated on the indicated CD3+CD8+ SP thymocyte subset.

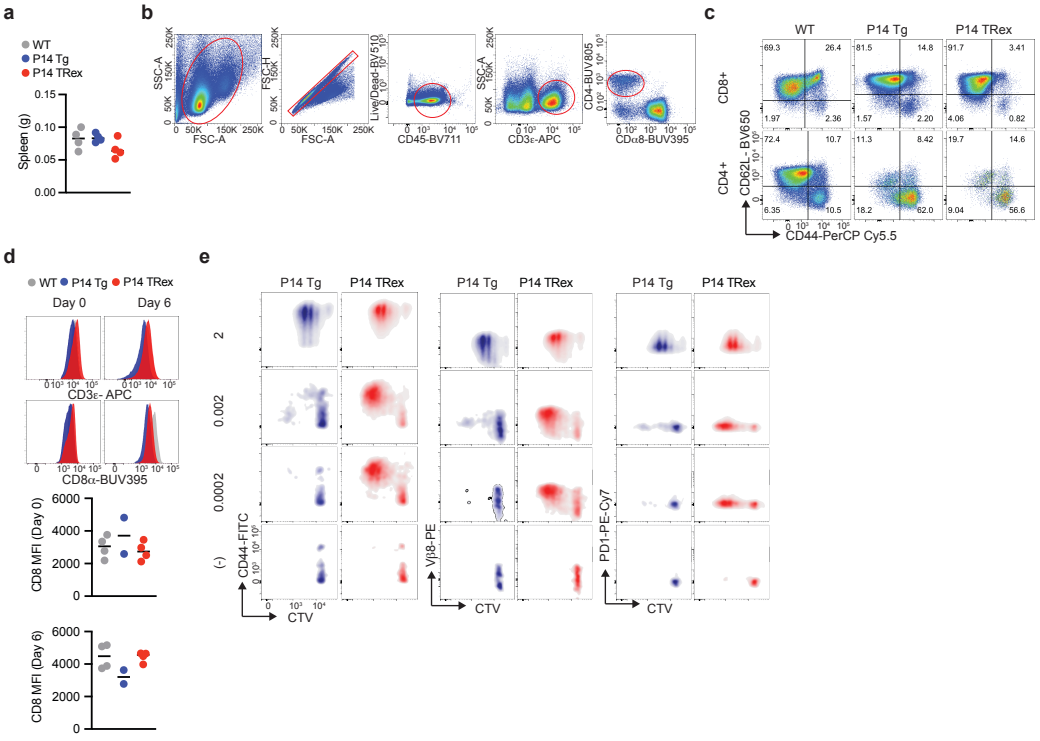

Fig S2.8. Targeting the P14 TCR to Trac enhances antigen sensitivity.
a Spleen weight in grams (g). Data are mean ± S.E.M. n=4 mice per group. **b** Representative gating schematic for splenic T cell analysis. **c** CD62L and CD44 staining to distinguish naïve/effector/memory phenotype gated on CD8+ or CD4+ T cells. **d** Histograms gated on CD8+ T cells either ex vivo (day 0) or 6 days post activation. CD8α MFI at both timepoints is quantified below. n=2-4 biologically independent animals per group. **e** Proliferation and phenotype gated on CD8+ T cells 3 days post activation with gp33 peptide without exogenous IL-2.

#	ID	Sex	P14[&]	%CD8[Φ]	%Vβ8 (CD8)	%CD4	%Vβ8 (CD4)
1	7043	F	-/-	n.d.	n.d.	n.d.	n.d.
2	7044	F	-/-	n.d.	n.d.	n.d.	n.d.
3	7045	F	-/-	n.d.	n.d.	n.d.	n.d.
4	7046	F	-/-	n.d.	n.d.	n.d.	n.d.
5	7047	F	+/-	29.6	99.2	1.15	48.6
6	7048	M	-/-	n.d.	n.d.	n.d.	n.d.
7	7049	F	-/-	n.d.	n.d.	n.d.	n.d.
8	7050	F	+/-	31.3	99.5	0.74	52.3
9	7051	F	-/-	n.d.	n.d.	n.d.	n.d.
10	7052	F	-/-	n.d.	n.d.	n.d.	n.d.
11	7053	M	-/-	11.7	6.27	19.2	5.07
12	7054	M	-/-	n.d.	n.d.	n.d.	n.d.
13	7055	M	-/-	1.19	1.9	1.7	1.07
14	7056	M	-/-	n.d.	n.d.	n.d.	n.d.
15	7057	F	-/-	n.d.	n.d.	n.d.	n.d.
16	7058	F	-/-	n.d.	n.d.	n.d.	n.d.
17	7059	F	+/-	n.d.	n.d.	n.d.	n.d.
18	7060	F	n.r.	11	6.97	16.4	4.83
19	7061	F	-/-	n.d.	n.d.	n.d.	n.d.
20	7062	M	+/-	30.1	91.7	6.32	21
21	7063	M	-/-	10.5	9.39	19.2	5.68
22	7064	F	-/-	n.d.	n.d.	n.d.	n.d.
23	7065	F	-/-	n.d.	n.d.	n.d.	n.d.
24	7066	F	-/-	n.d.	n.d.	n.d.	n.d.
25	7067	F	-/-	n.d.	n.d.	n.d.	n.d.
26	7068	F	+/+	n.d.	n.d.	n.d.	n.d.
27	7069	M	+/-	23.8	98.2	1.03	25.1
28	7070	M	+/+	29.8	95.8	3.72	18.4
29	7071	M	+/+	35	90.9	7.23	8.74
30	7072	M	n.r.	5.68	4.12	4.92	2.38
31	7073	M	+/-	27.1	95.5	2.34	36.1
32	7074	M	n.r.	11.4	7.97	14.5	4.41
33	7075	M	+/+	30.3	95	4.41	6.32
34	7076	M	-/-	n.d.	n.d.	n.d.	n.d.
35	7077	F	-/-	n.d.	n.d.	n.d.	n.d.
36	7078	M	-/-	n.d.	n.d.	n.d.	n.d.
37	7079	M	-/-	n.d.	n.d.	n.d.	n.d.
38	7080	M	+/+	25.1	98.1	0.9	55
39	7081	M	+/+	30.3	96.5	4.77	35.3
40	7082	M	+/-	30.9	96.3	3.36	26.2
41	7083	M	+/-	33	95.4	3.58	5.55
42	7084	F	+/-	26	99.1	0.75	55.3
43	7085	F	+/-	26.2	98.8	1.06	35
44	7086	F	-/-	9.71	7.54	14.4	5.16
45	7087	M	n.r.	23	98.7	1.29	33.2
46	7088	M	n.r.	10	6.54	16.3	4.41
47	7089	M	+/-	18.2	97.9	0.64	47.5
48	7090	M	n.r.	11.1	6.05	15.3	4.27
49	7091	M	+/-	25.7	97.9	1	53.5
50	7092	F	n.r.	11.3	7.6	13.4	4.76
51	7093	M	n.r.	31.1	91.2	6.84	5.97
52	7094	M	+/-	28	81.1	9.9	17.1

Table S2.1. Genomic and flow cytometric analysis of TCR expression in P14 TRex mice.
[&]P14 TCR *Trac* knock-in was determined by junction PCR of isolated tail DNA from pups; n.r., no results, sequence analysis was attempted but data were inconclusive.[Φ]n.d., not determined

Virus	Total # zygotes	# 2-cell embryos	# 1-cell embryos	# Lysed zygotes	# Pseudopregnant CD-1 females	# Pups
1045	91	61	27	3	2	15
7431	256	206	43	7	4	13
P14	471	235	226	10	8	52

Table S2.2. Summary of zygote engineering using CRISPR/Cas9.

Target	Fluorophore	Clone	Vendor	Cat no.	Lot #	Dilution
CD16/32	Purified	2.4G2	Tonbo Biosciences	70-0161-U500	D0161070920704	1:100
CD28 (for T cell activation)	Purified	37.51	BD Biosciences	553294	1039453	1:1000
CD3ε (for T cell activation)	Purified	145-2C11	BD Biosciences	553057	1307189	1:1000
CD24	FITC	M1/69	BD Biosciences	553261	8071818	1:100
CD25	BV711	PC61	BioLegend	102049	B359380	1:100
CD25	APC	PC61	BioLegend	102012	1284406	1:100
CD3ε	BV650	145-2C11	BD Biosciences	564378	B350667	1:100
CD3ε	PE-Cy7	145-2C11	BD Biosciences	56110	2489229	1:100
CD3ε	APC	145-2C11	Tonbo Biosciences	20-0031-U100	C0031081215203	1:100
CD4	APC	RM4-5	BD Biosciences	557681	7045882	1:100
CD4	BUV805	GK1.5	BD Biosciences	612900	1134156	1:100
CD44	PerCP/Cy5.5	IM7	BioLegend	103032	B333710	1:100
CD44	AF700	IM7	BioLegend	103026	B345604	1:100
CD44	BV786	IM7	BioLegend	103059	B357479	1:100
CD44	FITC	IM7	BioLegend	103006	B156153	1:100
CD45	BV711	30-F11	BD Biosciences	563709	1076257	1:100
CD45.1	APC/Cy7	A20	eBiosciences	47-0453-82	E10196-1636	1:100
CD45R/B220	BV786	RA3-6B2	BD Biosciences	563894	8250698	1:100
CD62L	BV650	MEL-14	BioLegend	104453	B324616	1:100
CD69	BUV737	H1.2F3	BD Biosciences	612793	1159821	1:100
CD8α	BUV395	53-6.7	BD Biosciences	563786	1207296	1:100
CD8α	BV421	53-6.7	BioLegend	100737	B284315	1:100
FoxP3	PE/Cy7	FJK-16s	Invitrogen	25-577382	2254250	1:75
IFNγ	APC	B27	BD Biosciences	554702	4031676	1:100
Ki67	AF488	B56	BD Biosciences	561165	1133448	1:75
Live/Dead	APC ef780	N/A	Tonbo Biosciences	13-0865-T100	D0865031422133	1:500
Live/Dead	BV510	N/A	Tonbo Biosciences	13-0870-T100	D0870111920133	1:1000
PD-1	PE-Cy7	J43	eBiosciences	25-9985-82	E15003-107	1:100
TCR βchain	BUV737	H57-597	BD Biosciences	564799	1069239	1:100
TCR Vβ8.1/8.2	PE	KJ16	eBiosciences	12-5813-80	E028050	1:100
TCR Vβ9	PE	MR10-2	BioLegend	139804	B252004	1:100
Thy1.1	PerCP/Cy5.5	Ox-7	BioLegend	202516	B234918	1:100
TNFα	BV711	MP6-XT22	BioLegend	506349	B361002	1:100
Vα2 TCR	APC	B20.1	BD Biosciences	560622	1308849	1:200
BD Mouse Vβ TCR screening panel KIT	FITC		BD Biosciences	557004	2140903	Pre-diluted
Vβ2 TCR (from screening kit)	FITC	B20.6	BD Biosciences	51-01634L	2098555	Pre-diluted
Vβ3 TCR (from screening kit)	FITC	KJ25	BD Biosciences	51-01404L	2098551	Pre-diluted
Vβ4 TCR (from screening kit)	FITC	KT4	BD Biosciences	51-01934L	2098568	Pre-diluted
Vβ5.1/5.2 TCR (from screening kit)	FITC	MR9-4	BD Biosciences	51-01354L	2098546	Pre-diluted
Vβ6 TCR (from screening kit)	FITC	RR4-7	BD Biosciences	51-01364L	2098547	Pre-diluted
Vβ7 TCR (from screening kit)	FITC	TR310	BD Biosciences	51-01424L	2098553	Pre-diluted
Vβ9 TCR (from screening kit)	FITC	MR10-2	BD Biosciences	51-01384L	2098549	Pre-diluted
Vβ10b TCR (from screening kit)	FITC	B21.5	BD Biosciences	51-01644L	2098556	Pre-diluted
Vβ11 TCR (from screening kit)	FITC	RR3-15	BD Biosciences	51-01374L	2098548	Pre-diluted
Vβ12 TCR (from screening kit)	FITC	MR11-1	BD Biosciences	51-01684L	2098557	Pre-diluted
Vβ13 TCR (from screening kit)	FITC	MR12-3	BD Biosciences	51-01394L	2098550	Pre-diluted
Vβ14 TCR (from screening kit)	FITC	14-2	BD Biosciences	51-01564L	2098554	Pre-diluted
Vβ17a TCR (from screening kit)	FITC	KJ23	BD Biosciences	51-01414L	2098552	Pre-diluted

Table S2.3. Antibodies used for flow cytometry and *in vitro* T cell activation.

2.5. Publications and Contributions:

Chapter modified with permission from the following published article:

Rollins, M.R., Raynor, J.F., Miller, E.A. *et al.* Germline T cell receptor exchange results in physiological T cell development and function. *Nat Commun* **14**, 528 (2023). https://doi-org.ezp3.lib.umn.edu/10.1038/s41467-023-36180-1

B.S.M., B.R.W., and I.M.S. conceptualized the study. I.M.S. and M.R.R. designed experiments. M.R.R. executed the experiments. B.R.W. designed rAAV TCR vectors and assisted with zygote engineering protocol. W.S.L. assisted with TCR vector generation. J.F.R. developed the TCR *Trac* knock-in protocol in murine primary T cells and the junction PCR. E.J.S. performed the Msln immunofluorescent staining of tissues. M.R.R and E.A.M. managed the maintenance and genotyping of the TRex colonies. E.A.M. and J.Z.B. performed experiments. A.L.B. assisted with F0 Blood genotyping experiments. Y.Y. performed zygote engineering. M.R.R. and I.M.S. analyzed and interpreted the data and generated the figures. M.R.R. and I.M.S. wrote the manuscript. M.R.R., B.R.W., and I.M.S. edited the final version of the manuscript. B.S.M., B.R.W., and I.M.S. secured funding. B.R.W. and I.M.S. supervised the study.

Chapter 3: Adoptive transfer of mesothelin TRex *Tgfbr2 -/-* T cells drive anti-tumor immunity in pancreatic ductal adenocarcinoma.

3.1 INTRODUCTION

Pancreatic ductal adenocarcinoma (PDA) is the third leading cause of cancer related deaths in the United States with a five year survival rate of 10% [231,232]. The incidence and mortality rate is on the rise and predicted to become the 2nd leading cause of cancer-related deaths by 2030[233]. Poor prognosis in PDA is attributed to its propensity for early metastasis, late diagnosis, and coordination of a dense stromal fibroinflammatory suppressive tumor microenvironment (TME)[114,169,231]. While immunotherapies, such as immune checkpoint blockade, have produced amazing clinical responses in many malignancies, PDA is almost always resistant[130,138,234]. Resistance is often attributed to constrained T cell access to the TME due to desmoplastic exclusion and immunosuppressive cytokines (e.g., TGFβ, IL-27, IL-10) and cells (e.g., MDSCs, CAFs, T_{regs}, TAMs) that inhibit CD8+ T cell functionality in the TME[38,110,132,181,235,236]. We have previously shown that antigen-specific T cells preferentially accumulate in primary tumors and metastasis, but still develop progressive markers of exhaustion [61,99,169,237].

Mesothelin (Msln) is a tumor-associated antigen that is highly overexpressed in PDA and other malignancies. Moreover, normal expression of Msln is generally limited with the highest levels of expression in the lining of the lungs (mesothelium) and the pericardium of the heart. The autochthonous PDA *KPC* (*Kras*$^{G12D/+}$;*Trp53*^{R172H};*p48*-Cre) mouse model is a robust predictor for therapeutic responses in patients and has been shown to overexpress Msln[176]. Our previous studies have shown that serial infusions of an engineered high affinity mesothelin specific TCR T cells (1045 TCR T cells) can infiltrate

tumors and significantly prolong survival in *KPC* mice with no apparent on target-off tissue toxicities[176]. Unsuitably, 1045 TCR T cells required serial T-cell infusions to achieve therapeutic benefit due to progressive T cell dysfunction[176]. Notably, 1045 TCR T cell function was unable to be rescued by combination immune checkpoint blockade or depletion of tumor associated macrophages[181,238]. These results suggest that 1045 TCR T cells need to be further engineered to overcome the suppressive tumor microenvironment.

Transforming growth factor beta (TGFβ) is a secreted cytokine that plays a critical role in immune homeostasis and tolerance by directly stimulating Treg expansion[41] and inhibiting generation and function of effector T cells and dendritic cells. Conversely it is central to immune suppression in tumors[38,239–241]. TGFβ signals through a heterodimeric transmembrane serine/threonine protein kinase complex composed of TGFβ receptor 1 (TGFβR1) and TGFβ receptor 2 (TGFβR2). TGFβR2 when engaged phosphorylates TGFβR1 which subsequently signals of SMADs, critical regulators of cytokine production, cell polarization, metabolism and many other pathways[242]. Thus, by knocking out TGFβR2 the entire downstream pathway is inhibited from occurring making it a very enticing target for enhancing cancer therapies [38,112,243,244].

Generation of the 1045 Msln-/- T cell receptor exchange (TRex) mice[245] provided a standardized source of naïve physiologic 1045 T cells for us to be able to test our hypothesis that TGFβ may be the significant driver of engineered T cell dysfunction in PDA. To test this hypothesis, we knocked out *Tgfbr2* using CRISPR/Cas9 in *in vitro* activated Msln-specific 1045 T cells. We identified that the abrogation of Tgfbr2 signaling in 1045 T cells increases markers of effector T cells such as Klrg1, Cxcr3, and CD44. When

transferred into *KPC*2 tumor bearing mice both *Tgbr2*-WT and *Tgbr2*-KO engineered T cells traffic to tumors and have long lasting interactions with XCR1+-cDC1s. With vaccination, the *Tgbr2*-WT and *Tgbr2*-KO T cells cause a 10-fold reduction in tumor weight at day 12 post tumor when compared to untreated and *Tgbr2*-KO T cells trend 2-fold smaller tumor weight than the *Tgbr2*-WT. Tumor infiltrating *Tgbr2*-KO cells upregulated IFNγ, TNFα, and Granzyme b and decreased markers of exhaustion PD1, Lag3 and Tox. Our studies suggest, interfering with TGFβ signaling can alter T cell fate prior to transfer and maintain this effector differentiation within the TME promoting cytotoxic Klrg1+ T cells at the expense of PD-1+ exhausted T cells leading to tumor control and *KPC* mouse survival.

3.2 Results

3.2.1 Targeting Tgfbr2 drives an early effector phenotype and Tumor cell killing by Msln-specific TRex primary murine T cells.

We previously generated and validated a methodology to target two murine Mesothelin $(Msln)_{406\text{-}414}$:H-2D^{b}-specific T cell receptor TCRs into the endogenous *Trac* locus in murine zygotes[176,245]. The high affinity Msln (1045) TCR was originally cloned from *Msln*$^{-/-}$ mice and utilized Vα4 and Vβ9[176]. These T cell receptor exchange (TRex) mice allow for a reliable and reproducible source of naïve antigen specific Msln T cells to study in a more robust manner how to enhance antitumor T cells in a suppressive pancreatic tumor microenvironment. To test the hypothesis that TGFβ is a driver of engineered T cell dysfunction in PDA[181,238,246,247], we knocked out *Tgfbr2* using CRISPR/Cas9 in *in vitro*

activated 1045 Msln$^{-/-}$ TRex T cells (**Figure 3.1A)**. Two single guide RNAs (sgRNAs) specific to the middle of *Tgfbr2* exon 3 were independently complexed to Cas9 ribonucleoprotein (RNP) and pooled to generate a 60-80% knockout efficiency as measured by Synthego intersection control evaluation (ICE) in activated 1045 *Tgfbr2-/-* T cells (**Fig. 3.1B**), using a previously described CRISPR protocol[188,245,248]. While both sgRNAs drove sufficient gene knockout, by protein, there was a log decrease in TGFβR2 on the surface of *in vivo* transferred T cells up to 6 days after CRISPR (**Fig. 3.1C**). Remaining cells expressing TGFβR2 on the surface suggests that there could be an outgrowth of unedited cells *in vivo* as TGFβR2 is quickly internalized and recycled off the cell surface[248,249]. To gain a better understanding of the phenotype and functionality of activated 1045 *Tgfbr2-/-* edited T cells were analyzed 72 hours post activation, the beginning of peak clonal T cell proliferation[250], by flow cytometry (**Fig. 3.1 D-I**). 1045 TRex mice were previously shown to have a significant skewing towards the CD8+ T cell linage due to the 1045 TCR being MHC I restricted[245]. *In vitro* culture D3 post activation showed 7 times greater CD8+ T cell population (30%) by percent over CD4+ T cells (4%) out of total CD45+ splenocytes replicating the previously reported T cell lineage skewing[245] (**Fig. 3.1 D**). 1045 *Tgfbr2-/-* cells saw slight but significant decreases in the frequency of CD8+ T cells (*Tgfbr2-/-* 25% vs WT 28%) and a slight increase in frequency of CD4+ T cells (*Tgfbr2-/-* 5% vs WT 4%) (**Fig. 3.1 D-E**). Understandably, because *Tgfbr2-/-* underwent CRISPR nucleofections 24 hours prior it is possible that these slight but significant changes in frequency of decreased CD8+ and increased CD4+ T cell populations could be due to the expected cell death arising from the protocol. Gating on CD8+ T cells, WT unlike *Tgfbr2-/-* cells fail to differentiate from naïve (CD62L+ CD44-,

31%) into CD8+ effector (CD62L- CD44+, 2%) T cells (**Fig. 3.1 F-G)**. Additionally, 43% of the CD4+ 1045 *Tgfbr2* -/- T cells in culture have differentiated into effector T cells (**Fig. 3.1 H)**. 1045 *Tgfbr2* -/- CD8+ T cells significantly downregulated CD69 (3%) while upregulating Klrg1(5%), PD-1 (20%), and CXCR3 (18%) strengthening an effector T cell phenotype. In comparison, 1045 WT cells lagged in differentiation as they lack upregulation of Klrg1 (1%), PD-1 (3%), and CXCR3 (5%) (**Fig. 3.1 I**). Similar trends were observed in CD4+ T cells but to a lesser extent (**Fig. 3.1 J**).

To assess 1045 *Tgfbr2*-/- cell functionality, we selected two different tumor cells lines, the *KPC*2 pancreatic tumor cell line[251] and E0771 breast cancer line[252], to perform an Incucyte tumor killing assay. Tumor cell lines were grown for 48 hours in tumor cell media with IFNγ to increase MHC I surface expression prior to plating for killing assay[251]. By flow cytometry, the *KPC*2 tumor cell line expressed both high intracellular and extracellular Msln protein (**Fig. 3.1 K**). While the E0771 only had intracellularly expressed Msln protein (**Fig. 3.1 K**). 1045 WT and 1045 *Tgfbr2-/-* cells were activated (**Fig 3.1 A**) and then were co-cultured with tumor cells in T cell media at a 5:1 and 20:1 T cell to tumor cell ratio (**Fig. 3.1 L)**. In the E0771 tumor line within 2 hours of co-culture 1045 T cells with and without *Tgfbr2-/-* robustly killed tumor cells by driving a negative fold proliferation (tumor cell death) (**Fig. 3.1 L**, bottom panels). By hour 46 of the killing assay, at the 5:1 ratio, the Tgfbr2-/- and 1045 WT zap only (underwent CRISPR protocol without mixing with RNPs) killed nearly 100% of the E0771 Tumor cells (**Fig. 3.1 L**, bottom panels). At 20:1 effector to tumor cell ratio, 100% of the E0771 tumor cells died in third of the time (~32 hours) (**Fig. 3.1 L**, bottom panels). 1045 *Tgfbr2-/-* cells were able to significantly control KPC2 tumor cell growth over 48 hours but, unlike the E0771 line,

elimination by WT, WT zap control, or *Tgfbr2-/-* of tumor cells was not achieved. At 20:1, 1045 WT cells were unable to control tumor cell growth and between 22-24 hours the *KPC*2 line escapes and began to proliferate in the wells. (**Fig. 3.1 L**, top panels**)**. When $Msln_{406-414}$ peptide was added into the T cell media, the 1045 T cells were able to induce negative fold proliferation in KPC2 tumor cells with the 1045 *Tgfbr2-/-* driving negative fold proliferation at the fastest time point (**Fig 3.1 L** top right panel**)**. These results suggest inherent differences in antigenicity between the two cell lines[158]. Overall, abrogation of TGFβR2 drives an early and robust effector T cell differentiation in 1045 *Tgfbr2-/-* in comparison to WT T cells but also drives significant tumor cell killing and control.

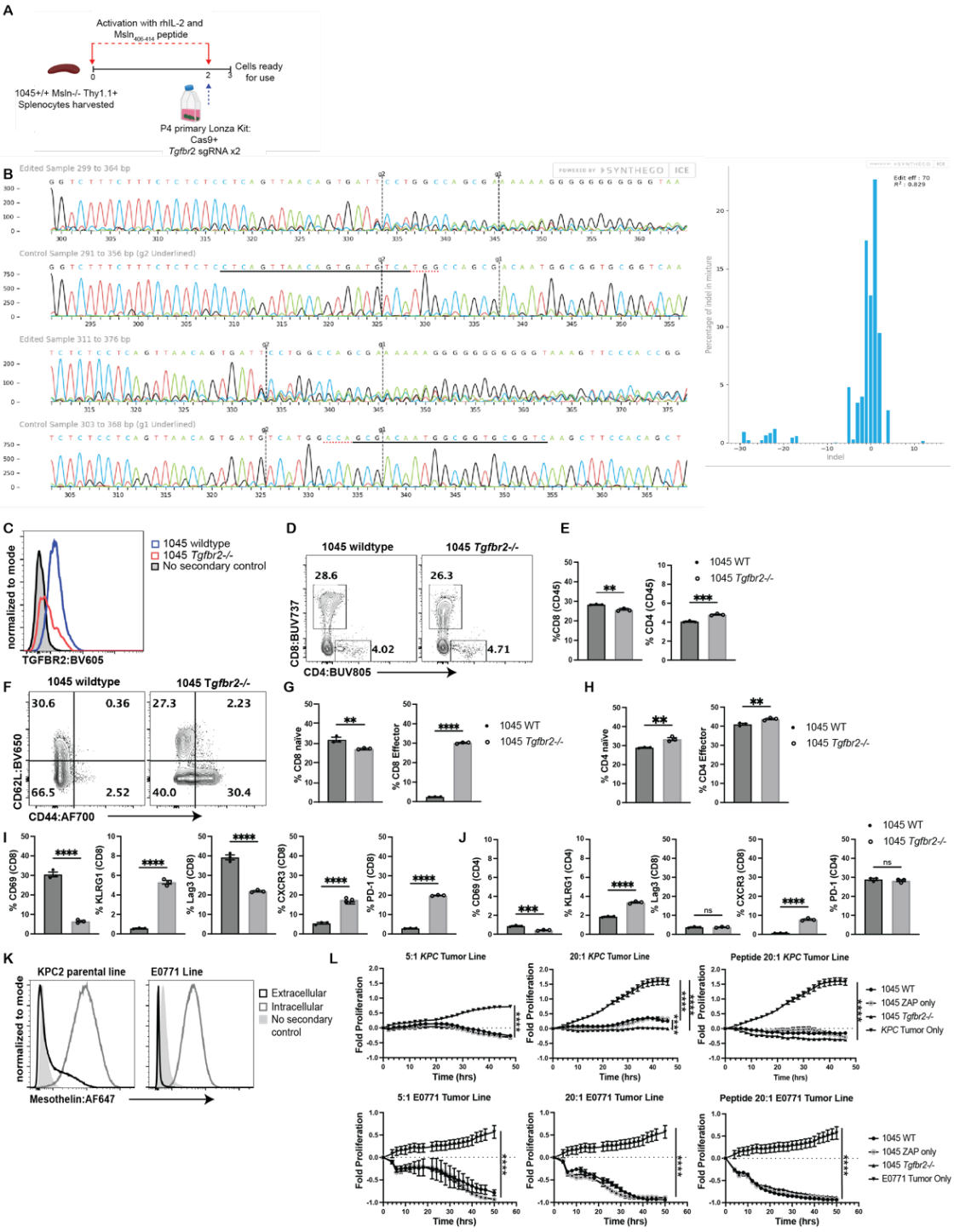

Figure 3.1. Targeting Tgfbr2 drives an early effector phenotype and tumor cell killing in 1045 TRex primary murine T cells.

A Simplified schematic of 1045 Msln-/- TRex splenocyte activation. CRISPR editing of *Tgfbr2* occurred 2 days after activation with +/- Msln$_{406-414}$ peptide and rhIL-2. **B** Representative ICE analysis of 1045 Msln-/- TRex cells electroporated with *Tgfbr2* two sgRNA (g1 and g2) complexed with Cas9. Editing efficiency was determined by ICE analysis (https://ice.synthego.com/#/). **C** Representative plot from gated on splenic

Live+CD45+CD8+ Thy1.1+ T cells isolated six days post CRISPR editing. **D** Representative plots gated on *in vitro* activation CD45+ T cells on day 3 post +/- $Msln_{406-414}$ peptide and rhIL-2, 24 hours post CRISPR editing for *Tgfbr2*. **E** Frequency of splenic CD8+ T cells (left) and frequency of CD4+ (right). **F** Representative plots gated on CD8+ T cells for naïve CD62L+ CD44- and effector CD62L-CD44+ T cell populations **G** Frequency of activated CD8+ T cells that express naïve (left) and frequency of CD8+ effector T cell phenotypes (right) **H** Frequency of activated CD4+ T cells that express naïve (left) and frequency of CD4+ effector T cell phenotypes (right) **I** Frequency of activated CD8+ T cells that express activation and T effector markers CD69 (left), Klrg1, Lag3, CXCR3, and PD-1 (right) **J** Frequency of activated CD4+ T cells that express T cell activation and T effector markers CD69 (left), Klrg1, Lag3, CXCR3, and PD-1 (right) Each dot is an independent mouse. $**p<0.005$, $***p<0.0005$, $****p<0.00001$. One-way ANOVA with a Tukey's posttest. Data are mean ± S.E.M. **K** Cell surface and intracellular expression of Msln in pancreatic cancer *KPC*2 cell line (left) and E0771 Breast cancer cell line (right) **L** KPC2 (top) and E0771 (bottom) were co-cultured with activated 1045 Msln-/- T cells +/- *tgfbr2* knock out and +/- electroporation (zap only). *KPC*2 and E0771 tumor cells were co-cultured at a 5:1 or 20:1 T cell to tumor cell ratio with a peptide media positive control. All tumor cells were treated with IFNγ for 48 hours prior to co-culture. Images are taken every two hours for a total of 48-50 hours. Fold proliferation of tumor cells is measure are shown in the graphs whereas any points above zero equal tumor proliferation and any numbers below zero indicate T cell killing. Maintenance of time points of fold proliferation at zero indicates tumor is in equilibrium with T cell response. Results are representative of three pooled biological replicates. Statistical analysis was performed using an unpaired student t-test. Data is the mean of 3 independent wells per time point ± SEM.

3.2.2 Abrogation of Tgfbr2 in antigen specific T cells maintains early effector phenotype and drives an effective early anti-tumor response in vivo.

We and others have previously showed that engineered T cells (TCR and CAR) knocked into the endogenous *TRAC* locus have been shown to have enhance functionality and resistance to T cell dysfunction[156,245]. Therefore, we hypothesized that therapeutic use of engineered 1045 *Tgfbr2*-/- TRex cells would result a highly functional and effective anti-tumor T cell response that would significantly impede T cell dysfunction in PDA. To test this hypothesis, we orthotopically implanted *KPC*2[230] tumor cells into the pancreas of WT C57BL/6J mice and treated cohorts with a congenically marked adoptive T cell therapy and harvested tissues 13 days post tumor implantation, D7 post therapy, and analyzed T cell infiltration and phenotype. We previously established a therapy protocol for administration of 1045 Msln T cells in PDA[176]. We replicated the TCR T-cell therapy protocol used in our previous study, but made a minor change by administering a more

clinically relevant TriVax vaccine[253] that included the $Msln_{406-414}$ peptide, Poly I:C adjuvant, and agonistic CD40 to expand the engineered T cells *in vivo*. Vigorous therapeutic controls were set up to account for any differences in tumor size or T cell responses that could be attributed to the vaccine or Cytoxan anti-tumor immune responses[99,109,254,255] (**Fig. 3.2 A-B**). There were trending increases in spleen weight in mice treated with 1045 TRex T cells + vaccine (**Fig. 3.2 C**). Surprisingly, any therapeutic treatment of KPC2 tumors at this timepoint led to significant decreases in tumor weight in tumor-bearing mice. Between the treated groups, there was at least a two-fold reduction in tumor size between the 1045 *Tgfbr2-/-* + vaccine group and all the other therapy-treated groups. (**Fig. 3.2 D**). 1045 *Tgfbr2*-/- + vaccine significantly increased the proportion and number of tumor-infiltrating CD8+ T cells (**Fig. 3.2 E**). There were significant decreases in total number of splenic and intratumoral CD8+ T cells in the Cytoxan only, vaccine + Cytoxan, and vaccine alone controls suggesting that the reduction in overall tumor weight may be a transient effect (**Fig. 3.2 D-E**). 1045 WT and 1045 *Tgfbr2*-/- + vaccine treated groups saw a significant decrease in intratumoral CD4 T cells. It is possible the decreased proportion and number of intratumoral CD4+ T cells is due to significant alterations in CD4+ polarization and elimination T_{regs} due to the rapid expansion and trafficking of helper CD4+ 1045 TRex cells (**Fig. 3.2 F**). Although this would require further study of CD4+ T helper subsets in this therapeutic model to better understand[47]. Critically, the TriVax vaccine is required to significantly expand adoptively transferred 1045 T cells. With vaccine, adoptively transferred engineered Thy1.1+ CD8+ T cell composed the majority of the intratumoral CD8+ T cell population (**Fig. 3.2 G-H**). Using Klrg1 and Lag3 surface markers to distinguish between effector and exhausted T cells, most 1045 *Tgfbr2*-/- T cells

found in the blood and spleen were Klrg1+ Lag3- effector phenotype in both vaccinated and unvaccinated mice (**Fig. 3.2 I-J**). Additionally, 1045 *Tgfbr2*-/- T cells highly expressed CD69, a marker of T cell activation, (**Fig. 3.2 K-L**) and regardless of TriVax vaccine were highly proliferative by Ki67+ staining in the TME (**Fig. 3.2 M**). Suggesting that the strong effector phenotype effector phenotype seen *in vitro* prior to transfer is maintained through antigen recognition in the TME[39,256]. Intriguingly though, only 20% of the intratumoral 1045 *Tgfbr2*-/- T cells + vaccine express Klrg1 but are not upregulating Lag3 (**Fig 3.2 I-J**), suggesting that these cells could be in the active process of differentiating from an effector phenotype to an exhausted phenotype. To determine if intratumoral T cells are differentiating into an exhausted phenotype, we gated on Tcf1 and PD-1 to distinguish between progenitor exhausted T cells (T_{ex}), TCF1+ PD-1+, and terminal T_{ex}, TCF1- PD-1+, populations[257–259]. 1045 *Tgfbr2*-/- in both the spleen and tumor decrease in frequency of progenitor T_{ex} and terminal T_{ex} (**Fig. 3.2 N-O**). Additionally, when looking at the actual effector functionality by cytokine and cytotoxic granzyme production, 1045 *Tgfbr2*-/- are still highly expressing IFNγ, TNFα, and Granzyme B (**Fig. 3.2 P-Q**). Overall, our results support that 1045 *Tgfbr2*-/- T cells are highly functional potent effector T cells.

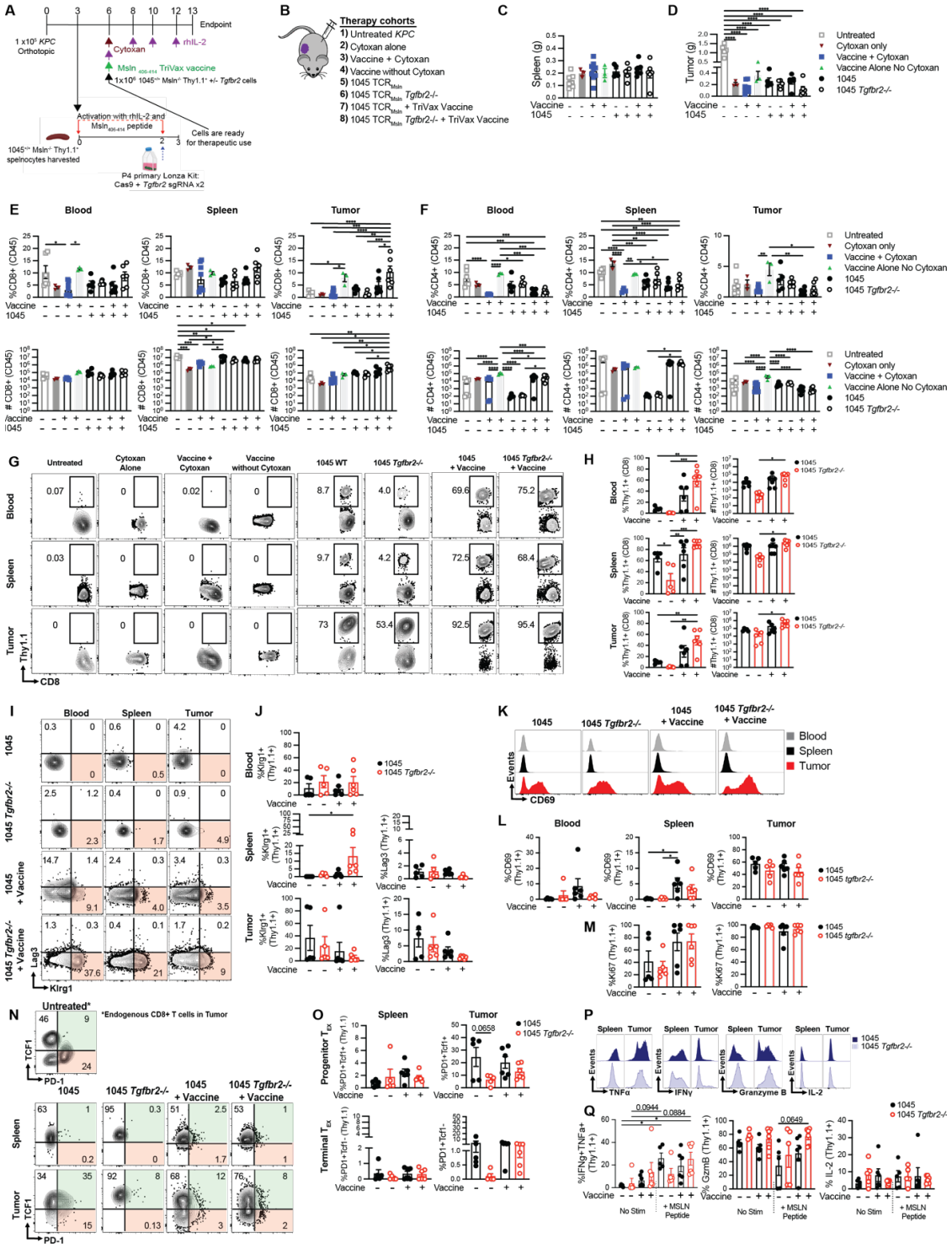

Figure 3.2. Abrogation of Tgfbr2 in antigen specific T cells maintains early effector phenotype and drives and effective early anti-tumor response in vivo.

A Experimental schematic for mice receiving orthotopic *KPC2* PDA cells, Cells for adoptive transfer were activated and edited in the same manner as **fig.3.1 A**. Therapeutic treatment began on day 6 post tumor implantation where mice received a single dose of Cytoxan to lymphodeplete 6 hours prior to the transfer of 1045 Msln$^{-/-}$ Thy1.1^{+} T cells +/-*Tgfbr2*-/-, a single dose of Msln$_{406-414}$ TriVax vaccine and rhIL-2. rhIL-2 was

given on D8,10,12 for the expansion of transferred cells. Experimental groups and controls are outlined in (**B**). All mice that received an adoptive cell transfer received Cytoxan. **C.** Orthotopic *KPC*2 spleen and Tumor **(D)** weights on day 13 post tumor, day 7 post start of therapy. Each dot is an independent animal. Data are mean ± SEM and $n = 3–9$ mice per group and 2-4 independent experiments. *$p<0.05$, **$p<0.005$, *$p<0.05$, ****$p<0.00001$ One-way ANOVA with a Tukey's posttest.
E. Frequency (top row, gated on live CD45+ cells) and number (bottom row, normalized to tissue gram) of all CD8+ T cells in blood (left), spleen (middle), and tumor (right) from controls or adoptive cell transfer immunotherapy-treated mice. **F.** Frequency (top row, gated on live CD45+ cells) and number (bottom row, normalized to tissue gram) of all CD4+ T cells in blood (left), spleen (middle), and tumor (right) from controls or adoptive cell transfer immunotherapy-treated mice. Data are mean ± SEM and $n = 3–9$ mice per group and 2-4 independent experiments. *$p<0.05$, **$p<0.005$, *$p<0.05$, ****$p<0.00001$ One-way ANOVA with a Tukey's posttest**.** Representative flow plots gated on live CD45+ Thy1.1+ CD8+ T cells. Thy1.1+ cells mark the adoptively transferred 1045 TRex T cells **H.** Quantification of Thy1.1+ cells in 1045 WT (black) and 1045 *Tgfbr2*-/- (red) cell therapy treated mice with and without vaccine from E by frequency (left) and number (right, normalized to tissue gram) in blood (top), spleen (middle), and tumor (bottom). **I.** Representative flow plots gated on Klrg1+ vs Lag3+ T cells in cell therapy treated mice in blood (left), spleen (middle), and tumor (right). **J.** Frequency of Klrg1+ (left) and Lag3+ (right) in blood (top), spleen (middle), and tumor (bottom) of I. **K.** Representative flow cytometric histograms plots gated on CD69+. **L.** Frequency of CD69+ T cells in blood (left), spleen (middle), and tumor (right). **M.** Frequency of Ki67+ proliferating T cells in 1045 WT (black) and 1045 *Tgfbr2*-/- (red) cell therapy treated mice from K in spleen (right), and tumor (left). **N.** Representative flow plots gated on TCF1+PD1+ (green) vs TCF1-PD-1+ (pink) T cells in spleen (middle) and tumor (bottom). Gating of TCF1 and PD-1 was determined by gating on Thy1.1- CD8+ T cells in the tumor of a control untreated mouse (top) **O.** Frequency of Progenitor T exhausted (TCF1+PD-1+, top) and terminal T exhausted (TCF1-PD-1+, bottom) from N in spleen (right), and tumor (left). **P.** Representative flow cytometric histograms plots gated on effector cytokines five hours post *in vitro* restimulation with $Msln_{406-414}$ in spleen (left), and tumor (right) in 1045 WT (Dark blue, top) and 1045 *Tgfbr2*-/- (Light blue, bottom) cell therapy treated mice with TriVax. Effector cytokines measure were (L-R) TNFα, IFNγ, Granzyme B, and IL-2. **Q.** Frequency of intratumoral T cell production of TNFα+ IFNγ+ (left), Granzyme B (middle), and IL-2 (right) without and with $Msln_{406-414}$ peptide restimulation. **G-Q.** Cells were first gated on live CD45+ Thy1.1+ CD8+ T cells as set in G in 1045 WT (black) and 1045 *Tgfbr2*-/- (red) cell therapy treated mice without and with TriVax Vaccine except P which only shows cell therapy treatments with vaccine. **G-Q**. Data are mean ± S.E.M. n=5-6 biologically independent animals per group. *$p<0.05$, **$p<0.005$, and ***$p<0.0005$. One-way ANOVA with a Tukey's posttest.

3.2.3 Intratumoral Dendritic cells drive maintenance of Klrg1+ effector phenotype and 1045 Tgfbr2-/- TRex migration into orthotopic KPC tumors.

Previous work from our lab showed that tumor antigenicity shapes myeloid cell composition and promotes accumulation of type 1 dendritic cells (cDC1), driven by Xcr1 signaling. Additionally, therapeutic activity of adoptive T cell therapies or immune checkpoint blockade required cDC1s to sustain functional Klrg1+ cytotoxic antitumor T cells[98]. 1045 *Tgfbr2*-/- TRex cell accumulation and Klrg1+ effector cells in the tumor suggests that this mechanism of tumor control may also occur in this model. To that extent, we first looked at the blood serum of therapy treated mice to look at systemic cytokine and

chemokine production (**Fig. 3.3 A-B**). Diagnostically, indications of a highly inflammatory anti-tumor immune response marked by increased concentrations of critical cytokines IL-12, IFNγ, TNFα, and chemokines Ccl3, Cxcl10, and Cxcl9, all of which are produced by cDC1s[44,100,260–262], was present in 1045 *Tgfbr2*-/- + vaccine treated mice. CXCR3, the receptor of CXCL9/10, was high on 1045 *Tgfbr2*-/- (**Fig. 3.1 I**) suggesting this could be the mechanism by which cDC1s drive T cell infiltration into tumor. By flow cytometry, gated on CD11c+ MHC+, Xcr1 and SIRPα surface markers distinguish the cDC1 and cDC2 dendritic cell populations, respectively (**Fig. 3.3 C**). We see that in 1045 *Tgfbr2*-/- + vaccine treated mice there is a significant increase in both frequency and number of cDC1s and cDC2s in the spleen and tumor (**Fig. 3.3 C-E**). When calculated as a total percentage of CD45+ lymphocytes, we see a significant increase in cDC1s in tumor of vaccine treated mice (**Fig. 3.3 E** right panel). Suggesting, that in combination with the T cell therapy, the TriVax vaccine is playing a critical role in shaping the myeloid compartment.

We next asked if XCR1+ cDC1s are directly interacting with 1045 TRex T cells treated with vaccine to drive the anti-tumor responses in the context of the TME. To answer this question, we performed two-photon microscopy to look directly at interactions between XCR1+ cDC1s and 1045 TRex T cells (**Fig 3.3 F-G**). XCR1-Venus mice were orthotopically implanted with mScarlet-*KPC2* PDA tumor cells into the pancreas, D6 post tumor, mice were treated (**Fig. 3.3 A**) with 1045 WT GFP+ (**Fig. 3.3 F**) or 1045 *Tgfbr2*-/- GFP+ TRex T cells + vaccine (**Fig. 3.3 G**). On D13 post tumor implantation, tumors were harvested out of mice and explanted tumors were imaged within 1 hour. Tumors were imaged over a thirty-minute period with captures occurring every 30 seconds for a total of 60 frames. Data was collected in the X, Y, and Z directions allowing for 3D imaging of the

tumor microenvironment. Imaris Software was used to perform Spots (1045 GFP+ T cells, green) and Surfaces (Xcr1-Venus, yellow) interaction analysis (**Fig 3.3 G**) as well as tracking of GFP+ T cell trafficking. As seen in fig.3.3 E, there was no significant difference between WT and *Tgfbr2-/-* cells in the number of Xcr1-venus cDC1s in the TME. Additionally, the average track speed was not significantly different from between (< 10μm/min^{-1}) WT and *Tgfbr2-/-* cells but it does indicated that both groups are activated actively scanning for antigen[263,264]. cDC1 and T cell interactions were determined to be present when a spot measured < 7μm from a surface (**Fig 3.3 G,** indicated by black arrows). When measured 1045 WT T cells are found significantly closer distance to XCR1+ cDC1s in the TME (**Fig. 3.3 J)**. This result is likely inaccurately skewed since there were over double the total number of GFP+ 1045 *Tgfbr2-/-* T cells in the TME significantly increasing the mean distance between spots and surfaces as there were more cells to be found on outer margins of the imaged tumor location. Further, there is a significant increase in the frequency of 1045 *Tgfbr2-/-* T cells and cDC1 cell-to-cell interactions within the TME and of those interactions they are longer lasting meaningful interactions (**Fig 3.3 K**). Overall, this suggest that intratumoral XCR1+ cDC1s are driving 1045 TRex T cell migration and maintenance of the Klrg1+ effector phenotype in 1045 *Tgfbr2-/-* TRex T cells in orthotopic *KPC2* tumors through direct and meaningful cell-cell interactions.

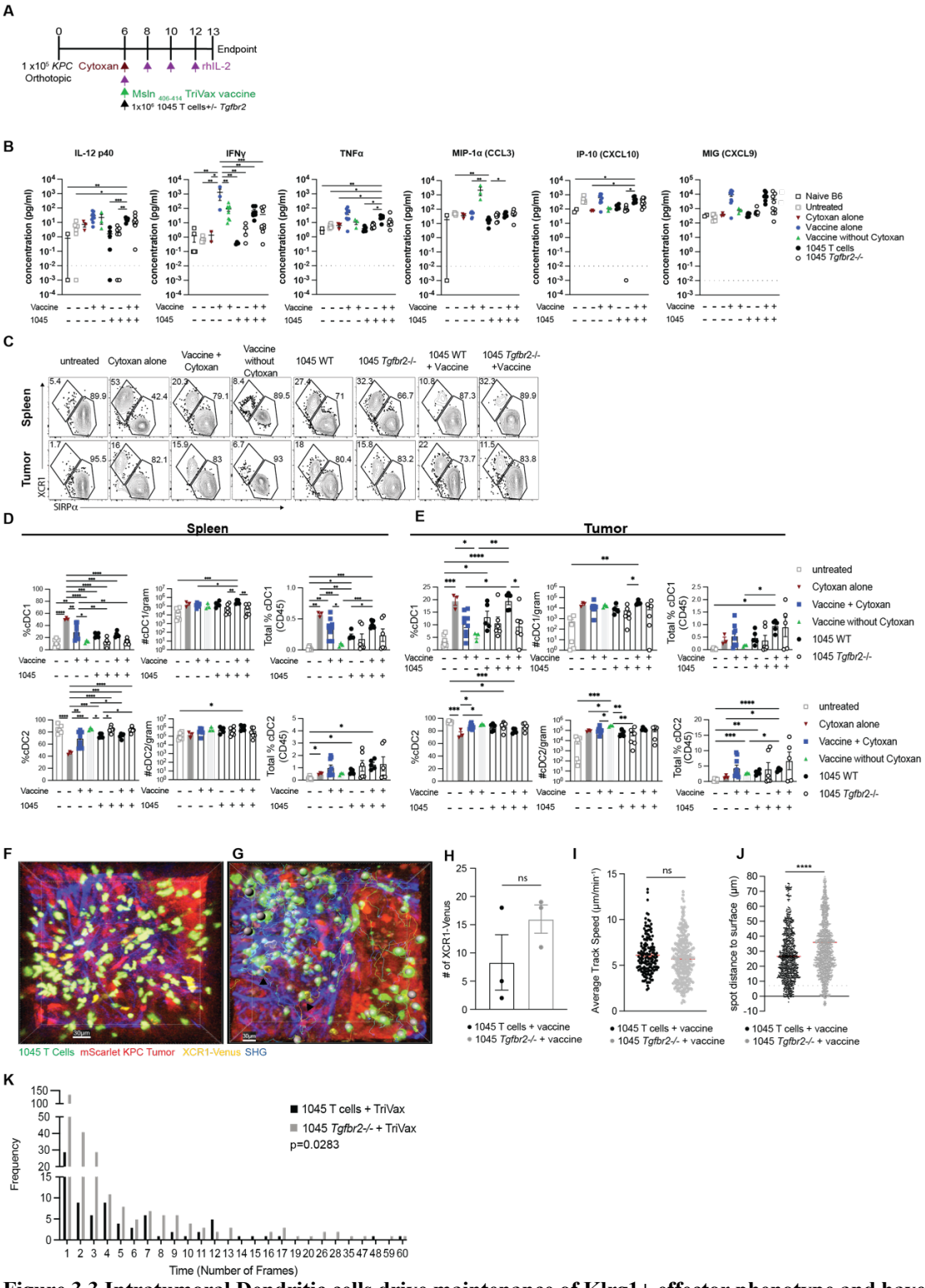

Figure 3.3 Intratumoral Dendritic cells drive maintenance of Klrg1+ effector phenotype and have meaningful interactions in orthotopic KPC tumors.

A Experimental schematic for mice receiving orthotopic KPC2 or mScarlet-KPC2 PDA cells, 1045 adoptive transfer were activated and edited in the same manner as fig.3.2 A. **B.** Serum cytokine concentration measure

by Luminex mouse XL cytokine performance screening panel. Data points that fall below 10^{-2} were considered undetectable. Data are mean ± S.E.M. n=2-6 biologically independent animals per group. *p<0.05, **p<0.005, and ***p<0.0005. One-way ANOVA with a Tukey's posttest. **C.** Representative flow plots gated on CD11c+ MHCI +. Xcr1+ cells mark cDC1s, whereas S1RPα + mark cDC2s **D.** Quantification of (C) splenic CD11c+ MHCI+ Xcr1+ cDC1s (top) and S1RPα + cDC2s (bottom) treated mice by frequency (left) and number (right, normalized to tissue gram) and frequency of cDC population of total CD45+ cells. **E.** Quantification of (C) tumor CD11c+ MHCI+ Xcr1+ cDC1s (top) and S1RPα + cDC2s (bottom) treated mice by frequency (left) and number (right, normalized to tissue gram) and frequency of cDC population of total CD45+ cells. Data are mean ± S.E.M. n=5-6 biologically independent animals per group. *p<0.05, **p<0.005, and ***p<0.0005. One-way ANOVA with a Tukey's posttest. F Representative image of two-photon on D13 post tumor implantation, from 1045 WT + vaccine treated mouse tumor. Spot and surface layers for analysis were removed to show representative fluorescence intensity after spectral unmixing. mScarlet-*KPC2* PDA tumor cells (red), Xcr1+ cDC1 (yellow), 1045 *Msln-/-* GFP+ TRex T cells (Green), Second-harmonic generation (blue) denotes collagen. **F**. Representative image of video collect from 1045 *Tgfbr2-/-* + vaccine treated mouse tumor. Spot and surface layers were generated using the Imaris analysis software. Spots (grey) were applied to the 1045 T cells and cell tracks (red--> blue) were generated to follow as an individual T cell moves within the TME over the 60 frames of imaging collection (**I**). Surfaces (yellow) were applied to the XCR1-venus+ cells (H). T cell spot distance to surfaces was in contact (**G,** black arrows) in when the center of the spot was < 7μm at all given time points, an unpaired students T Test was performer to determine significance ****p<0.00001 t=10.04, df=2787 (**J**). **K.** Length of interactions was calculated by determining the number of frames in a row a single spot was < 7μm from surface. Frequency denotes how many spots in each therapy group made contact for that given length of time i.e., 1 WT T cell and 1 *Tgfbr2-/-* T cell maintained in contact with a cDC1 the entire time of imaging. A Chi-squared test was calculated df =40.12, 25 p=0.0283

3.2.4 Serial infusions of 1045 TRex T cells with vaccination lead to significant survival in KPC Mice.

Previous work with 1045 T cells required 6 rounds of serial T cell infusions to see a significant survival benefit[238] due to progressive engineered T cell dysfunction. We hypothesized that due to the superior effector functionality, shown in the orthotopic tumor model, 1045 *Tgfbr2-/-* TRex T cells will drive a significant survival benefit with fewer rounds of therapy in the autochthonous *KPC* Model. To test this, we enrolled *KPC* mice, who spontaneously develop pancreatic cancer[265], based off of ultrasound tumor measurements of 3-6mm (50-400 mm^3) into the study where they would receive three total rounds of therapy (**Fig. 3.4 A**). 1045 TRex T cells undergo a 10-fold expansion when given with a TriVax vaccine as measured in the blood D8 after therapy (**Fig. 3.4 B**). All *KPC* mice tumor volume at enrollment was not significantly different (p<0.05, **Fig 3.4 C**). Unfortunately, serial infusions of TriVax vaccines lead to toxicity likely caused by previously seen autoimmune pathology[157] (**Fig. 3.4 D,** Green line**)**. Thus to avoid off target autoimmune toxicity a BiVax vaccine[266] (Msln406-414 peptide and Poly I:C adjuvant) was administered with the first and last infusion. No apparent toxicity was seen in mice that

received Cytoxan and BiVax/TriVax/BiVax infusions vaccinations, thus we felt safe moving forward with enrolling mice with T cell therapies and BiVax/TriVax/BiVax. *KPC* mice enrolled in1045 WT TRex T cells + BiVax/TriVax/BiVax therapies had a significant survival benefit (median survival n=133 days post enrollment p=0.0030) after just three rounds of cell therapy. Unfortunately, although not significant *KPC* that were randomized into the 1045 *Tgfbr2-/-* + BiVax/TriVax/BiVax vaccine enrolled with a larger tumor volume (median=34.48mm^3) just shy of being significantly different form 1045 WT alone (p=0.0579) and 1045+ BiVax/TriVax/BiVax (p=0.0617). Suggesting that the difference in survival between WT and *Tgfbr2-/-* is not necessarily that different. More *KPC* mice will need to be randomized and enrolled in therapy arms to be able to make confident conclusions on the therapeutic benefit of 1045 *Tgfbr2-/-* + BiVax/TriVax/BiVax. Overall, though this data does show immense promise as the changes we made in our engineering strategy in 1045 TRex T cells with a clinically relevant vaccine already significantly extends *KPC* mouse survival in as little as three rounds of therapy.

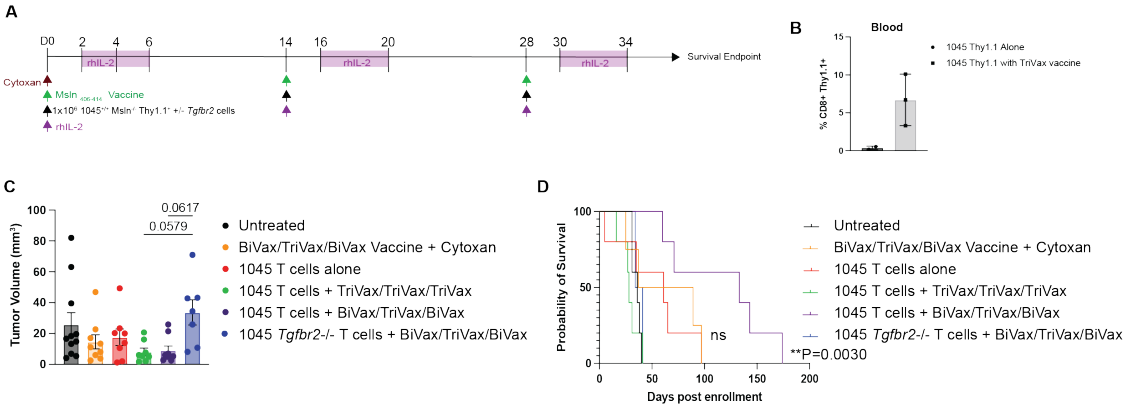

Figure 3.4. Serial infusions of 1045 TRex T cells with vaccination leads to significant survival in *KPC* Mice.

A Experimental Therapy schematic for *KPC* mice receiving, cells for adoptive transfer were activated and edited in the same manner as **fig.3.1 A**. Therapeutic treatment enrollment was defined as the first day therapy was administered <1 week post ultrasound that confirmed enrollment criteria (tumor =3-6mm). *KPC* mice received a single dose of Cytoxan, only with the first therapy round, to lymphodeplete 6 hours prior to the transfer of 1045 Msln$^{-/-}$ Thy1.1$^+$ T cells +/-*Tgfbr2*-/-, an I.P. injection of Msln$_{406-414}$ BiVax or TriVax vaccine and rhIL-2. rhIL-2 was given on D2, 4, 6 for the expansion of transferred cells. A total of three rounds of therapy were administered. **B.** Frequency of CD8+ Thy1.1+ 1045 WT TRex T cells in the blood 8 days after transfer with and without TriVax in non-tumor bearing B6 mice. Data are mean ± SEM and *n* = 3 mice per group. Unpaired Two-tailed students T Test p=0.0882 **C.** Ultrasound Tumor volume at time of enrollment. Mice were randomized into a given therapy group based off my experimental schedule and how busy I was and the difficulty for generation of therapy. Data are mean ± SEM and *n* = 4–5 mice per group and 1-4 independently measured tumors per mouse. $p<0.05$. One-way ANOVA with a Tukey's posttest. **(D)** Kaplan-

Meier curve measuring KPC mouse survival days post enrollment. Each step is an independent animal. P values are calculated by a log rank test with a 95% CI and $n = 4–5$ mice per group. $^{**}p<0.005$

3.3 Discussion

High levels of TGFβ in the PDA TME[242] are known to drive T cell dysfunction. Here, we show potent killing, by a physiologically controlled TCR, that is driven by abrogation of the TGFβ signaling receptor Tgfbr2 in a majority of the 1045 TRex T cells. An early effector phenotype in 1045 *Tgfbr2-/-* T cell defined by high expression of effector T cell markers KLRG1+, CD44+, CD69+, CXCR3+. *In vitro* incucyte killing assays looked at two malignant cell lines, KPC2 and E0771. In both cell lines malignancy is driven by the mutant tumor suppressor gene p53 with and additional *Kras* driving mutation in the KPC2 line. 1045 TRex T cells recognize its cognate $Msln_{406-414}$ peptide in the context of MHC I H-$2D^b$ presentation and thus the differences in intracellular and extracellular Msln expression are relatively moot as both can be internally processed and presented on MHC I. Where the E0771 tumor cell line was easily killed by both WT and *Tgfbr2-/-* T cells, the *KPC*2 tumor line growth was mostly held in a state of equilibrium for the entirety of the 48-hour co-culture. Promising results showed that *Tgfbr2-/-* TRex T cells due to the decreased negative regulatory intracellular inhbibtion[21,243] do eventually induce killing *in vitro* of the *KPC*2.

After therapeutic adoptive transfer we saw a significant reduction in tumor burden in all therapeutically treated groups with the greatest reduction in mice treated with 1045 *Tgfbr2-/-* + vaccine. Adoptively transferred cells traffic to the tumors with a significant increase in groups given a TriVax vaccine. A lower frequency (20%) of intratumoral 1045 *Tgfbr2-/-* + vaccine T cells expressed Klrg1 suggesting that these T cells may be differentiating into Klrg1 negative memory subsets[267]. This could be possible due to

outgrowth of unedited 1045 T cells in these mice, further studies will be needed to determine the level at which this outgrowth occurs. Moreover, 1045 *Tgfbr2-/-* appear resistant to progressive T cell dysfunction as they lack high expression of T cell exhaustion markers Lag3, PD-1, and the progenitor T exhausted subset defined by TCF1+PD1+ expression. We show that the maintenance of this highly potent Klrg1+ effector T cell response is driven by XCR1+ cDC1s[98,268] in the tumor in likely highly inflammatory chemokine (CCL2, CXCL9/10) and cytokine (IL-12, IFNγ and TNFα) rich microenvironments through meaningful long lasting cell to cell contact. Finally, we show that overall engineered Msln-specific TRex T cells do indeed have a highly potent effector T cell killing response to *in vitro* cultured tumor cells, orthotopically implanted *in vivo* tumors, and *in vivo* autochthonous KPC tumor. The outstanding question remains though if 1045 *Tgfbr2-/-* T cells + BiVax/TriVax/BiVax responses can control tumor burden and extend survival long term as enrollment of *KPC* mice with more similar tumor burden is greatly needed. Synchronously, as TGFβ is an important cytokine in the polarization of T cells from SLEC into MPECs and memory T cell formation[239,269] long term memory studies will need to be completed to better understand if the1045 *Tgfbr2-/-* T cell response is sufficient for tumor elimination.

3.4 Methods

3.4.1 Animals

The University of Minnesota Institutional Animal Care and Use Committee approved all animal studies that conformed to ethical regulations for animal testing and research. Animals were co-housed in SPF vivarium which is maintained at a 14:10 hour

light: dark cycle, at 68-70°F and 20-70% humidity range. Both female and male mice between the ages of 6-12 weeks old were used in this study. Mice for these studies were euthanized according to IACUC approved methods of isoflurane overdose followed by cervical dislocation. C57BL/6J wild type (WT) mice were purchased from Jackson Labs (#000664). 1045 TRex animals[245] were backcrossed onto the Thy1.1 congenic marker B6.PL-*Thy1*^{a}/CyJ mouse strain purchased from Jackson Labs (#000406) for two generations and subsequently bred for homozygous 1045$^{+/+}$ Msln$^{-/-}$ Thy1.1$^{+/+}$. *Kras*$^{LSL\text{-}G12D/+}$;*Trp53*$^{LSL\text{-}R172H/+}$;*p48*^{Cre} (*KPC*) mice initially generated on a mixed background[270] and were serially backcrossed to C57Bl/6J mice (The Jackson Laboratory; Stock No 00664) and determined to be >99.6% pure by SNP analyses as previously described[176]. XCR1-Venus mice were acquired from Dr. Brian Fife.

3.4.2 Primary tumor epithelial cells

Autochthonous tumors from C57BL/6J *KPC* mice were cultured in vitro to generate primary PDA tumor epithelial cells as described[230,246]. The *KPC*2[251] were maintained below passage 15 in basic media (in 500 ml of DMEM [Life Technologies] + 10% FBS [Life Technologies] + 2.5 μg/ml amphotericin B [Life Technologies] + 100 μg/ml penicillin/streptomycin [Life Technologies] + 2.5 mg dextrose [Fisher Chemical]) at 37°C and 5% CO_2. Medium was sterile-filtered and stored in the dark at 4°C. Cell lines were negative for Mycoplasma.

3.4.3 Orthotopic tumor cell implantation

For orthotopic tumor implantation, mice received slow-release buprenorphine injected subcutaneously 2 hours prior to surgery for analgesia according to approved protocols. Mice were anesthetized using continuous flow of 2–5% isoflurane. Hair was removed using clean clippers followed by 30-60 seconds of Nair. The abdomen was sterilized using a series of EtOH and Betadine washes. Following washes the mice were place on a fresh sterile drape and covered with clear sterile drape to only expose the surgical site. After reaching surgical plane anesthesia, a 2-3 mm incision was made in the right abdomen followed by a 1-2 mm incision in the peritoneum to access the pancreas. A total of 1×10^5 tumor cells were injected into the pancreas in 20 µl of 60% Matrigel (Discovery Labware) using an insulin syringe (Covidien)[251]. Separate sets of sutures were used to close the peritoneum and skin (Ethicon).

3.4.4 Primary murine T cell activation

T cell media was sterile filtered DMEM (Life Technologies) + 10% FBS (Life Technologies), 100 µg/ml penicillin/streptomycin (Life Technologies), 20 mM l-glutamine (Life Technologies), 1X NEAA (Life Technologies) and 50 µM 2-betamercaptoethanal (Sigma-Aldrich) and was used to culture T cells *in vitro*. Spleens were mechanically dissociated using a 40 µm filter. RBCs were lysed by resuspension in 1 ml ACK lysis buffer for 2 minutes. Lysis was quenched by addition of 10 mls of T cell media. T cells were centrifuged at 350 x g for 5 minutes at 4°C and resuspended in 10 ml of T cell media containing 10 ng/µl recombinant human IL-2 (rhIL-2, Peprotech) and 10 µg/ml $Msln_{406-414}$ peptide (GQKMNAQAI, Genscript). Splenocytes were cultured in T25 flask

for 48 (*Tgfbr2* knockout cells) - 72 hours at 37°C, 5% CO2. Cells were counted using a hemocytometer and Trypan blue exclusion.

3.4.5 Adoptive T-cell therapy

Adoptive cell therapies were based off of previously described protocol optimized to promote the expansion of mesothelin TCR-engineered cells in mice[181,238,246]. $1045^{+/+}$ $Msln^{-/-}$ $Thy1.1^{+}$ TRex T cells were activated prior to transfer as described (described above). Orthotopic tumor implanted mice were enrolled in therapy six days post orthotopic tumor implantation. *KPC* mice are enrolled in treatment studies when they achieve 3–6 mm pancreatic tumors as determined by serial monitoring with high-resolution ultrasound (Vevo 2100). All Therapy enrolled mice received Cytoxan (cyclophosphamide, 180 mg/kg, IP, Amneal Pharmaceuticals), and 6 hours later received i.p. 1×10^{6} $1045^{+/+}$ $Msln^{-/-}$ $Thy1.1^{+}$ TRex T cells +/- *Tgfbr2*, a $Msln_{406-414}$ TriVax vaccine (100 μg/ml $Msln_{406-414}$ peptide, 2μg/ml Poly I:C (Sigma) and 50μg/ml αCD40 (FGK45; BioXCell)) and 2×10^{4} U rhIL-2. Each therapy component was diluted in sterile bacteriostatic saline. For serial T cell infusions, mice received the same treatment protocol every 2 weeks except excluding Cytoxan after the first dose and two groups received a BiVax vaccine (100 μg/ml $Msln_{406-414}$ peptide and 2μg/ml Poly I:C) for the first and last infusions. Therapy recipients also received rhIL-2 (2×10^{4} U/i.p. every other day for 8 days) to promote T-cell expansion after T cell transfer.

3.4.6 CRISPR of primary murine T cells

Primary $1045^{+/+}$ $Msln^{-/-}$ $Thy1.1^{+}$ TRex T cells were activated with peptide and rhIL-2 as described above and after 2 days, T cells were centrifuged for 10 minutes at 200 x g

at 4°C. T cells were counted using trypan blue exclusion and resuspended at 1 x 10^6 cells per 20 µl reaction in P4 solution with supplement (Lonza, V4XP-4024) and 1µl per reaction of 4 µM Alt-R Cas9 Electroporation Enhancer (100µM, Integrated DNA Technologies, #10007805). Synthego sgRNAs were resuspended at 50 µM. 2 µl TrueCut Cas9 v2 (5µg/mL, ThermoFisher Scientific, A36498) was combined with 1.5 µl of *Tgfbr2* sgRNA at a 1:1 molar ratio and mixed gently by pipetting similar to as described[188] and incubated at room temperature for 10 minutes. Two sgRNAs specific to murine *Tgfbr2* exon 3 were used, *Tgfbr2* sgRNA 1: GACCGCACCGCCAUUGUCGC (+116131690) and *Tgfbr2* sgRNA 2: CUCAGUUAACAGUGAUGUCA (-116131702). RNPs were diluted four-fold in the cell suspension and cells were transferred to the nucleofection cuvette and incubated at room temperature for 2 minutes with the cover on. Cells were nucleofected using the Amaxa 4D Nucleofector, pulse code CM137, rested for 15 minutes in the cuvette at room temperature. Cells were promptly diluted 1:10 in pre-warmed (37°C) T cell recovery media (T cell media without antibiotics) in the cuvette and transferred to a 96well plate and moved into an incubator (37°C, 5% CO2) to recover for 2 hours. T cells were then transferred to pre-warmed (37°C) T cell media and returned to the incubator (37°C, 5% CO2) for 24 hours before to *in vivo* transfer or *in vitro* analysis. Primary $1045^{+/+}$ $Msln^{-/-}$ $Thy1.1^{+}$ TRex T cells viability ranged from 40-50% following this protocol.

3.4.6 PCR genotyping and ICE

DNA was isolated from 1045 TRex tail snips using the REDExtract Kit (Sigma Aldrich). PCR was run using Q5 HiFi Master Mix (New England Biolabs) for *Trac* KO, *Msln* KO, and *Trac* junction PCR protocols using conditions previously described[245]. DNA

was isolated from edited isolate the genomic DNA with a DNeasy Blood and Tissue Kit (Qiagen). *Tgfbr2* KO PCR products were purified using a PCR Clean-Up Kit (Qiagen) and submitted for Sanger sequencing through Eurofins genomics using the following gene-specific PCR primers to detect both cut sites: *Tgfbr2* sgRNA 1 forward: TGTGGCCGCTGCATATC and reverse: GTTCTTGTCGTTCTTCCTCCA and *Tgfbr2* sgRNA 2 forward: CCCAAGTCGGATGTGGAAAT reverse: CAGACTTCATGCGGCTTCT primers. PCR was run on an Eppendorf Vapo Protect thermocycler. Sequence results were analyzed using Snapgene and Interference with Crispr Edits (ICE) software (https://ice.synthego.com). Mutant sequences were directly compared to Cas9 alone control sequence.

3.4.7 Preparation of mononuclear cells from spleen, blood, and tumor

Spleens were mechanically dissociated to single cells. RBCs were lysed by incubation in 1 mL of Tris-ammonium chloride (ACK) lysis buffer (GIBCO) for 1-2 minutes at room temperature. 9 mL of T cell media was added to quench lysis. Tumors were mechanically and enzymatically digested to single-cell suspensions using 1mg/ml collagenase type IV digested for 20 minutes at 37° C and washed 2X with DMEM to remove cell debris and pancreatic enzymes. Tumor and Spleen Cells were spun at 1400 rpm for 5 minutes at 4° C and resuspended in T cell media and stored on ice until further use. For PBMCs, 100-200 µl of blood was collected per animal in 20 mM EDTA in an Eppendorf tube. RBCs were lysed by resuspension in 150 µl ACK lysis buffer (GIBCO) for 10 minutes at room temperature. 1 mL of T cell media was added to quench cell lysis.

Cells were spun at 350 x g for 5 minutes at 4°C, supernatant decanted. Cells were stored in T cell media on ice until further use.

3.4.8 Monoclonal antibody staining for flow cytometry.

Mononuclear cells were stained in the presence of Fc block (αCD16/32) and a live/dead stain (Tonbo Ghost dye in BV510 or APC ef780). For analysis of immune cells, fluorescently conjugated monoclonal antibodies were diluted 1:100 in FACs buffer and include CD45 (30F-11, BioLegend), CD3e (17A2, BioLegend), CD8α (53–6.7, Tonbo), CD44 (IM7, BD), CD4+ (RM4.5, Tonbo), Klrg1 (2F1, BioLegend), Thy1.1 (OX-7), Cxcr3 (Cxcr3-173, BioLegend), PD-1 (J43, Invitrogen), Lag-3 (C9B7W, BioLegend), CD69 (H1.2F3, BD), CD62L (Mel14, BioLegend), CD11b (M1/70, Tonbo), CD19 (1D3, BD), NK1.1 (PK136, eBiosciences), Ly6G (1A8, eBiosciences), F4/80 (T45-2342, BD), CD11c (N418, BD), I-A^b (M5/114 15.2, Invitrogen), Ly6C (HK1.4, eBiosciences) and Xcr1 (ZET, BioLegend). Cells were stained for 30 min at 4 °C in the dark and washed 2X with FACs buffer. Cells were fixed in 2% PFA or fixation buffer (Tonbo) for 10–15 min at 4 °C in the dark prior to data acquisition. For intracellular TCF7 and Ki67 staining, cells were fixed using Foxp3 transcription factor reagent (Tonbo) for 30 minutes at 4°C, washed and intracellular stained with diluted antibodies in permeabilization buffer (Tonbo) and stained overnight. The next day, cells were washed 2X with perm/wash buffer and resuspended in FACs buffer. All samples were resuspended in FACs buffer and 100 µl of Countbright Absolute Counting Beads (Thermo Fisher). Cells were acquired with a Fortessa 1770 or Fortessa X-20 using Facs Diva software (BD Biosciences). Data were analyzed using FlowJo software (version 10).

3.4.9 Intracellular cytokine staining

Cells were incubated in round-bottom 96-well plates in a total volume of 200 µl of T cell media + Golgiplug + Golgistop (BD Biosciences) +/- $Msln_{406-414}$ peptide for 5 hours at 37°C, 5% CO_2. Cells were then stained in the dark with antibodies to CD8+ (1:100) and Thy1.1 (1:100) diluted in FACs buffer for 30 min on ice. Cells were washed x2 with FACs buffer and fixed for 20 min on ice with BD Biosciences Fix/Perm. Cells were washed with 1X BD Biosciences Perm/Wash and incubated with antibodies to IFNγ (1:100), IL-2 (1:100), and TNFα (1:100) overnight in the dark at 4°C. Cells were washed 2X and resuspended in FACs buffer and 100 µl of Countbright Absolute Counting Beads (Thermo Fisher). Acquisition was performed using a Fortessa 1770 or Fortessa X-20 using FACs Diva software (BD Biosciences). Data were analyzed using FlowJo software (version 10).

3.4.10 Two-photon laser scanning microscopy and analysis microscopy procedure

Tumor was harvested out of the treated XCR1-Venus mice. The entire tumor was embedded in 0.5% agarose and cut at 3 different tumor depths using a microtome into 20-micron slices, mounted on a coverslip, and was placed into warm RPMI 1640 containing 5% FBS. Movies were acquired using a MP SP5 two photon microscope TCS (Leica) equipped with a Mai Tai HP Deep See lasers (SpectraPhysics), an 8,000-Hz resonant scanner, a 25 3 /0.95 NA objective, two non-descanned detector and two hybrid detectors. During imaging, continuous oxygenated DMEM high glucose media lacking phenol red (Hyclone) was exchanged in the chamber containing the sample. Tissue was excited at 860 or 890nm and multiple fluorophores were imaged using the custom dichroic mirrors with

the following collections: SHG < 440nm, mScarlet 569-593nm, GFP 500-520nm, Venus 515-528nm. Data were processed with Imaris software (version 9.9. and version 10.0.0). Migration analysis was performed using the Imaris spot (GFP+ cells) function and surface (Venus+ cells) functions. The drift correct function in Imaris was used during imaging analysis where necessary to fix drift due to media flow. For each individual animal, we collected movies of at least three different locations within the tumor separated by at least 1 mm. Within each of these macroscopic locations, we imaged 2-3 positions concurrently. Videos were collected over a thirty-minute period for a total of sixty frames. We removed positions that contained excessive numbers of GFP+ T cells and were left with 3 unique positions/animal per a given treatment condition. These individual positions were separately analyzed and averaged to identify typical cell behavior. For presentation in figures, we showed data from one mouse per group that pools all data points from each location collected. Each dot in the average speed measurement graphs represents one cell which was defined by the spot function in Imaris. Spots (GFP+ T cells) were defined as 14 microns in size and to travel no greater than 20 microns between frames. XCR1-Venus DCs was defined using the surface function in Imaris and were defined as 25 microns in size and to track no greater than 10 microns between frames. Individual GFP+ spots and Venus+ surfaces cell had to be adjusted frame by frame to account for not all cells fitting the set parameters. Track distance traversed by the spot (mm3) is divided by the time the cell was observed (in seconds). As the spot (GFP+ cell) moved through the tumor, the distance between the cell and each of the surfaces was calculated. An Imaris algorithm was used to compute these distances. If the distance between the center of the spot cell and a surface center was less than 7 microns, then the spot was considered to be directly

interacting with the surface. The total length of time of these interactions was measured by the number of frames that specific spot was < 7 microns from a surface. For every experimental track, T cells sample from the speed and spot Error bars plot the maximum and minimum volume patrolled over the 100 simulations at a specific time. Data were compiled using Microsoft Excel (v16.15.1) and all statistical analyses were conducted using Prism (version 9.0).

3.4.11 Cell numbers normalized to tissue gram.

The number of live CD45+ cells collected per tissue was determined by FlowJo analysis software and the equation: # CD45+ cells per tube (*n*) = (# Beads/# Cells) x (Concentration of beads x Volume of beads added). Total number of cells collected from the entire single cell suspension was determined by multiplying n by total number of stains. Cell numbers were normalized to tissue weight or organ as indicated.

3.4.12 Incucyte Killing Assay

T cell killing efficacy was determined via a IncuCyte S3 Live-Cell Analysis System (Essen BioScience). Sartorius Incucyte® Cell-by-Cell enables real-time quantification of viable tumor cells by measuring near-IR signal expansion and T cell killing through tracking a Capase-3/7 Green Dye. Two mouse tumor lines, KPC2 and E0771, were transduced with a lentivirus encoding Near-IR (NIR) and a puromycin selection marker. NIR KPC2 and NIR E0771 target cancer cells were treated with 10 ng/mL of IFNγ in media for 48 hours prior to seeding (3,000/well in 100 µl of TCM) in a 96-well flat bottom plate. Prior to seeding, the plate was coated with 50 µl of 0.01% poly-L-ornithine

solution. Plates were incubated at 37°C for one hour, the solution was aspirated, and the plate was washed 2x with 200 µl of PBS. After four hours, to allow for initial tumor adherence and quantification, the plates were removed from the incubator. 50 µl of T cell suspension (activated 1045 WT, 1045 Zap only, or 1045 Tgfbr2-/-) was introduced to each experimental well at an E: T (effector: target) ratio of 20:1 and 5:1 in triplicate. 50 µl of T cell media was added to the no T cell control wells. 50 µl of Caspase 3/7 solution (1 µM working concentration) was added to each well to track tumor death. Plates were immediately returned to the Incucyte® Live-Cell Analysis System for continuous analysis: Objective: 20X; Channel selection: Phase Contrast + Fluorescence; Scan type: Standard (8 images per well); Scan interval: Every 2 hours. After 48-52 hours, Incucyte® Cell-by-Cell Analysis Software was used to measure target tumor cell growth and export data to Microsoft excel. Statistics were calculated using Prism software (v9.0).

3.4.13 Immunofluorescence

Tissues were embedded in OCT (Tissue-Tek) and stored at −80°C. 7 µm sections were cut using a Cryostat and fixed in acetone at −20°C for 10 min. Sections were rehydrated with PBS + 1% bovine serum albumin (BSA) and incubated for 1 hr with primary antibodies to rat anti-mouse Msln (MBL, B35, 1:100) diluted in PBS + 1% BSA at rt. Slides were washed 3X in PBS + 1% BSA and incubated with anti-rat AF546 (Invitrogen, 1:500) for 1 hr in the dark at room temperature. Stained slides were then washed 3X with PBS + 1% BSA, washed 3X with PBS, and mounted in DAPI Prolong Gold (Life Technologies). Images were acquired on a Leica DM6000 epifluorescent

microscope at the University of Minnesota Center for Immunology using Imaris 9.1.0 (Bitplane).

3.4.14 Statistical Analysis

N=3-9 mice in each group were used and data are a minimum of 2 independent experiments, except for two photon which was collected in a single experiment. Data were compiled using Microsoft Excel (v16.15.1) and all statistical analyses were conducted using Prism (version 9.0). Appropriate statistical methods were used to calculate significance as described in the figure legends. Where no *P* value is provided for a relevant comparison, the result was not significant. The data were analyzed using the two-tailed unpaired Student *t* test, with or without a Welch correction, depending on whether the data had possible unequal or equal variances, respectively. One-way analysis of variance (ANOVA) and Tukey post-test were used for >2-group data. For ANOVA of non-Gaussian distribution, a Kruskal-Wallis test was used. Graphed data are presented as mean ± standard error of the mean (S.E.M.) unless otherwise indicated and $p<0.05$ was considered significant. *$p<0.05$, **$p<0.005$, ***$p<0.0005$, and ****$p<0.0001$.

3.5 Publications:

The data from this chapter is currently unpublished.

Data for this chapter contained experimental contributions from: Jonah Butler, Ebony Miller, and Dr. Adam Burrack who have contributed to aspects of experimental set up and data collection. To that I am immensely grateful.

Chapter 4: Conclusions

4.1: Overview

It's been over ten years since the FDA approved the first immune checkpoint blockade therapy. Since then, we have seen an explosion of innovation in immunotherapies that have changed the outlook for cancer survival and care in both solid and hematological malignancies[93,271,272]. T cell exhaustion is a common feature found in chronic infection and cancer. T cell exhaustion is defined by a maintained phenotypic expression of inhibitory receptors such as PD-1 and Lag3, metabolic dysregulation, loss of effector functions such as production of IFNγ, and meager recall and maintenance of the memory cell population[48]. Previous work showed exhaustion occurs in the engineered Msln TCR T cells as early as day 8 post transfer and required 6 rounds of Msln TCR T cell transferred every two weeks[169]. Not only would this clinical therapy be extremely expensive for a patient, it also doesn't solve the primary issue that drove the need for serial infusions, the T cell exhaustion[138,273]. Any way that we can abrogate T cell exhaustion, to require fewer serial T cell transfers and allow for memory T cell persistence will greatly reduce cost and increase quality of patient care. My thesis work presented here furthers our understanding of 1) how to generate robust high affinity exhaustion resistant preclinical mouse model and 2) abrogation of TGFβ signaling in Msln TCR TRex cells shows great clinical promise in therapeutic treatment of pancreatic ductal adenocarcinoma.

4.2: Implications on T cell engineering strategies

Engineered CARs and TCRs are typically transduced into the T cells of a patient using γ-retroviral vectors or other randomly integrating vectors [202,274]. Random integration of the receptor construct can result in clonal expansion, variegated transgene expression,

and oncogenic transformation [154,207,275,276]. Recent advances in genome editing through the discovery of CRISPR/Cas9 have allowed for an efficient sequence-specific insertion of receptor constructs in human cells, including targeted gene delivery into site specific regions of the genome [184,277–279]. Previous work by Eyquem *et. al.* showed that insertion of a CD19-CAR into the endogenous *TRAC* locus in human T cells resulted in uniform CAR expression, enhanced T cell potency, averts tonic signaling that leads to exhaustion, and outperformed conventionally γ-retroviral generated CD19-CAR T cells in a leukemia mouse model[277]. Here, we developed a methodology to integrate a desired exogenous TCR into the physiological endogenous *Trac* locus in murine T cells and zygotes by adapting the CRISPR-READI approach[184]. By combining an AAV-mediated donor TCR delivery with Cas9/sgRNA RNP electroporation to induce site-specific modifications in *Trac* we were able to integrate the exogenous TCR of interest effectively replacing the endogenous murine T cell repertoire. We independently generated multiple T cell receptor exchange (TRex) mouse strains supporting the highly efficiency, reproducibility, quick methodology for generating a TRex strain over historical TCR transgenic strains. Furthermore, in Mesothelin TCR TRex strains we induced *Msln* null mutations to successfully circumvent mechanisms of T cell central tolerance and negative selection. P14 and Msln -/- TRex mice appear to have no defects in normal T cell development.

Despite differences in TCR affinity, 7431 TRex effector T cells were as sensitive to low antigen concentrations as the high affinity 1045 TRex effector T cells. P14 TRex T cells were also more sensitive to antigen as compared to historical and identical TCR P14 transgenic T cells, which may be explained in part due to higher TCR expression in P14 TRex T cells. Overall, this data supports that TCR integration into the endogenous *Trac*

locus may improve antigen sensitivity. Most importantly, we identified that targeting a TCR to *Trac* sustained primary murine T cell function over multiple stimulations *in vitro* compared to retrovirally transduced T cells. Our study further supports and expands the previous work by Eyquem *et.al.* that the genomic location of engineered TCR can impact T cell functionality and exhaustion[277].

As Msln is a commonly overexpressed tumor-associated antigen[163–167,176], the 1045 and 7431 TRex mice will provide a standardized source of naïve T cells with TCRs specific to a native and clinically relevant tumor antigen to identify engineering strategies to sustain T cell function in solid tumors. TRex mice are a robust tool to generate and track any native self/tumor-specific T cell responses, not limited to Msln. As many cancers are poorly immunogenic, in part through defects in antigen processing and presentation, the demonstrated increased antigen sensitivity in TRex T cells which may be beneficial in such cancer settings where antigen is limited[77,79,245]. Thus, Msln-specific TRex mice will permit efficient investigation into how to enhance antitumor engineered T cells therapies in cancer. Particularly, experiments to further engineer the T cells to overcome the suppressive tumor microenvironment by expressing chimeric costimulatory proteins, cytokines or are now easily feasible since all TRex T cells express the Msln-specific TCR [112,143,154,245,277,280]. Thus, the TRex methodology is an exciting technology to generate heritable alleles encoding a desired TCR and easily permit studies to uncover facets of TCR immunobiology and underscore the potential of CRISPR/Cas9 genome editing to further advance immunotherapies.

4.3: Therapeutic inhibition of TGFβ signaling in Engineered Msln-TRex T cells

Currently, there are no effective treatments for long term survival of patients with advanced pancreatic ductal adenocarcinoma (PDA). Transforming Growth Factor β (TGFβ) is a ubiquitously expressed cytokine in the PDA tumor microenvironment (TME) and has been linked in several hallmark features of PDA including but not limited to driving T cell dysfunction [242,281]. TGFβ signaling can be a double-edged sword as TGFβ signaling in epithelial cells can have strong tumor-suppressive effects by inducing cell cycle arrest thru upregulation of cyclin dependent kinases[281]. Alternatively, TGFβ signaling also accelerates PDA tumorigenesis by boosting epithelial-to-mesenchymal transition (EMT), fibrosis, and the evasion of immune surveillance[282,283]. Clinical use of TGFβ inhibitors alone have shown to be relatively unremarkable and, in some cases, administration lead to tumor growth [113,284,285]. Additionally, several *in vivo* studies have shown that cytotoxic T cells deficient in TGFβ signaling are capable driving a robust anti-tumor effector immune response[112,286,287]. Thus, I desired to target TGFβ signaling only in the engineered T cells in a way to limit off target effects of TGFβ depletion in the TME. Here, my thesis work shows an innovative and potent therapy in an *in vivo* orthotopic *KPC* PDA mouse model that is driven by abrogation of TGFβ signaling through genomic knockout of TGFβ receptor 2 (Tgfbr2) in a majority of high affinity (1045) Msln-TRex T cells.

First, we showed that abrogation of *Tgfbr2* using CRISPR/cas9 drives an early effector phenotype in 1045 *Tgfbr2-/-* T cell defined by high expression of effector T cell markers KLRG1+, CD44+, CD69+, CXCR3+. When challenged *In vitro*, 1045 Msln-TRex T cells with and without Tgfbr2 annihilated the E0771 breast cancer cell line at both a low and high effector to tumor cell ratio in an incucyte killing assay. This result shows for the

first time that activated TRex T cells are capable of inducing target cell apoptosis and tumor cell control through their robust effector functions. When challenged against a KPC2 PDA tumor cell line, 1045 *Tgfbr2-/-* T cells at late timepoints were able to induce PDA tumor cell apoptosis. 1045 WT cells were unable to maintain control of tumor cell growth. These results indicate inherent differences in immunogenicity between the tumor cell lines and confirms our previous prediction that TRex T cells could be a potent therapy in multiple cancer models. Unlike CAR T cells, TCR T cell therapies can be used to treat cancer with both intracellular and extracellular Msln expression as both can be internally processed and presented on MHC I[166,167,288,289].

We next tested the therapeutic efficacy of 1045 *Tgfbr2-/-* vs 1045 WT TRex T cells in an orthotopically implanted KPC2 tumor model. Using a previously established therapy protocol, we treated mice with Cytoxan to lymphodeplete 6 hours prior to an adoptive T cell therapy with or without a TriVax vaccine. After therapeutic adoptive transfer we saw a significant reduction in tumor burden in all therapeutically treated groups with the greatest reduction in mice treated with 1045 *Tgfbr2-/-* + vaccine. We found that 1045 +/- *Tgfbr2-/-* plus vaccine significantly expanded *in vivo* and trafficked to the tumors. A portion of intratumoral 1045 *Tgfbr2-/-* + vaccine T cells expressed Klrg1 a marker of effector T cells[64,267]. Moreover, 1045 *Tgfbr2-/-* appear resistant to progressive T cell dysfunction as they lack high expression of T cell exhaustion markers Lag3, PD-1, and the progenitor T exhausted subset defined by TCF1+PD1+ expression. The highly inflammatory chemokine (CCL2, CXCL9/10) and cytokine (IL-12, IFNγ and TNFα) rich microenvironment after T cell transfer is critical in supporting the effector functionality through recruitment innate immune populations critical in supporting cytotoxic T cells[39,260].

To that point we critically showed that maintenance of the highly potent Klrg1+ effector T cell response is driven by meaningful and long lasting cell to cell contact XCR1+ cDC1s[98,268]. Overall, the orthotopic PDA studies highlight a significant reduction in engineered Msln-T cell dysfunction that we previously saw at day 8 post therapeutic transfer (**Fig. 4.1**). Although outstanding questions remain if 1045 *Tgfbr2-/-* T cells + BiVax/TriVax/BiVax responses can control tumor burden and extend *KPC* mouse survival long term. We were able to show that by changing the engineering strategy, Msln-specific TRex T cells can significantly increase autochthonous *KPC* mouse survival with fewer rounds of therapy and significantly fewer cells transferred in each round. Giving immense hope for the use of this as the new baseline engineering strategy for all adoptive CAR and TCR cell therapies going forward.

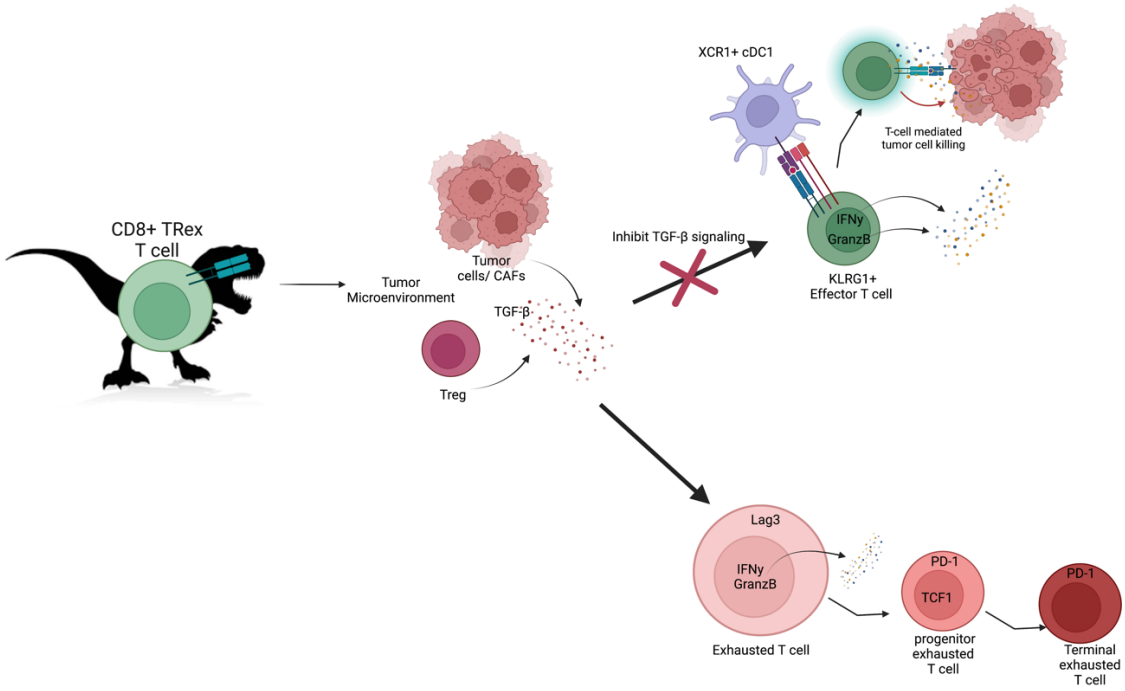

Figure 4.1. Orthotopic model for enhancing engineered T cell therapies in PDA.
(Left to right) The engineering strategy chosen to generate engineered T cell therapies can establish cell therapy success even prior to transfer. Here we use high affinity T cell receptor exchange (TRex) Msln TCR-T cells which show resistance to exhaustion due to directed insertion of the TCR into the endogenous *Trac* locus. When adoptively into the TGFβ rich PDA TME, 1045 WT TRex cells show signs of progressive T cell exhaustion through upregulation of Lag3, decreased production of IFNγ and Granzyme B and increases in the progenitor (TCF1+ PD-1+) exhausted T cell and Terminally (PD-1+ TCF1-) exhausted T cell population (**bottom right**). By abrogating TGFβ signaling, through knocking out Tgfbr2, we drive effector T cell differentiation, and it is maintained through direct and meaningful interactions with XCR1+ cDCs. TRex T cells maintain high production of IFNγ and Granzyme B leading to overall T cell mediated tumor cell killing and may drive tumor control (**top right**).

4.2: Final thoughts on future clinical implications of Msln TRex T cells

The field of cancer immunotherapy is growing at an exponential pace, with new therapies and combination therapies being published almost every week. Furthermore development of robust preclinical models, like the TRex mice, allow for a more rapid and reproducible source of antigen specific TCR-T cells[245], opening the door be able to screen tumor associated antigen and neoantigen specific TCRs in *in vitro* and *in vivo*. Generation of strong preclinical data that truly encapsulates the complex interactions between cancer and the immune system will be more likely to succeed when translated into the clinic. Adoptive cell therapies such as the Msln TCR-T cell therapy have emerged as a promising treatment

for many different types of solid tumors and the clinical implications of this work cannot be overlooked as the current clinical trial testing the efficacy of Msln TCR-T cells is ongoing right now (NCT04809766). As scientists, we do research to help expand our understanding of the world around us and to improve the lives of others. It is easy to get caught in a cycle of our own exhaustion and forget that. This project was a constant reminder to me as to why we push scientific boundaries, why collaboration is so critically important and why we can't lose our drive to share our knowledge with others. What we do in the lab matters greatly. Someone, in this vast expansive world, has been waiting or searching for our results as they hold the potential to provide the hope they need to keep going.

References:

1. Marshall, J. S., Warrington, R., Watson, W. & Kim, H. L. An introduction to immunology and immunopathology. *Allergy Asthma Clin. Immunol.* **14**, 49 (2018).
2. Baxby, D. Edward Jenner's Inquiry; a bicentenary analysis. *Vaccine* **17**, 301–307 (1999).
3. Murphy, K. & Weaver, C. *Janeway's immunobiology*. (2017).
4. Andersen, M. H., Schrama, D., Thor Straten, P. & Becker, J. C. Cytotoxic T cells. *J. Invest. Dermatol.* **126**, 32–41 (2006).
5. Dong, Y. *et al.* Genome-Wide Analysis Identifies Rag1 and Rag2 as Novel Notch1 Transcriptional Targets in Thymocytes. *Front. Cell Dev. Biol.* **9**, (2021).
6. Khor, B. & Sleckman, B. P. Allelic exclusion at the TCRbeta locus. *Curr. Opin. Immunol.* **14**, 230–234 (2002).
7. Hogquist, K. A., Baldwin, T. A. & Jameson, S. C. Central tolerance: learning self-control in the thymus. *Nat. Rev. Immunol.* **5**, 772–782 (2005).
8. Hogquist, K. A. *et al.* T cell receptor antagonist peptides induce positive selection. *Cell* **76**, 17–27 (1994).
9. Moran, A. E. & Hogquist, K. A. T-cell receptor affinity in thymic development. *Immunology* **135**, 261–267 (2012).
10. Starr, T. K., Jameson, S. C. & Hogquist, K. A. Positive and negative selection of T cells. *Annu. Rev. Immunol.* **21**, 139–176 (2003).
11. Perniola, R. Twenty Years of AIRE. *Front. Immunol.* **9**, (2018).
12. Yun, T. J. & Bevan, M. J. The Goldilocks conditions applied to T cell development. *Nat. Immunol.* **2**, 13–14 (2001).
13. Henrickson, S. E. & von Andrian, U. H. Single-cell dynamics of T-cell priming. *Curr. Opin. Immunol.* **19**, 249–258 (2007).
14. Henrickson, S. E. *et al.* Antigen availability determines CD8+ T cell-dendritic cell interaction kinetics and memory fate decisions. *Immunity* **39**, 496–507 (2013).
15. Cyster, J. G. & Schwab, S. R. Sphingosine-1-phosphate and lymphocyte egress from lymphoid organs. *Annu. Rev. Immunol.* **30**, 69–94 (2012).
16. Lo, C. G., Lu, T. T. & Cyster, J. G. Integrin-dependence of Lymphocyte Entry into the Splenic White Pulp. *J Exp Med* **197**, 353–361 (2003).
17. Laudanna, C., Kim, J. Y., Constantin, G. & Butcher, E. C. Rapid leukocyte integrin activation by chemokines. *Immunol. Rev.* **186**, 37–46 (2002).
18. Rosen, H. & Goetzl, E. J. Sphingosine 1-phosphate and its receptors: an autocrine and paracrine network. *Nat. Rev. Immunol.* **5**, 560–570 (2005).
19. Lee, S. & Ditko, S. *Spider-Man!* vol. Amazing Fantasy #15 (Marvel Comics, 1962).
20. Guermonprez, P., Valladeau, J., Zitvogel, L., Théry, C. & Amigorena, S. Antigen Presentation and T Cell Stimulation by Dendritic Cells. *Annu. Rev. Immunol.* **20**, 621–667 (2002).
21. Pircher, H., Bürki, K., Lang, R., Hengartner, H. & Zinkernagel, R. M. Tolerance induction in double specific T-cell receptor transgenic mice varies with antigen. *Nature* **342**, 559–561 (1989).
22. Au-Yeung, B. B. *et al.* The structure, regulation, and function of ZAP-70. *Immunol. Rev.* **228**, 41–57 (2009).

23. Iwashima, M., Irving, B. A., van Oers, N. S., Chan, A. C. & Weiss, A. Sequential interactions of the TCR with two distinct cytoplasmic tyrosine kinases. *Science* **263**, 1136–1139 (1994).
24. Okkenhaug, K. & Vanhaesebroeck, B. PI3K in lymphocyte development, differentiation and activation. *Nat. Rev. Immunol.* **3**, 317–330 (2003).
25. Bossi, G. *et al.* The secretory synapse: the secrets of a serial killer. *Immunol. Rev.* **189**, 152–160 (2002).
26. Čemerski, S. & Shaw, A. Immune synapses in T-cell activation. *Curr. Opin. Immunol.* **18**, 298–304 (2006).
27. Dustin, M. L. T-cell activation through immunological synapses and kinapses. *Immunol. Rev.* **221**, 77–89 (2008).
28. Grakoui, A., Donermeyer, D. L., Kanagawa, O., Murphy, K. M. & Allen, P. M. TCR-independent pathways mediate the effects of antigen dose and altered peptide ligands on Th cell polarization. *J. Immunol. Baltim. Md 1950* **162**, 1923–1930 (1999).
29. Mor, A., Dustin, M. L. & Philips, M. R. Small GTPases and LFA-1 reciprocally modulate adhesion and signaling. *Immunol. Rev.* **218**, 114–125 (2007).
30. Gaffen, S. L. SIGNALING DOMAINS OF THE INTERLEUKIN 2 RECEPTOR. *Cytokine* **14**, 63–77 (2001).
31. Bezman, N. & Koretzky, G. A. Compartmentalization of ITAM and integrin signaling by adapter molecules. *Immunol. Rev.* **218**, 9–28 (2007).
32. Acuto, O. & Michel, F. CD28-mediated co-stimulation: a quantitative support for TCR signalling. *Nat. Rev. Immunol.* **3**, 939–951 (2003).
33. Watts, T. H. TNF/TNFR family members in costimulation of T cell responses. *Annu. Rev. Immunol.* **23**, 23–68 (2005).
34. Toyooka, K. *et al.* CD28 co-stimulatory signals induce IL-2 receptor expression on antigen-stimulated virgin T cells by an IL-2-independent mechanism. *Int. Immunol.* **8**, 159–169 (1996).
35. Bachmann, M. F. & Oxenius, A. Interleukin 2: from immunostimulation to immunoregulation and back again. *EMBO Rep.* **8**, 1142–1148 (2007).
36. Acuto, O., Bartolo, V. D. & Michel, F. Tailoring T-cell receptor signals by proximal negative feedback mechanisms. *Nat. Rev. Immunol.* **8**, 699–712 (2008).
37. Curtsinger, J. M., Lins, D. C. & Mescher, M. F. Signal 3 Determines Tolerance versus Full Activation of Naive CD8 T Cells. *J. Exp. Med.* **197**, 1141–1151 (2003).
38. Flavell, R. A., Sanjabi, S., Wrzesinski, S. H. & Licona-Limón, P. The polarization of immune cells in the tumour environment by TGFbeta. *Nat Rev Immunol* **10**, 554–567 (2010).
39. Croft, M., Carter, L., Swain, S. L. & Dutton, R. W. Generation of polarized antigen-specific CD8 effector populations: reciprocal action of interleukin (IL)-4 and IL-12 in promoting type 2 versus type 1 cytokine profiles. *J Exp Med* **180**, 1715–1728 (1994).
40. Trinschek, B. *et al.* Kinetics of IL-6 Production Defines T Effector Cell Responsiveness to Regulatory T Cells in Multiple Sclerosis. *PLoS One* **8**, (2013).

41. Levings, M. K., Bacchetta, R., Schulz, U. & Roncarolo, M. G. The Role of IL-10 and TGF-β in the Differentiation and Effector Function of T Regulatory Cells. *Int. Arch. Allergy Immunol.* **129**, 263–276 (2002).
42. Harrington, L. E. *et al.* Interleukin 17-producing CD4+ effector T cells develop via a lineage distinct from the T helper type 1 and 2 lineages. *Nat. Immunol.* **6**, 1123–1132 (2005).
43. Weichsel, R. *et al.* Profound Inhibition of Antigen-Specific T-Cell Effector Functions by Dasatinib. *Clin Cancer Res* **14**, 2484–2491 (2008).
44. Spranger, S., Dai, D., Horton, B. & Gajewski, T. F. Tumor-Residing Batf3 Dendritic Cells Are Required for Effector T Cell Trafficking and Adoptive T Cell Therapy. *Cancer Cell* **31**, 711-723.e4 (2017).
45. Zhang, N. & Bevan, M. J. Transforming growth factor-β signaling to T cells inhibits autoimmunity during lymphopenia-driven proliferation. *Nat. Immunol.* **13**, 667–673 (2012).
46. Evrard, M. *et al.* Sphingosine 1-phosphate receptor 5 (S1PR5) regulates the peripheral retention of tissue-resident lymphocytes. *J Exp Med* **219**, e20210116 (2022).
47. Shiner, E. K., Holbrook, B. C. & Alexander-Miller, M. A. CD4+ T Cell Subset Differentiation and Avidity Setpoint Are Dictated by the Interplay of Cytokine and Antigen Mediated Signals. *PLoS One* **9**, (2014).
48. McLane, L. M., Abdel-Hakeem, M. S. & Wherry, E. J. CD8 T Cell Exhaustion During Chronic Viral Infection and Cancer. *Annu. Rev. Immunol.* **37**, 457–495 (2015).
49. Reiser, J. & Banerjee, A. Effector, Memory, and Dysfunctional CD8+ T Cell Fates in the Antitumor Immune Response. (2016) doi:https://doi.org/10.1155/2016/8941260.
50. Schietinger, A. & Greenberg, P. D. Tolerance and exhaustion: defining mechanisms of T cell dysfunction. *Trends Immunol.* **35**, 51–60 (2014).
51. Schönrich, G. *et al.* Down-regulation of T cell receptors on self-reactive T cells as a novel mechanism for extrathymic tolerance induction. *Cell* **65**, 293–304 (1991).
52. Tomofuji, Y. *et al.* Chd4 choreographs self-antigen expression for central immune tolerance. *Nat. Immunol.* **21**, 892–901 (2020).
53. Wu, Y., Guo, Y., Huang, A., Zheng, P. & Liu, Y. CTLA-4–B7 Interaction Is Sufficient to Costimulate T Cell Clonal Expansion. *J. Exp. Med.* **185**, 1327–1336 (1997).
54. Butte, M. J., Keir, M. E., Phamduy, T. B., Freeman, G. J. & Sharpe, A. H. PD-L1 interacts specifically with B7-1 to inhibit T cell proliferation. *Immunity* **27**, 111–122 (2007).
55. Gibbons, R. M. *et al.* B7-H1 limits the entry of effector CD8+ T cells to the memory pool by upregulating Bim. *OncoImmunology* **1**, 1061–1073 (2012).
56. Tourdot, B. E. *et al.* Immunoreceptor Tyrosine-based Inhibitory Motif (ITIM)-mediated Inhibitory Signaling is Regulated by Sequential Phosphorylation Mediated by Distinct Nonreceptor Tyrosine Kinases: A Case Study Involving PECAM-1. *Biochemistry* **52**, 2597–2608 (2013).

57. Xu, X. *et al.* PD-1 and BTLA regulate T cell signaling differentially and only partially through SHP1 and SHP2. *J. Cell Biol.* **219**, e201905085 (2020).
58. Rollins, M. R. & Gibbons Johnson, R. M. CD80 Expressed by CD8+ T Cells Contributes to PD-L1-Induced Apoptosis of Activated CD8+ T Cells. *J. Immunol. Res.* **2017**, 7659462 (2017).
59. Gao, J. *et al.* Loss of IFN-γ Pathway Genes in Tumor Cells as a Mechanism of Resistance to Anti-CTLA-4 Therapy. *Cell* **167**, 397-404.e9 (2016).
60. Winograd, R. *et al.* Induction of T-cell Immunity Overcomes Complete Resistance to PD-1 and CTLA-4 Blockade and Improves Survival in Pancreatic Carcinoma. *Cancer Immunol Res* **3**, 399–411 (2015).
61. Burrack, A. L. *et al.* Combination PD-1 and PD-L1 Blockade Promotes Durable Neoantigen-Specific T Cell-Mediated Immunity in Pancreatic Ductal Adenocarcinoma. *Cell Rep* **28**, 2140-2155.e6 (2019).
62. Moral, J. A. *et al.* ILC2s amplify PD-1 blockade by activating tissue-specific cancer immunity. *Nature* **579**, 130–135 (2020).
63. Teixeiro, E. *et al.* Different T Cell Receptor Signals Determine CD8+ Memory Versus Effector Development. *Science* **323**, 502–505 (2009).
64. Duckworth, B. C. *et al.* Effector and stem-like memory cell fates are imprinted in distinct lymph node niches directed by CXCR3 ligands. *Nat Immunol* **22**, 434–448 (2021).
65. Jameson, S. & Hamilton, S. CD8 T cell memory: it takes all kinds. *Front. Immunol.* **3**, (2012).
66. Jameson, S. C. & Masopust, D. Understanding Subset Diversity in T Cell Memory. *Immunity* **48**, 214–226 (2018).
67. Plumlee, C. R. *et al.* Early Effector CD8 T Cells Display Plasticity in Populating the Short-Lived Effector and Memory-Precursor Pools Following Bacterial or Viral Infection. *Sci. Rep.* **5**, 12264 (2015).
68. Kurachi, M. *et al.* Chemokine receptor CXCR3 facilitates CD8+ T cell differentiation into short-lived effector cells leading to memory degeneration. *J. Exp. Med.* **208**, 1605–1620 (2011).
69. Cremasco, V. *et al.* FAP Delineates Heterogeneous and Functionally Divergent Stromal Cells in Immune-Excluded Breast Tumors. *Cancer Immunol. Res.* **6**, 1472–1485 (2018).
70. Weninger, W., Manjunath, N. & von Andrian, U. H. Migration and differentiation of CD8+ T cells. *Immunol. Rev.* **186**, 221–233 (2002).
71. Salmon, H. *et al.* Matrix architecture defines the preferential localization and migration of T cells into the stroma of human lung tumors. *J Clin Invest* **122**, 899–910 (2012).
72. Janssen, O., Sanzenbacher, R. & Kabelitz, D. Regulation of activation-induced cell death of mature T-lymphocyte populations. *Cell Tissue Res* **301**, 85–99 (2000).
73. Groscurth, P. & Filgueira, L. Killing Mechanisms of Cytotoxic T Lymphocytes. *Physiology* **13**, 17–21 (1998).
74. Hassin, D., Garber, O. G., Meiraz, A., Schiffenbauer, Y. S. & Berke, G. Cytotoxic T lymphocyte perforin and Fas ligand working in concert even when Fas ligand lytic action is still not detectable. *Immunology* **133**, 190–196 (2011).

75. Volpe, E., Sambucci, M., Battistini, L. & Borsellino, G. Fas–Fas Ligand: Checkpoint of T Cell Functions in Multiple Sclerosis. *Front. Immunol.* **7**, (2016).
76. Karki, R. *et al.* Synergism of TNF-α and IFN-γ Triggers Inflammatory Cell Death, Tissue Damage, and Mortality in SARS-CoV-2 Infection and Cytokine Shock Syndromes. *Cell* **184**, 149-168.e17 (2021).
77. Zhou, F. Molecular mechanisms of IFN-gamma to up-regulate MHC class I antigen processing and presentation. *Int. Rev. Immunol.* **28**, 239–260 (2009).
78. Tsuyuki, Y. *et al.* IFN-gamma induces coordinate expression of MHC class I-mediated antigen presentation machinery molecules in adult mouse Schwann cells. *Neuroreport* **9**, 2071–2075 (1998).
79. Dhatchinamoorthy, K., Colbert, J. D. & Rock, K. L. Cancer Immune Evasion Through Loss of MHC Class I Antigen Presentation. *Front Immunol* **12**, 636568 (2021).
80. D'Cruz, L. M., Rubinstein, M. P. & Goldrath, A. W. Surviving the crash: transitioning from effector to memory CD8+ T cell. *Semin Immunol* **21**, 92–98 (2009).
81. Garrod, K. R. *et al.* Dissecting T cell contraction in vivo using a genetically encoded reporter of apoptosis. *Cell Rep* **2**, 1438–1447 (2012).
82. Butz, E. A. & Bevan, M. J. Massive Expansion of Antigen-Specific CD8+ T Cells during an Acute Virus Infection. *Immunity* **8**, 167–175 (1998).
83. Prlic, M. & Bevan, M. J. Exploring regulatory mechanisms of CD8+ T cell contraction. *Proc. Natl. Acad. Sci.* **105**, 16689–16694 (2008).
84. Kok, L., Masopust, D. & Schumacher, T. N. The precursors of CD8+ tissue resident memory T cells: from lymphoid organs to infected tissues. *Nat. Rev. Immunol.* **22**, 283–293 (2022).
85. Van Beek, M., Nussenzweig, M. C. & Chakraborty, A. K. Two complementary features of humoral immune memory confer protection against the same or variant antigens. *Proc. Natl. Acad. Sci.* **119**, e2205598119 (2022).
86. Joag, V. *et al.* Sensing and alarm function of vaccine-elicited SIV-gag specific CD8 TRM in the reproductive mucosa of rhesus macaques. *J. Immunol.* **208**, 114.15 (2022).
87. Soerens, A. G. *et al.* Functional T cells are capable of supernumerary cell division and longevity. *Nature* **614**, 762–766 (2023).
88. Kaufmann, S. H. E. Immunology's foundation: the 100-year anniversary of the Nobel Prize to Paul Ehrlich and Elie Metchnikoff. *Nat. Immunol.* **9**, 705–712 (2008).
89. Burnet, F. M. Cancer—A Biological Approach. (1957).
90. Schreiber, R. D., Old, L. J. & Smyth, M. J. Cancer immunoediting: integrating immunity's roles in cancer suppression and promotion. *Science* **331**, 1565–1570 (2011).
91. Hanahan, D. & Weinberg, R. A. Hallmarks of Cancer: The Next Generation. *Cell* **144**, 646–674 (2011).
92. Burnet, F. M. A modification of Jerne's theory of antibody production using the concept of clonal selection. *CA. Cancer J. Clin.* **26**, 119–121 (1976).

93. Gubin, M. M. & Vesely, M. D. Cancer Immunoediting in the Era of Immuno-oncology. *Clin. Cancer Res.* **28**, 3917–3928 (2022).
94. Kaplan, D. H. *et al.* Demonstration of an interferon gamma-dependent tumor surveillance system in immunocompetent mice. *Proc. Natl. Acad. Sci. U. S. A.* **95**, 7556–7561 (1998).
95. Shankaran, V. *et al.* IFNγ and lymphocytes prevent primary tumour development and shape tumour immunogenicity. *Nature* **410**, 1107–1111 (2001).
96. Aguirre-Ghiso, J. A. Models, mechanisms and clinical evidence for cancer dormancy. *Nat. Rev. Cancer* **7**, 834–846 (2007).
97. Koebel, C. M. *et al.* Adaptive immunity maintains occult cancer in an equilibrium state. *Nature* **450**, 903–907 (2007).
98. Burrack, A. L. *et al.* Distinct myeloid antigen-presenting cells dictate differential fates of tumor-specific CD8+ T cells in pancreatic cancer. *JCI Insight* **7**, e151593 (2022).
99. Burrack, A. L. *et al.* CD40 Agonist Overcomes T Cell Exhaustion Induced by Chronic Myeloid Cell IL-27 Production in a Pancreatic Cancer Preclinical Model. *J. Immunol.* ji2000765 (2021) doi:10.4049/jimmunol.2000765.
100. Yamazaki, C. *et al.* Critical Roles of a Dendritic Cell Subset Expressing a Chemokine Receptor, XCR1. *J. Immunol.* **190**, 6071–6082 (2013).
101. Hegde, S. *et al.* Dendritic Cell Paucity Leads to Dysfunctional Immune Surveillance in Pancreatic Cancer. *Cancer Cell* **37**, 289-307.e9 (2020).
102. Croft, M., Carter, L., Swain, S. L. & Dutton, R. W. Generation of polarized antigen-specific CD8 effector populations: reciprocal action of interleukin (IL)-4 and IL-12 in promoting type 2 versus type 1 cytokine profiles. *J. Exp. Med.* **180**, 1715–1728 (1994).
103. Burrack, A. L. *et al.* Cxcr3 constrains pancreatic cancer dissemination through instructing T cell fate. *Cancer Immunol. Immunother.* (2022) doi:10.1007/s00262-022-03338-7.
104. Hu, J. K., Kagari, T., Clingan, J. M. & Matloubian, M. Expression of chemokine receptor CXCR3 on T cells affects the balance between effector and memory CD8 T-cell generation. *Proc. Natl. Acad. Sci.* **108**, E118–E127 (2011).
105. Duckworth, B. C. *et al.* Effector and stem-like memory cell fates are imprinted in distinct lymph node niches directed by CXCR3 ligands. *Nat. Immunol.* **22**, 434–448 (2021).
106. Dhatchinamoorthy, K., Colbert, J. D. & Rock, K. L. Cancer Immune Evasion Through Loss of MHC Class I Antigen Presentation. *Front. Immunol.* **12**, 636568 (2021).
107. Khong, H. T. & Restifo, N. P. Natural selection of tumor variants in the generation of 'tumor escape' phenotypes. *Nat. Immunol.* **3**, 999–1005 (2002).
108. Eyles, J. *et al.* Tumor cells disseminate early, but immunosurveillance limits metastatic outgrowth, in a mouse model of melanoma. *J. Clin. Invest.* **120**, 2030–2039 (2010).
109. Beatty, G. L. *et al.* CD40 Agonists Alter Tumor Stroma and Show Efficacy Against Pancreatic Carcinoma in Mice and Humans. *Science* **331**, 1612–1616 (2011).

110. Pereira, B. A. *et al.* CAF Subpopulations: A New Reservoir of Stromal Targets in Pancreatic Cancer. *Trends Cancer* **5**, 724–741 (2019).
111. Roberts, E. W. *et al.* Depletion of stromal cells expressing fibroblast activation protein-α from skeletal muscle and bone marrow results in cachexia and anemia. *J Exp Med* **210**, 1137–1151 (2013).
112. Fix, S. M. *et al.* CRISPR-mediated TGFBR2 knockout renders human ovarian cancer tumor-infiltrating lymphocytes resistant to TGF-β signaling. *J Immunother Cancer* **10**, e003750 (2022).
113. Biffi, G. *et al.* IL1-Induced JAK/STAT Signaling Is Antagonized by TGFβ to Shape CAF Heterogeneity in Pancreatic Ductal Adenocarcinoma. *Cancer Discov* **9**, 282–301 (2019).
114. Feig, C. *et al.* Targeting CXCL12 from FAP-expressing carcinoma-associated fibroblasts synergizes with anti–PD-L1 immunotherapy in pancreatic cancer. *PNAS* **110**, 20212–20217 (2013).
115. Witkiewicz, A. *et al.* Expression of Indoleamine 2,3-Dioxygenase in Metastatic Pancreatic Ductal Adenocarcinoma Recruits Regulatory T Cells to Avoid Immune Detection. *J. Am. Coll. Surg.* **206**, 849 (2008).
116. Tang, Y. *et al.* An Increased Abundance of Tumor-Infiltrating Regulatory T Cells Is Correlated with the Progression and Prognosis of Pancreatic Ductal Adenocarcinoma. *PLoS ONE* **9**, e91551 (2014).
117. Zhang, Y. *et al.* Regulatory T-cell Depletion Alters the Tumor Microenvironment and Accelerates Pancreatic Carcinogenesis. *Cancer Discov.* **10**, 422–439 (2020).
118. Tai, X. *et al.* Foxp3 Transcription Factor Is Proapoptotic and Lethal to Developing Regulatory T Cells unless Counterbalanced by Cytokine Survival Signals. *Immunity* **38**, (2013).
119. Bensinger, S. J. *et al.* Distinct IL-2 Receptor Signaling Pattern in CD4+CD25+ Regulatory T Cells. *J. Immunol. Baltim. Md 1950* **172**, 5287–5296 (2004).
120. Catakovic, K., Klieser, E., Neureiter, D. & Geisberger, R. T cell exhaustion: from pathophysiological basics to tumor immunotherapy. *Cell Commun. Signal.* **15**, 1 (2017).
121. Harjes, U. States of exhaustion. *Nat. Rev. Cancer* **19**, 185 (2019).
122. Khan, O. *et al.* TOX transcriptionally and epigenetically programs CD8+ T cell exhaustion. *Nature* (2019) doi:10.1038/s41586-019-1325-x.
123. Gabrilovich, D. I. & Nagaraj, S. Myeloid-derived suppressor cells as regulators of the immune system. *Nat. Rev. Immunol.* **9**, 162–174 (2009).
124. Mace, T. A. *et al.* Pancreatic cancer-associated stellate cells promote differentiation of myeloid-derived suppressor cells in a STAT3-dependent manner. *Cancer Res* **73**, 3007–3018 (2013).
125. Schmiechen, Z. C. & Stromnes, I. M. Mechanisms Governing Immunotherapy Resistance in Pancreatic Ductal Adenocarcinoma. *Front. Immunol.* **11**, (2021).
126. McCarthy, E. F. The Toxins of William B. Coley and the Treatment of Bone and Soft-Tissue Sarcomas. *Iowa Orthop. J.* **26**, 154–158 (2006).
127. Cann, S. A. H., Netten, J. P. van & Netten, C. van. Dr William Coley and tumour regression: a place in history or in the future. *Postgrad. Med. J.* **79**, 672–680 (2003).

128. Wei, S. C., Duffy, C. R. & Allison, J. P. Fundamental Mechanisms of Immune Checkpoint Blockade Therapy. *Cancer Discov.* **8**, 1069–1086 (2018).
129. Darvin, P., Toor, S. M., Sasidharan Nair, V. & Elkord, E. Immune checkpoint inhibitors: recent progress and potential biomarkers. *Exp. Mol. Med.* **50**, 1–11 (2018).
130. Kalbasi, A. & Ribas, A. Tumour-intrinsic resistance to immune checkpoint blockade. *Nat. Rev. Immunol.* **20**, 25–39 (2020).
131. Tumeh, P. C. *et al.* PD-1 blockade induces responses by inhibiting adaptive immune resistance. *Nature* **515**, 568–571 (2014).
132. Mariathasan, S. *et al.* TGFβ attenuates tumour response to PD-L1 blockade by contributing to exclusion of T cells. *Nature* **554**, 544–548 (2018).
133. Spain, L., Diem, S. & Larkin, J. Management of toxicities of immune checkpoint inhibitors. *Cancer Treat. Rev.* **44**, 51–60 (2016).
134. Gibbons Johnson, R. M. & Dong, H. Functional Expression of Programmed Death-Ligand 1 (B7-H1) by Immune Cells and Tumor Cells. *Front. Immunol.* **8**, (2017).
135. Meléndez, B. *et al.* Methods of measurement for tumor mutational burden in tumor tissue. *Transl. Lung Cancer Res.* **7**, (2018).
136. Chan, T. A. *et al.* Development of tumor mutation burden as an immunotherapy biomarker: utility for the oncology clinic. *Ann. Oncol.* **30**, 44–56 (2019).
137. Ottaviano, M., De Placido, S. & Ascierto, P. A. Recent success and limitations of immune checkpoint inhibitors for cancer: a lesson from melanoma. *Virchows Arch. Int. J. Pathol.* **474**, 421–432 (2019).
138. Stromnes, I. M. *et al.* Insufficiency of compound immune checkpoint blockade to overcome engineered T cell exhaustion in pancreatic cancer. *J Immunother Cancer* **10**, e003525 (2022).
139. Chapuis, A. G. *et al.* T cell receptor gene therapy targeting WT1 prevents acute myeloid leukemia relapse post-transplant. *Nat. Med.* **25**, 1064–1072 (2019).
140. Chapuis, A. G. *et al.* Transferred WT1-reactive CD8+ T cells can mediate antileukemic activity and persist in post-transplant patients. *Sci. Transl. Med.* **5**, 174ra27 (2013).
141. Chapuis, A. G. *et al.* Regression of metastatic Merkel cell carcinoma following transfer of polyomavirus-specific T cells and therapies capable of re-inducing HLA class-I. *Cancer Immunol. Res.* **2**, 27–36 (2014).
142. Stromnes, I. M., Schmitt, T. M., Chapuis, A. G., Hingorani, S. R. & Greenberg, P. D. Re-adapting T cells for cancer therapy: from mouse models to clinical trials. *Immunol. Rev.* **257**, 145–164 (2014).
143. Rollins, M. R. M. R., Spartz, E. J. E. J. & Stromnes, I. M. I. M. T Cell Receptor Engineered Lymphocytes for Cancer Therapy. *Curr. Protoc. Immunol.* **129**, (2020).
144. Alspach, E. *et al.* MHC-II neoantigens shape tumour immunity and response to immunotherapy. *Nature* **574**, 696–701 (2019).
145. Yee, C. *et al.* Melanocyte destruction after antigen-specific immunotherapy of melanoma: direct evidence of t cell-mediated vitiligo. *J. Exp. Med.* **192**, 1637–1644 (2000).
146. Lee, J. W. *et al.* Hepatocytes direct the formation of a pro-metastatic niche in the liver. *Nature* **567**, 249–252 (2019).

147. Zacharakis, N. *et al.* Immune recognition of somatic mutations leading to complete durable regression in metastatic breast cancer. *Nat. Med.* **24**, 724–730 (2018).
148. Tran, E. *et al.* T-Cell Transfer Therapy Targeting Mutant KRAS in Cancer. *N. Engl. J. Med.* **375**, 2255–2262 (2016).
149. Robbins, P. F. *et al.* Single and dual amino acid substitutions in TCR CDRs can enhance antigen-specific T cell functions. *J. Immunol. Baltim. Md 1950* **180**, 6116–6131 (2008).
150. Beatty, G. L. *et al.* Activity of Mesothelin-Specific Chimeric Antigen Receptor T Cells Against Pancreatic Carcinoma Metastases in a Phase 1 Trial. *Gastroenterology* **155**, 29–32 (2018).
151. June, C., Rosenberg, S. A., Sadelain, M. & Weber, J. S. T-cell therapy at the threshold. *Nat. Biotechnol.* **30**, 611–614 (2012).
152. Kalos, M. *et al.* T Cells with Chimeric Antigen Receptors Have Potent Antitumor Effects and Can Establish Memory in Patients with Advanced Leukemia. *Sci. Transl. Med.* **3**, 95ra73-95ra73 (2011).
153. Maus, M. V. *et al.* T cells expressing chimeric antigen receptors can cause anaphylaxis in humans. *Cancer Immunol. Res.* **1**, 26–31 (2013).
154. Shah, N. N. *et al.* Clonal expansion of CAR T cells harboring lentivector integration in the CBL gene following anti-CD22 CAR T-cell therapy. *Blood Adv.* (2019) doi:10.1182/bloodadvances.2019000219.
155. Fraietta, J. A. *et al.* Disruption of TET2 promotes the therapeutic efficacy of CD19-targeted T cells. *Nature* **558**, 307–312 (2018).
156. Eyquem, J. *et al.* Targeting a CAR to the TRAC locus with CRISPR/Cas9 enhances tumour rejection. *Nature* **543**, 113–117 (2017).
157. Sultan, H., Trillo-Tinoco, J., Rodriguez, P. & Celis, E. Effective antitumor peptide vaccines can induce severe autoimmune pathology. *Oncotarget* **8**, 70317–70331 (2017).
158. Pircher, H., Bürki, K., Lang, R., Hengartner, H. & Zinkernagel, R. M. Tolerance induction in double specific T-cell receptor transgenic mice varies with antigen. *Nature* **342**, 559–561 (1989).
159. Mamalaki, C. *et al.* Positive and Negative Selection in Transgenic Mice Expressing a T-Cell Receptor Specific for Influenza Nucleoprotein and Endogenous Superantigen. *Dev. Immunol.* (1993) doi:10.1155/1993/98015.
160. Xue, S. A., Bendle, G. M., Holler, A. & Stauss, H. J. Generation and characterization of transgenic mice expressing a T-cell receptor specific for the tumour-associated antigen MDM2. *Immunology* (2008) doi:10.1111/j.1365-2567.2007.02793.x.
161. Kouskoff, V., Signorelli, K., Benoist, C. & Mathis, D. Cassette vectors directing expression of T cell receptor genes in transgenic mice. *J. Immunol. Methods* (1995) doi:10.1016/0022-1759(95)00002-R.
162. Katz, J. D., Wang, B., Haskins, K., Benoist, C. & Mathis, D. Following a diabetogenic T cell from genesis through pathogenesis. *Cell* (1993) doi:10.1016/0092-8674(93)90730-E.

163. Argani, P. *et al.* Mesothelin is overexpressed in the vast majority of ductal adenocarcinomas of the pancreas: Identification of a new pancreatic cancer marker by serial analysis of gene expression (SAGE). *Clin. Cancer Res.* (2001).
164. Coelho, R. *et al.* Regulation of invasion and peritoneal dissemination of ovarian cancer by mesothelin manipulation. *Oncogenesis* (2020) doi:10.1038/s41389-020-00246-2.
165. Inaguma, S. *et al.* Comprehensive immunohistochemical study of mesothelin (MSLN) using different monoclonal antibodies 5B2 and MN-1 in 1562 tumors with evaluation of its prognostic value in malignant pleural mesothelioma. *Oncotarget* (2017) doi:10.18632/oncotarget.15814.
166. Thomas, A. *et al.* High mesothelin expression in advanced lung adenocarcinoma is associated with KRAS mutations and a poor prognosis. *Oncotarget* (2015) doi:10.18632/oncotarget.3429.
167. Tchou, J. *et al.* Mesothelin, a novel immunotherapy target for triple negative breast cancer. *Breast Cancer Res. Treat.* (2012) doi:10.1007/s10549-012-2018-4.
168. Anderson, K. G. *et al.* Engineered Adoptive T-cell Therapy Prolongs Survival in a Preclinical Model of Advanced-Stage Ovarian Cancer. *Cancer Immunol. Res.* **7**, 1412–1425 (2019).
169. Stromnes, I. M. *et al.* T Cells Engineered against a Native Antigen Can Surmount Immunologic and Physical Barriers to Treat Pancreatic Ductal Adenocarcinoma. *Cancer Cell* **28**, 638–652 (2015).
170. Hassan, R. *et al.* Mesothelin immunotherapy for cancer: Ready for prime time? *J. Clin. Oncol.* (2016) doi:10.1200/JCO.2016.68.3672.
171. Thomas, A. M. *et al.* Mesothelin-specific CD8+ T cell responses provide evidence of in vivo cross-priming by antigen-presenting cells in vaccinated pancreatic cancer patients. *J. Exp. Med.* (2004) doi:10.1084/jem.20031435.
172. Beatty, G. L. *et al.* Activity of Mesothelin-Specific Chimeric Antigen Receptor T Cells Against Pancreatic Carcinoma Metastases in a Phase 1 Trial. *Gastroenterology* (2018) doi:10.1053/j.gastro.2018.03.029.
173. Maus, M. V. *et al.* T cells expressing chimeric antigen receptors can cause anaphylaxis in humans. *Cancer Immunol. Res.* (2013) doi:10.1158/2326-6066.CIR-13-0006.
174. Adusumilli, P. S. *et al.* A phase i trial of regional mesothelin-targeted car t-cell therapy in patients with malignant pleural disease, in combination with the anti–pd-1 agent pembrolizumab. *Cancer Discov.* **11**, (2021).
175. Bera, T. K. & Pastan, I. Mesothelin Is Not Required for Normal Mouse Development or Reproduction. *Mol. Cell. Biol.* **20**, (2000).
176. Stromnes, I. M. *et al.* T Cells Engineered against a Native Antigen Can Surmount Immunologic and Physical Barriers to Treat Pancreatic Ductal Adenocarcinoma. *Cancer Cell* **28**, 638–652 (2015).
177. Border, E. C., Sanderson, J. P., Weissensteiner, T., Gerry, A. B. & Pumphrey, N. J. Affinity-enhanced T-cell receptors for adoptive T-cell therapy targeting MAGE-A10: strategy for selection of an optimal candidate. *OncoImmunology* **8**, (2019).

178. Pircher, H., Bürki, K., Lang, R., Hengartner, H. & Zinkernagel, R. M. Tolerance induction in double specific T-cell receptor transgenic mice varies with antigen. *Nature* (1989) doi:10.1038/342559a0.
179. Anderson, K. G. *et al.* Engineered Adoptive T-cell Therapy Prolongs Survival in a Preclinical Model of Advanced-Stage Ovarian Cancer. *Cancer Immunol. Res.* **7**, 1412–1425 (2019).
180. Stromnes, IM, Hulbertm AH, Rollins, MR Basom, RS, Delrow, J, Bonson, P, Burrack, AL, Hingorani, SR and Greenberg, P. Insufficiency of compound immune checkpoint blockade to overcome engineered T cell exhaustion in pancreatic cancer. *J. Immunother. Cancer* **In Press**, (2022).
181. Stromnes, I. M. *et al.* Differential Effects of Depleting versus Programming Tumor-Associated Macrophages on Engineered T Cells in Pancreatic Ductal Adenocarcinoma. *Cancer Immunol. Res.* **7**, 977–989 (2019).
182. Eyquem, J. *et al.* Targeting a CAR to the TRAC locus with CRISPR/Cas9 enhances tumour rejection. *Nature* (2017) doi:10.1038/nature21405.
183. Schober, K. *et al.* Orthotopic replacement of T-cell receptor α- and β-chains with preservation of near-physiological T-cell function. *Nat. Biomed. Eng.* **3**, (2019).
184. Chen, S. *et al.* CRISPR-READI: Efficient Generation of Knockin Mice by CRISPR RNP Electroporation and AAV Donor Infection. *Cell Rep.* (2019) doi:10.1016/j.celrep.2019.05.103.
185. Sant'Angelo, D. B. *et al.* The specificity and orientation of a TCR to its peptide-MHC class II ligands. *Immunity* **4**, (1996).
186. Wang, J. *et al.* Highly efficient homology-driven genome editing in human T cells by combining zinc-finger nuclease mRNA and AAV6 donor delivery. *Nucleic Acids Res.* **44**, (2016).
187. Liu, Z. *et al.* Systematic comparison of 2A peptides for cloning multi-genes in a polycistronic vector. *Sci. Rep.* **7**, (2017).
188. Seki, A. & Rutz, S. Optimized RNP transfection for highly efficient CRI SPR/Cas9-mediated gene knockout in primary T cells. *J. Exp. Med.* (2018) doi:10.1084/jem.20171626.
189. Starr, T. K., Jameson, S. C. & Hogquist, K. A. Positive and negative selection of T cells. *Annual Review of Immunology* Preprint at https://doi.org/10.1146/annurev.immunol.21.120601.141107 (2003).
190. Godfrey, D. I., Kennedy, J., Suda, T. & Zlotnik, A. A developmental pathway involving four phenotypically and functionally distinct subsets of CD3-CD4-CD8-triple-negative adult mouse thymocytes defined by CD44 and CD25 expression. *J. Immunol. Baltim. Md 1950* **150**, (1993).
191. Koyasu, S. *et al.* Pre-TCR signaling components trigger transcriptional activation of a rearranged TCRα gene locus and silencing of the pre-TCRα locus: Implications for intrathymic differentiation. *Int. Immunol.* **9**, (1997).
192. Koller, B. H., Marrack, P., Kappler, J. W. & Smithies, O. Normal development of mice deficient in β2M, MHC class I proteins, and CD8+ T cells. *J. Immunol.* **184**, (2010).

193. Schuster, M., Plaza-Sirvent, C., Visekruna, A., Huehn, J. & Schmitz, I. Generation of Foxp3+CD25− regulatory T-cell precursors requires c-rel and IκBNS. *Front. Immunol.* **10**, (2019).
194. Hogquist, K. A. *et al.* T cell receptor antagonist peptides induce positive selection. *Cell* **76**, (1994).
195. Amir, E. A. D. *et al.* ViSNE enables visualization of high dimensional single-cell data and reveals phenotypic heterogeneity of leukemia. *Nat. Biotechnol.* **31**, (2013).
196. Crawford, F., Kozono, H., White, J., Marrack, P. & Kappler, J. Detection of antigen-specific T cells with multivalent soluble class II MHC covalent peptide complexes. *Immunity* **8**, (1998).
197. Yee, C., Savage, P. A., Lee, P. P., Davis, M. M. & Greenberg, P. D. Isolation of high avidity melanoma-reactive CTL from heterogeneous populations using peptide-MHC tetramers. *J. Immunol. Baltim. Md 1950* **162**, (1999).
198. Stone, J. D., Chervin, A. S. & Kranz, D. M. T-cell receptor binding affinities and kinetics: impact on T-cell activity and specificity. *Immunology* vol. 126 Preprint at https://doi.org/10.1111/j.1365-2567.2008.03015.x (2009).
199. Viganò, S. *et al.* Functional avidity: A measure to predict the efficacy of effector T cells? *Clinical and Developmental Immunology* vol. 2012 Preprint at https://doi.org/10.1155/2012/153863 (2012).
200. Schönrich, G. *et al.* Down-regulation of T cell receptors on self-reactive T cells as a novel mechanism for extrathymic tolerance induction. *Cell* **65**, (1991).
201. Valitutti, S., Müller, S., Salio, M. & Lanzavecchia, A. Degradation of T cell receptor (TCR)-CD3-ζ complexes after antigenic stimulation. *Journal of Experimental Medicine* vol. 185 Preprint at https://doi.org/10.1084/jem.185.10.1859 (1997).
202. Roth, T. L. *et al.* Reprogramming human T cell function and specificity with non-viral genome targeting. *Nature* **559**, (2018).
203. Soto, C. M. *et al.* MHC-class I-restricted CD4 T cells: A nanomolar affinity TCR has improved anti-tumor efficacy in vivo compared to the micromolar wild-type TCR. *Cancer Immunol. Immunother.* **62**, (2013).
204. Khor, B. & Sleckman, B. P. Allelic exclusion at the TCRβ locus. *Current Opinion in Immunology* vol. 14 Preprint at https://doi.org/10.1016/S0952-7915(02)00326-6 (2002).
205. Benjamini, Y., Krieger, A. M. & Yekutieli, D. Adaptive linear step-up procedures that control the false discovery rate. *Biometrika* **93**, (2006).
206. Baldwin, T. A., Sandau, M. M., Jameson, S. C. & Hogquist, K. A. The timing of TCRα expression critically influences T cell development and selection. *J. Exp. Med.* **202**, (2005).
207. Steinel, N. C., Brady, B. L., Carpenter, A. C., Yang-Iott, K. S. & Bassing, C. H. Posttranscriptional Silencing of VβDJβCβ Genes Contributes to TCRβ Allelic Exclusion in Mammalian Lymphocytes. *J. Immunol.* **185**, (2010).
208. Levin-Klein, R. & Bergman, Y. Epigenetic regulation of monoallelic rearrangement (allelic exclusion) of antigen receptor genes. *Frontiers in Immunology* vol. 5 Preprint at https://doi.org/10.3389/fimmu.2014.00625 (2014).

209. Derbinski, J. *et al.* Promiscuous gene expression in thymic epithelial cells is regulated at multiple levels. *J. Exp. Med.* **202**, (2005).
210. Villaseñor, J., Besse, W., Benoist, C. & Mathis, D. Ectopic expression of peripheral-tissue antigens in the thymic epithelium: Probabilistic, monoallelic, misinitiated. *Proc. Natl. Acad. Sci. U. S. A.* **105**, (2008).
211. Takaba, H. *et al.* Fezf2 Orchestrates a Thymic Program of Self-Antigen Expression for Immune Tolerance. *Cell* **163**, (2015).
212. Tomofuji, Y. *et al.* Chd4 choreographs self-antigen expression for central immune tolerance. *Nat. Immunol.* **21**, (2020).
213. Wang, J. *et al.* Hassall's corpuscles with cellular-senescence features maintain IFNα production through neutrophils and pDC activation in the thymus. *Int. Immunol.* **31**, (2019).
214. Bautista, J. L. *et al.* Single-cell transcriptional profiling of human thymic stroma uncovers novel cellular heterogeneity in the thymic medulla. *Nat. Commun.* **12**, (2021).
215. Chen, Y. *et al.* Mesothelin expression in thymic epithelial tumors (TETs). *J. Clin. Oncol.* **32**, (2014).
216. Fraietta, J. A. *et al.* Disruption of TET2 promotes the therapeutic efficacy of CD19-targeted T cells. *Nature* (2018) doi:10.1038/s41586-018-0178-z.
217. Von Kalle, C., Deichmann, A. & Schmidt, M. Vector integration and tumorigenesis. *Human Gene Therapy* Preprint at https://doi.org/10.1089/hum.2014.2525 (2014).
218. Ellis, J. Silencing and variegation of gammaretrovirus and lentivirus vectors. *Human Gene Therapy* Preprint at https://doi.org/10.1089/hum.2005.16.1241 (2005).
219. Stromnes, I. M., Schmitt, T. M., Chapuis, A. G., Hingorani, S. R. & Greenberg, P. D. Re-adapting T cells for cancer therapy: from mouse models to clinical trials. *Immunol. Rev.* **257**, 145–164 (2014).
220. Le, D. T. *et al.* Safety and survival with GVAX pancreas prime and Listeria monocytogenes-expressing mesothelin (CRS-207) boost vaccines for metastatic pancreatic cancer. *J. Clin. Oncol.* (2015) doi:10.1200/JCO.2014.57.4244.
221. Ahmadi, M. *et al.* CD3 limits the efficacy of TCR gene therapy in vivo. *Blood* (2011) doi:10.1182/blood-2011-04-346338.
222. Legut, M., Dolton, G., Mian, A. A., Ottmann, O. G. & Sewell, A. K. CRISPR-mediated TCR replacement generates superior anticancer transgenic t cells. *Blood* (2018) doi:10.1182/blood-2017-05-787598.
223. Turtle, C. J. *et al.* CD19 CAR-T cells of defined CD4+:CD8+ composition in adult B cell ALL patients. *J. Clin. Invest.* (2016) doi:10.1172/JCI85309.
224. Rius, C. *et al.* Peptide–MHC Class I Tetramers Can Fail To Detect Relevant Functional T Cell Clonotypes and Underestimate Antigen-Reactive T Cell Populations. *J. Immunol.* **200**, (2018).
225. Tungatt, K. *et al.* Antibody Stabilization of Peptide–MHC Multimers Reveals Functional T Cells Bearing Extremely Low-Affinity TCRs. *J. Immunol.* **194**, (2015).
226. Yang, S. *et al.* Development of optimal bicistronic lentiviral vectors facilitates high-level TCR gene expression and robust tumor cell recognition. *Gene Ther.* **15**, (2008).

227. Gibson, D. G. Enzymatic assembly of overlapping DNA fragments. in *Methods in Enzymology* vol. 498 (2011).
228. Behringer, R., Gertsenstein, M., Vintersen Nagy, K. & Nagy, A. *Manipulating the Mouse Embryo*. *Cold Spring Harbor, NY: Cold Spring Harbor Laboratory Press* (2014).
229. Kito, S. *et al.* Improved in vitro fertilization and development by use of modified human tubal fluid and applicability of pronucleate embryos for cryopreservation by rapid freezing in inbred mice. *Comp. Med.* (2004).
230. Burrack, A. L. *et al.* Combination PD-1 and PD-L1 Blockade Promotes Durable Neoantigen-Specific T Cell-Mediated Immunity in Pancreatic Ductal Adenocarcinoma. *Cell Rep.* **28**, 2140-2155.e6 (2019).
231. Kolbeinsson, H. M., Chandana, S., Wright, G. P. & Chung, M. Pancreatic Cancer: A Review of Current Treatment and Novel Therapies. *J. Invest. Surg.* **36**, 2129884 (2023).
232. Vincent, A., Herman, J., Schulick, R., Hruban, R. H. & Goggins, M. Pancreatic cancer. *The Lancet* **378**, 607–620 (2011).
233. Rahib, L. *et al.* Projecting Cancer Incidence and Deaths to 2030: The Unexpected Burden of Thyroid, Liver, and Pancreas Cancers in the United States. *Cancer Res.* **74**, 2913–2921 (2014).
234. Robert, C. A decade of immune-checkpoint inhibitors in cancer therapy. *Nat. Commun.* **11**, 3801 (2020).
235. Krishnamurty, A. T. *et al.* LRRC15+ myofibroblasts dictate the stromal setpoint to suppress tumour immunity. *Nature* **611**, 148–154 (2022).
236. Diskin, B. *et al.* PD-L1 engagement on T cells promotes self-tolerance and suppression of neighboring macrophages and effector T cells in cancer. *Nat. Immunol.* **21**, 442–454 (2020).
237. Burrack, A. L. *et al.* Distinct myeloid antigen-presenting cells dictate differential fates of tumor-specific CD8+ T cells in pancreatic cancer. *JCI Insight* **7**, e151593 (2022).
238. Stromnes, I. M. *et al.* Insufficiency of compound immune checkpoint blockade to overcome engineered T cell exhaustion in pancreatic cancer. *J. Immunother. Cancer* **10**, e003525 (2022).
239. Chaudhury, A. & Howe, P. H. The Tale of Transforming Growth Factor-β (TGFβ) Signaling: A Soigné Enigma. *IUBMB Life* **61**, 929–939 (2009).
240. Schwartzkopff, S. *et al.* TGF-β downregulates KLRG1 expression in mouse and human CD8+ T cells. *Eur. J. Immunol.* **45**, 2212–2217 (2015).
241. Esebanmen, G. E. & Langridge, W. H. R. The role of TGF-beta signaling in dendritic cell tolerance. *Immunol. Res.* **65**, 987–994 (2017).
242. Batlle, E. & Massagué, J. Transforming Growth Factor-β Signaling in Immunity and Cancer. *Immunity* **50**, 924–940 (2019).
243. Li, M. O., Sanjabi, S. & Flavell, R. A. Transforming Growth Factor-β Controls Development, Homeostasis, and Tolerance of T Cells by Regulatory T Cell-Dependent and -Independent Mechanisms. *Immunity* **25**, 455–471 (2006).

244. Yang, H. *et al.* Concomitant underexpression of TGFBR2 and overexpression of hTERT are associated with poor prognosis in cervical cancer. *Sci. Rep.* **7**, 41670 (2017).
245. Rollins, M. R. *et al.* Germline T cell receptor exchange results in physiological T cell development and function. *Nat. Commun.* **14**, 528 (2023).
246. Stromnes, I. M. *et al.* T Cells Engineered against a Native Antigen Can Surmount Immunologic and Physical Barriers to Treat Pancreatic Ductal Adenocarcinoma. *Cancer Cell* **28**, 638–652 (2015).
247. Zhou, B., Guo, W., Sun, C., Zhang, B. & Zheng, F. Linc00462 promotes pancreatic cancer invasiveness through the miR-665/TGFBR1-TGFBR2/SMAD2/3 pathway. *Cell Death Dis.* **9**, 1–15 (2018).
248. Evrard, M. *et al.* Sphingosine 1-phosphate receptor 5 (S1PR5) regulates the peripheral retention of tissue-resident lymphocytes. *J. Exp. Med.* **219**, e20210116 (2022).
249. Fix, S. M. *et al.* CRISPR-mediated TGFBR2 knockout renders human ovarian cancer tumor-infiltrating lymphocytes resistant to TGF-β signaling. *J. Immunother. Cancer* **10**, e003750 (2022).
250. Obst, R. The Timing of T Cell Priming and Cycling. *Front. Immunol.* **6**, (2015).
251. Burrack, A. L. *et al.* Combination PD-1 and PD-L1 Blockade Promotes Durable Neoantigen-Specific T Cell-Mediated Immunity in Pancreatic Ductal Adenocarcinoma. *Cell Rep.* **28**, 2140-2155.e6 (2019).
252. Le Naour, A., Rossary, A. & Vasson, M. EO771, is it a well-characterized cell line for mouse mammary cancer model? Limit and uncertainty. *Cancer Med.* **9**, 8074–8085 (2020).
253. Barrios, K. & Celis, E. TriVax: an improved peptide-based therapeutic vaccination strategy against Human Papillomavirus-induced cancers. *Cancer Immunol. Immunother. CII* **61**, 1307–1317 (2012).
254. Dasatinib, Temsirolimus, and Cyclophosphamide in Treating Patients with Advanced, Recurrent, or Refractory Solid Tumors - NCT02389309. *Natl. Cancer Inst.* (2011).
255. Cham, K. K. Y. *et al.* Metronomic gemcitabine suppresses tumour growth, improves perfusion, and reduces hypoxia in human pancreatic ductal adenocarcinoma. *Br. J. Cancer* **103**, 52–60 (2010).
256. Kaech, S. M., Wherry, E. J. & Ahmed, R. Effector and memory T-cell differentiation: implications for vaccine development. *Nat. Rev. Immunol.* **2**, 251–262 (2002).
257. Wherry, E. J. T cell exhaustion. *Nat Immunol* **12**, 492–499 (2011).
258. Paley, M. A. *et al.* Progenitor and Terminal Subsets of CD8+ T Cells Cooperate to Contain Chronic Viral Infection. *Science* **338**, 1220–1225 (2012).
259. Miller, B. C. *et al.* Subsets of exhausted CD8+ T cells differentially mediate tumor control and respond to checkpoint blockade. *Nat. Immunol.* **20**, 326–336 (2019).
260. Mittal, D. *et al.* Interleukin-12 from CD103+ Batf3-Dependent Dendritic Cells Required for NK-Cell Suppression of Metastasis. *Cancer Immunol. Res.* **5**, 1098–1108 (2017).

261. Brewitz, A. *et al.* CD8+ T Cells Orchestrate pDC-XCR1+ Dendritic Cell Spatial and Functional Cooperativity to Optimize Priming. *Immunity* **46**, 205–219 (2017).
262. He, S., Wang, L., Wu, Y., Li, D. & Zhang, Y. CCL3 and CCL20-recruited dendritic cells modified by melanoma antigen gene-1 induce anti-tumor immunity against gastric cancer ex vivo and in vivo. *J. Exp. Clin. Cancer Res. CR* **29**, 37 (2010).
263. Fowell, D. J. & Kim, M. The spatio-temporal control of effector T cell migration. *Nat. Rev. Immunol.* **21**, 582–596 (2021).
264. Lämmermann, T. *et al.* Rapid leukocyte migration by integrin-independent flowing and squeezing. *Nature* **453**, 51–55 (2008).
265. Stromnes, I. M., DelGiorno, K. E., Greenberg, P. D. & Hingorani, S. R. Stromal reengineering to treat pancreas cancer. *Carcinogenesis* **35**, 1451–1460 (2014).
266. Cho, H.-I., Barrios, K., Lee, Y.-R., Linowski, A. K. & Celis, E. BiVax: A peptide/poly-IC subunit vaccine that mimics an acute infection elicits vast and effective anti-tumor CD8 T cell responses. *Cancer Immunol. Immunother. CII* **62**, 787–799 (2013).
267. Herndler-Brandstetter, D. *et al.* KLRG1+ Effector CD8+ T Cells Lose KLRG1, Differentiate into All Memory T Cell Lineages, and Convey Enhanced Protective Immunity. *Immunity* **48**, 716-729.e8 (2018).
268. Burrack, A. L. *et al.* Cxcr3 constrains pancreatic cancer dissemination through instructing T cell fate. *Cancer Immunol. Immunother.* (2022) doi:10.1007/s00262-022-03338-7.
269. Ma, C. & Zhang, N. Transforming growth factor-β signaling is constantly shaping memory T-cell population. *Proc. Natl. Acad. Sci. U. S. A.* **112**, 11013–11017 (2015).
270. Hingorani, S. R. *et al.* Trp53R172H and KrasG12D cooperate to promote chromosomal instability and widely metastatic pancreatic ductal adenocarcinoma in mice. *Cancer Cell* **7**, 469–483 (2005).
271. Kalos, M. *et al.* T Cells with Chimeric Antigen Receptors Have Potent Antitumor Effects and Can Establish Memory in Patients with Advanced Leukemia. *Sci. Transl. Med.* **3**, 95ra73 (2011).
272. Darvin, P., Toor, S. M., Sasidharan Nair, V. & Elkord, E. Immune checkpoint inhibitors: recent progress and potential biomarkers. *Exp Mol Med* **50**, 1–11 (2018).
273. Stromnes, I. M. *et al.* T Cells Engineered against a Native Antigen Can Surmount Immunologic and Physical Barriers to Treat Pancreatic Ductal Adenocarcinoma. *Cancer Cell* **28**, 638–652 (2015).
274. Rivière, I., Gallardo, H. F., Hagani, A. B. & Sadelain, M. Retroviral-mediated gene transfer in primary murine and human T-lymphocytes. *Mol. Biotechnol.* **15**, 133–142 (2000).
275. Kouskoff, V., Signorelli, K., Benoist, C. & Mathis, D. Cassette vectors directing expression of T cell receptor genes in transgenic mice. *J. Immunol. Methods* **180**, 273–280 (1995).
276. von Kalle, C., Deichmann, A. & Schmidt, M. Vector Integration and Tumorigenesis. *Hum. Gene Ther.* **25**, 475–481 (2014).
277. Eyquem, J. *et al.* Targeting a CAR to the TRAC locus with CRISPR/Cas9 enhances tumour rejection. *Nature* **543**, 113–117 (2017).

278. Chan, K. Y. *et al.* Engineered AAVs for efficient noninvasive gene delivery to the central and peripheral nervous systems. *Nat Neurosci* **20**, 1172–1179 (2017).
279. Sather, B. D. *et al.* Efficient modification of CCR5 in primary human hematopoietic cells using a megaTAL nuclease and AAV donor template. *Sci. Transl. Med.* **7**, 307ra156-307ra156 (2015).
280. Chen, S. *et al.* CRISPR-READI: Efficient Generation of Knockin Mice by CRISPR RNP Electroporation and AAV Donor Infection. *Cell Rep.* **27**, 3780-3789.e4 (2019).
281. Principe, D. R., Timbers, K. E., Atia, L. G., Koch, R. M. & Rana, A. TGFβ Signaling in the Pancreatic Tumor Microenvironment. *Cancers* **13**, 5086 (2021).
282. Principe, D. R., Timbers, K. E., Atia, L. G., Koch, R. M. & Rana, A. TGFβ Signaling in the Pancreatic Tumor Microenvironment. *Cancers* **13**, 5086 (2021).
283. Dardare, J., Witz, A., Merlin, J.-L., Gilson, P. & Harlé, A. SMAD4 and the TGFβ Pathway in Patients with Pancreatic Ductal Adenocarcinoma. *Int. J. Mol. Sci.* **21**, 3534 (2020).
284. Mariathasan, S. *et al.* TGFβ attenuates tumour response to PD-L1 blockade by contributing to exclusion of T cells. *Nature* **554**, 544–548 (2018).
285. Hussain, S. M. *et al.* Role of TGF-β in pancreatic ductal adenocarcinoma progression and PD-L1 expression. *Cell. Oncol.* **44**, 673–687 (2021).
286. Dardare, J., Witz, A., Merlin, J.-L., Gilson, P. & Harlé, A. SMAD4 and the TGFβ Pathway in Patients with Pancreatic Ductal Adenocarcinoma. *Int. J. Mol. Sci.* **21**, 3534 (2020).
287. Principe, D. R. *et al.* TGFβ Blockade Augments PD-1 Inhibition to Promote T-Cell–Mediated Regression of Pancreatic Cancer. *Mol. Cancer Ther.* **18**, 613–620 (2019).
288. Robbins, P. F. *et al.* Single and dual amino acid substitutions in TCR CDRs can enhance antigen-specific T cell functions. *J. Immunol. Baltim. Md 1950* **180**, 6116–6131 (2008).
289. Border, E. C., Sanderson, J. P., Weissensteiner, T., Gerry, A. B. & Pumphrey, N. J. Affinity-enhanced T-cell receptors for adoptive T-cell therapy targeting MAGE-A10: strategy for selection of an optimal candidate. *Oncoimmunology* **8**, e1532759 (2019).